

論文 / 著書情報  
Article / Book Information

題目(和文)	L10-CoPt/TiN薄膜の組織と垂直磁気異方性に関する研究
Title(English)	Structure and Magnetic properties of L10-CoPt/TiN thin films
著者(和文)	安紅雨
Author(English)	Hongyu An
出典(和文)	学位:博士(工学), 学位授与機関:東京工業大学, 報告番号:甲第9966号, 授与年月日:2015年9月25日, 学位の種別:課程博士, 審査員:史 蹟,中村 吉男,村石 信二,三宮 工,中川 茂樹
Citation(English)	Degree:., Conferring organization: Tokyo Institute of Technology, Report number:甲第9966号, Conferred date:2015/9/25, Degree Type:Course doctor, Examiner:,,,,,
学位種別(和文)	博士論文
Type(English)	Doctoral Thesis

**Structure and magnetic properties of L1<sub>0</sub>-CoPt/TiN  
thin films**

**Hongyu AN**

**Directed by**

**Professor Ji SHI**

**Professor Yoshio NAKAMURA**

**Department of Metallurgy and Ceramics Science**

**Tokyo Institute of Technology**

**May, 2015**



## Preface

During the last decade,  $L1_0$ -ordered CoPt and FePt structures have attracted researchers' interests due to their high magnetocrystalline anisotropy, large coercivity and high thermal stability, which make them promising candidates for the emerging spintronic devices and ultrahigh density recording media. On one hand, the layered  $L1_0$  structure can be used for perpendicular pseudo spin valves, which are the core elements in magnetic sensors, hard disk read heads, and magnetic random access memories (MRAM). On the other hand,  $L1_0$  granular films can be used for the heat-assisted magnetic recording media (HAMR), which is the most promising recording media in the next 10 years.

In the present work, the microstructure and magnetic properties of the  $L1_0$ -CoPt structure have been systematically studied by using TiN seed layers.

Firstly, we have successfully fabricated highly (001) oriented  $L1_0$ -CoPt/TiN multilayer films with strong perpendicular magnetic anisotropy (PMA) on glass substrates by controlling the deposition process of TiN layer. It is found that by alternate depositing TiN and CoPt layers, (001) orientation of CoPt layers is gradually prompted by TiN layers, leading to the enhancement of PMA.

Secondly, we have successfully observed the perpendicular exchange-bias-like effect in CoPt/TiN multilayer films. It is well known that exchange bias (EB) effect generally exists in the ferromagnetic (FM)/antiferromagnetic (AFM) material systems due to the coupling effect of the spins at the interface between FM and AFM materials. Similar to this effect, it is found

that the coupling effect also exists between A1-CoPt and L1<sub>0</sub>-CoPt phases in the CoPt/TiN multilayer films.

Finally, we have successfully fabricated L1<sub>0</sub>-CoPt single layer films with large perpendicular coercivity on glass substrates by using TiN seed layer. We also provide an innovative method for fabricating highly ordered L1<sub>0</sub>-CoPt films on glass substrates, which is to apply an appropriate amount of nitrogen during the deposition of CoPt films. During deposition, incorporated N in CoPt layer partially relieves the tensile stress, and favors the epitaxial growth of CoPt on TiN. During the post annealing process, nitrogen effuses from CoPt layer, and promotes the diffusion mobility of Co and Pt atoms, enhancing L1<sub>0</sub> structure transformation.

# Contents

<b>Preface</b> .....	i
<b>Contents</b> .....	iii
<b>Chapter 1 Introduction</b> .....	1
1.1 Development of HDD technology.....	1
1.2 Perpendicular magnetic recording media.....	2
1.3 Heat-assisted magnetic recording media.....	3
1.4 Introduction of A1 and L1 <sub>0</sub> structure.....	4
1.5 Exchange bias effect.....	6
1.6 Spin valve and pseudo spin valve.....	8
1.7 Background of this work .....	10
1.8 Objectives of this work.....	12
1.9 Organization of this thesis .....	13
Reference.....	15
<b>Chapter 2 Fabrication and characterization of CoPt/TiN films</b> .....	19
2.1 Film fabrication and heat treatment.....	19
2.1.1 dc magnetron sputtering.....	19
2.1.2 Heat treatment.....	20
2.2 Structure characterization.....	20
2.2.1 X-ray diffraction .....	21
2.2.1.1 Fundamentals of XRD.....	21
2.2.1.2 XRD measurement of TiN single layer .....	22
2.2.1.3 XRD measurement of CoPt/TiN multilayer films.....	25
2.2.2 X-ray reflectivity.....	26
2.2.2.1 Fundamentals of XRR.....	26
2.2.2.2 XRR Measurement of CoPt/TiN multilayer films.....	26
2.2.3 Transmission electron microscopy.....	27
2.2.3.1 Fundamentals of TEM.....	27
2.2.3.2 Observations of CoPt/TiN multilayer films.....	30
2.2.4 Atomic force microscopy.....	33
2.2.4.1 Fundamentals of AFM.....	33
2.2.4.2 Surface observations of CoPt/TiN films.....	34

2.3 Magnetic properties measurement.....	35
2.3.1 Fundamentals of magnetic hysteresis loops.....	35
2.3.2 Magnetic properties measurement of CoPt/TiN multilayer films.....	36
2.4 Summary .....	36
Reference.....	38

### **Chapter 3 Effect of period on the structure and magnetic properties of L1<sub>0</sub>-CoPt/TiN**

<b>multilayer films</b> .....	39
3.1 Deposition of CoPt/TiN multilayer films .....	39
3.2 Experimental results of TiN(5 nm)[CoPt(4 nm)/TiN(2 nm)] <sub>5</sub> .....	40
3.2.1 Structure characterization .....	40
3.2.2 Magnetic properties measurement .....	41
3.3 Experimental results by increasing multilayer periods .....	42
3.3.1 Structure characterization .....	42
3.3.2 Magnetic properties measurement .....	47
3.3.3 In-plane residual stress and magnetoelastic anisotropy .....	48
3.4 Summary .....	49
Reference.....	51

### **Chapter 4 Effect of TiN layer thickness on the structure and magnetic properties of**

<b>L1<sub>0</sub>-CoPt/TiN multilayer films</b> .....	53
4.1 Deposition of CoPt/TiN multilayer films .....	53
4.2 Magnetic properties measurement.....	53
4.3 Structure characterization.....	60
4.3.1 XRD measurement.....	60
4.3.2 Calculation of chemical ordering parameter.....	61
4.3.3 Mechanism for the change of magnetic anisotropy and ordering parameter.....	63
4.4 Summary .....	66
Reference.....	68

### **Chapter 5 Perpendicular exchange-bias-like effect in CoPt/TiN multilayer films** ..... 69 |

5.1 Fabrication of L1 <sub>0</sub> -CoPt/TiN multilayer films .....	70
5.2 Observation of perpendicular exchange-bias-like effect.....	71
5.3 The origin of exchange-bias-like effect.....	75
5.4 2D micromagnetic simulations.....	79
5.5 Summary .....	80
Reference.....	82

<b>Chapter 6 Realization of PMA in L1<sub>0</sub>-CoPt/TiN single layer films</b> .....	84
6.1 Fabrication of L1 <sub>0</sub> -CoPt/TiN single layer films .....	85
6.2 structure characterization of TiN single layer .....	86
6.3 Magnetic properties measurement of CoPt/TiN films.....	86
6.4 Effect of N <sub>2</sub> doping during deposition .....	88
6.5 Summary .....	96
Reference.....	97
<b>Chapter 7 Conclusions</b> .....	99
<b>Publications</b> .....	102
<b>Acknowledgements</b> .....	105



## Chapter 1 Introduction

As information technology society develops, information becomes more significant in our human being's world no matter in personal life or public work than never before. However, the storage of the huge amount of the information data also comes out as an unavoidable problem. According to the investigation of IDC Corporation, data storage requirement increases by about 40 percent per annum. Such amount of data can be stored by optical storage media, magnetic-optical storage media, semiconductor storage media, magnetic storage media, etc.<sup>[1]</sup> Among these storage medias, hard disk drives (HDDs) which is based on magnetic storage technology, is the cheapest way to store data with a cost of less than \$0.10 per gigabyte.<sup>[2]</sup> and as the new perpendicular magnetic recording technology evolves, this cost is continuously decreasing.

### 1.1 Development of HDD technology

Since IBM released the first HDD product, IBM305 RAMAC with a total storage capacity of 4.4 megabytes and a price of \$10 M per gigabyte in 1956, HDD technology has been developed for over 50 years.<sup>[2]</sup> As the dominant storage devices, HDDs nowadays with a 2.5 inch diameter can store data at 750 Gb/inch at a price of less than \$0.10 per gigabyte.<sup>[2]</sup> Due to the insatiable demand for information data storage, HDDs with larger capacities are still eagerly needed at present and in the near future. Figure 1-1 shows the HDD roadmap released by Advanced Storage Technology Consortium in 2014. It can be seen that perpendicular magnetic recording (PMR) is currently applied for HDDs, and heat-assisted

magnetic recording (HAMR) will be the most promising technology for magnetic recording in the next 10 years.

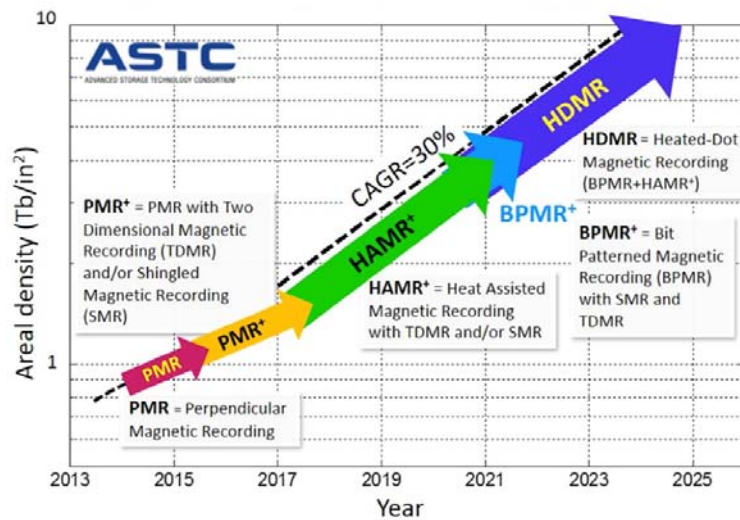


Figure 1-1 HDD roadmap released by Advanced Storage Technology Consortium

## 1.2 Perpendicular magnetic recording media

Since Iwasaki and Takemura proposed the concept of perpendicular magnetic recording in 1975,<sup>[3]</sup> it has been intensively studied around the world due to the potential to drastically increase areal recording density than longitudinal recording.<sup>[4-7]</sup> Different from that the longitudinal magnetic recording media has magnetization direction along the in-plane direction of media plane (Fig. 1-2(a)); perpendicular magnetic recording has magnetization perpendicular to the media plane (Fig. 1-2(b)). The latter arrangement increased the amount of recording grains, leading to a break through of recording capacity in HDDs industry. However, in spite of the advantage it owns, the development of perpendicular magnetic recording was lagging behind of the longitudinal recording in the last century, since no appropriate material could be used to segregate recording grains without impairing the

perpendicular magnetic anisotropy. In 2002, Oikawa *et al.* found that adding SiO<sub>2</sub> in CoCrPt films was very effective in isolating the grains.<sup>[8]</sup> From then on, the systematical study on CoCrPt: SiO<sub>2</sub> granular films has been gradually completed. At present, CoCrPt: SiO<sub>2</sub> granular films have already been widely used in the commercial HDDs.

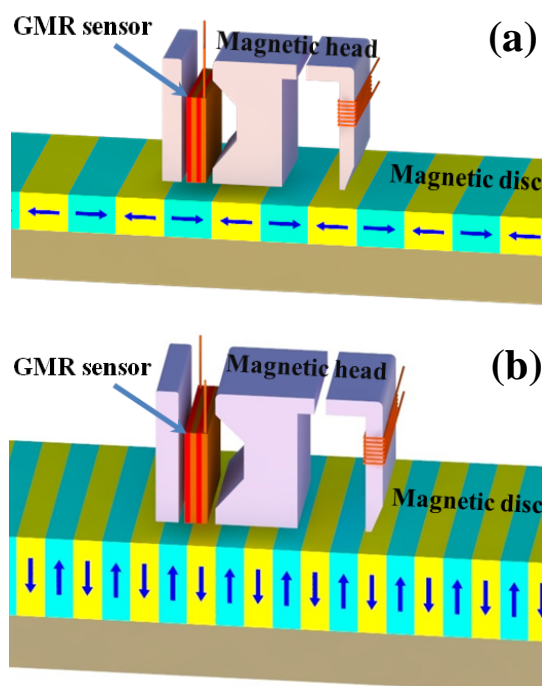


Figure 1-2 Schematic illustration of (a) longitudinal magnetic recording, (b) perpendicular magnetic recording.

### 1.3 Heat-assisted magnetic recording media

The urgent demand for large capacity HDDs has never been stopped. Although perpendicular magnetic recording drastically increased the areal recording density up to 500-1000 Gb/in<sup>2</sup>,<sup>[9]</sup> the limitation has already come. If the recording grains are further reduced to increase the recording density, thermal instability problem will occur, which is prohibited for reliable magnetic recording. Therefore, alternative materials or methods are

needed to push forward the development of magnetic recording industry. Heat-assisted magnetic recording (HAMR) offers an innovative way to avoid such a problem. By applying a laser, the media can be locally heated (Fig. 1-3(a)). For recording, the coercivity will be lowered below the available read field by temporarily heating the media (Fig. 1-3(b)).<sup>[10]</sup> After recording, the laser will be removed and the media can be rapidly cooled down to room temperature. Since this method is able to allow large coercivity at room temperature, areal recording density can be drastically increased by reducing the recording grain size without thermal instability problem. If the grain size can be reduced to 3-4 nm, it is feasible that the areal recording density can be increased to 5 Tbit/in<sup>2</sup>.<sup>[2]</sup>

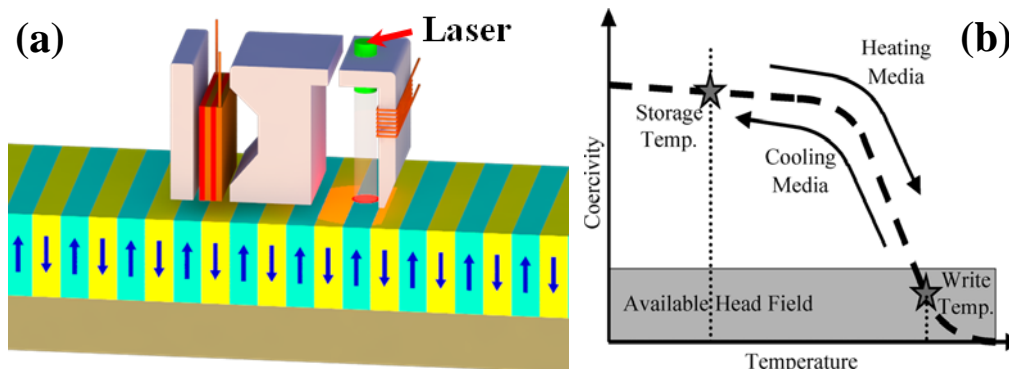


Figure 1-3 Heat-assisted magnetic recording of (a) schematic illustration, (b) recording principle.

#### 1.4 Introduction of A1 and L1<sub>0</sub> structure

As introduced in previous section, to increase recording density, media material is requested for large coercivity to keep it thermally stable at room temperature, and the most promising materials can satisfy this rigid request is L1<sub>0</sub> FePt or CoPt due to its large coercivity and high magnetocrystalline anisotropy.<sup>[10-12]</sup> Since FePt and CoPt have very

similar structure and magnetic properties, and we used CoPt in our study, hereafter, we will only representatively mention CoPt. Generally, CoPt has A1 and L1<sub>0</sub> two main structures. A1 structure is a face-centered cubic (fcc) structure with each position randomly occupied by Co or Pt atom, as shown in (Fig. 1-4(a)). After heat treatment, A1 structure can transform to L1<sub>0</sub> structure, which is a face-centered tetragonal (fct) structure with each atom layers alternately occupied by Co and Pt, as shown in (Fig. 1-4(b)). It is noteworthy that L1<sub>0</sub> structure has high magnetocrystalline anisotropy in [001] crystal orientation. Therefore, in order to obtain strong perpendicular magnetic anisotropy (PMA), the c-axis ([001] crystal orientation) must be oriented to the normal of the film plane.<sup>[13]</sup> However, it is difficult to control the fcc metallic crystal growth, since (111) plane has the lowest surface energy and tends to form (111) oriented columnar texture during deposition.<sup>[14,15]</sup> In most previous studies, single crystalline MgO (001) substrates were used to promote the epitaxial growth of L1<sub>0</sub> structure by depositing at elevated temperatures or post-annealing (Fig. 1-5 (a)).<sup>[16,17]</sup> However, MgO substrate is unsuitable for practical application due to its high cost, poor mechanical properties and hydrophilic nature. Recently, amounts of studies on L1<sub>0</sub> structure fabrication also focused on depositing different kinds of seed layers, such as: Au, Ag, C, TiN/RuAl, Cu, TiN, MgO and TiN/CrRu on glass or other amorphous substrates (Fig. 1-5 (b)).<sup>[18-25]</sup> By controlling the orientation of the seed layers, (001) oriented L1<sub>0</sub> CoPt can be obtained.

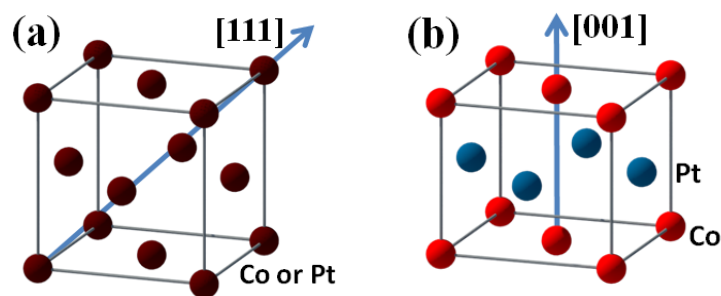


Figure 1-4 Schematic illustrations of (a) A1 structure (b) L1<sub>0</sub> structure. Arrows indicate the magnetocrystalline anisotropy direction.

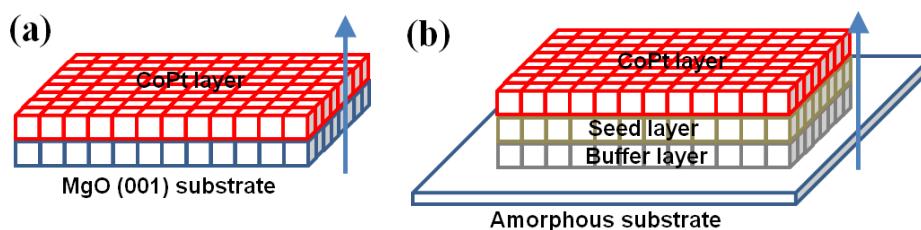


Figure 1-5 Schematic illustrations for fabricating L1<sub>0</sub>-CoPt (a) on MgO (001) substrate (b) on amorphous substrate with seed layer. Arrows indicate the magnetic anisotropy direction.

### 1.5 Exchange bias effect

Exchange bias (EB) refers to a shift of the magnetic hysteresis loop along the magnetic field axis. It generally occurs in ferromagnetic (FM)/antiferromagnetic (AFM) material systems.<sup>[44]</sup> As shown in Fig. 1-6, by increasing the temperature to above Néel temperature but below Curie temperature, AFM shows paramagnetic property and spins in FM material are switched parallel to the direction of applied external magnetic field. After cooling down to below Néel temperature, AFM shows antiferromagnetic property. Spins in FM are pinned by the spins in AFM at the interface between FM and AFM. This coupling cost additional energy for the spin switching in FM by applying magnetic field in opposite direction, and

lead to a shift in the opposite direction of the magnetic field. Similar to the common in-plane EB effect, perpendicular exchange bias (PEB) effect also can be observed in the FM/AFM system with the easy magnetization axis in perpendicular direction of the film plane.<sup>[45,46]</sup> PEB is considered to be an promising technology in the perpendicular spin valves.

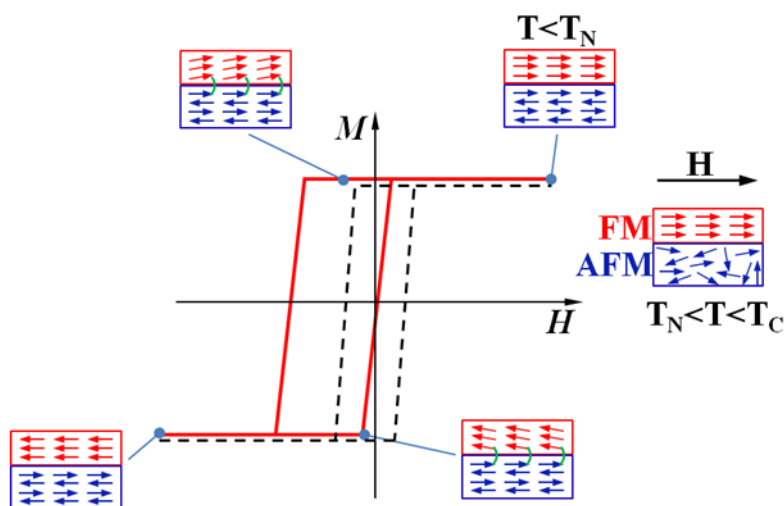


Figure 1-6 Schematic illustration of exchange bias effect.

Exchange bias effect exists not only in FM/AFM material systems, but also in ferromagnetic/ferromagnetic (Ferri/Ferri)<sup>[48]</sup>, Ferri/FM<sup>[49]</sup> and FM/FM<sup>[50]</sup> material systems, where it is called exchange-bias-like (EB-like) effect. As shown in Fig. 1-7, the system is generally composed a soft magnetic material with a coercivity  $H_{C1}$  and a hard magnetic material with coercivity  $H_{C2}$ . Firstly, both materials are magnetized by an external magnetic field larger than  $H_{C2}$ , or a smaller field at high temperature. Then by measuring the system in a magnetic field larger than  $H_{C1}$ , but smaller than  $H_{C2}$ , hysteresis loop with shifts both in vertical and horizontal direction can be obtained. Vertical shift is due to the remained not

switched spins from the hard magnetic material. The coupling between the spins at the interface from both materials generates the EB-like effect.

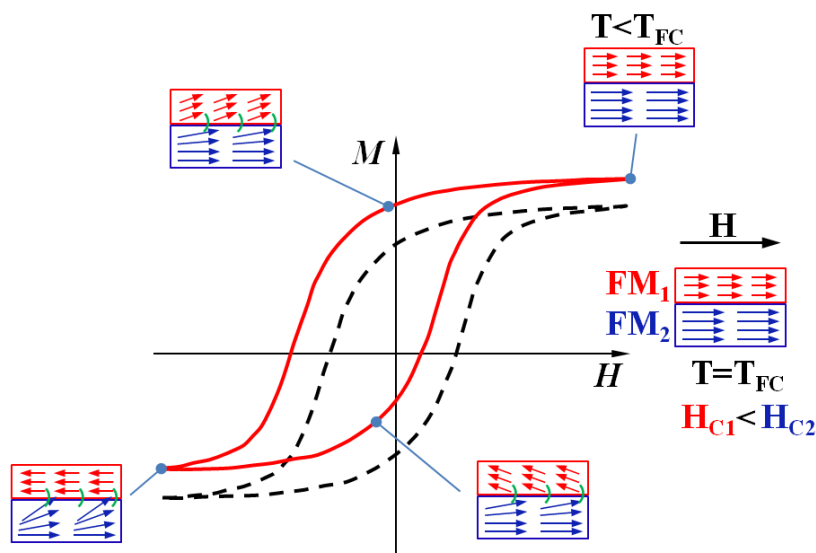


Figure 1-7 Schematic illustration of exchange-bias-like effect.

## 1.6 Spin valve and pseudo spin valve

Spin valve is the core element in magnetic sensors, hard disk read heads, and magnetic random access memories (MRAM). It is a layered structure consisting of two ferromagnetic (FM) layers, whose electrical resistivity can be changed by controlling the magnetization alignment of the two layers.<sup>[47]</sup> Generally, in a spin valve, the two FM layers are separated by a nonmagnetic (NM) layer (Fig. 1-8(a)). The magnetization direction of one FM layer is pinned by an antiferromagnetic (AFM) layer, and the magnetization direction of the other FM layer can be freely controlled by the external magnetic field. By controlling the two magnetization direction between parallel and antiparallel, the electrical resistivity can be controlled.

Pseudo spin valve is similar with normal spin valve, except for the absence of the AFM layer (Fig. 1-8(b)). It is composed by two FM layers with different coercivity. A magnetic field larger than the coercivities of both layers can change the two magnetization directions to be parallel. While, a magnetic field between the two coercivities can control the magnetization direction of the FM layer with small coercivity.

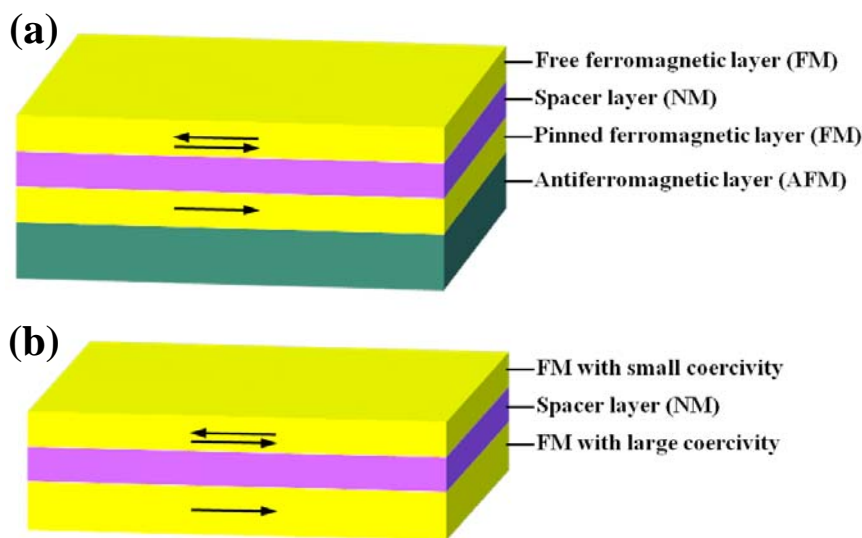


Figure 1-8 Schematic illustrations of (a) spin valve (b) pseudo spin valve.

Figure 1-9 shows the working principle of spin valves with perpendicular magnetic anisotropy. Spin valves with perpendicular magnetic anisotropy has same working principle with conventional spin valves (has in-plane magnetic anisotropy), except for the magnetization direction perpendicular to the film plane. In magnetic materials, the electrical resistivity is significantly affected by the scattering of electrons. When the magnetization directions are uniparallel in the two FM layers (Fig. 1-9(a)), the scattering is strongest resulting a largest electrical resistivity. By switching the magnetization directions to parallel,

the scattering becomes weakest, and leads to a smallest electrical resistivity (Fig. 1-9(a)). By applying a current into the system, resistivity can be calculated through measuring the electromotive force. Generally, current in plane (CIP) and current perpendicular to plane (CPP) can be applied, as shown in Fig. 1-9 (c) and (d).

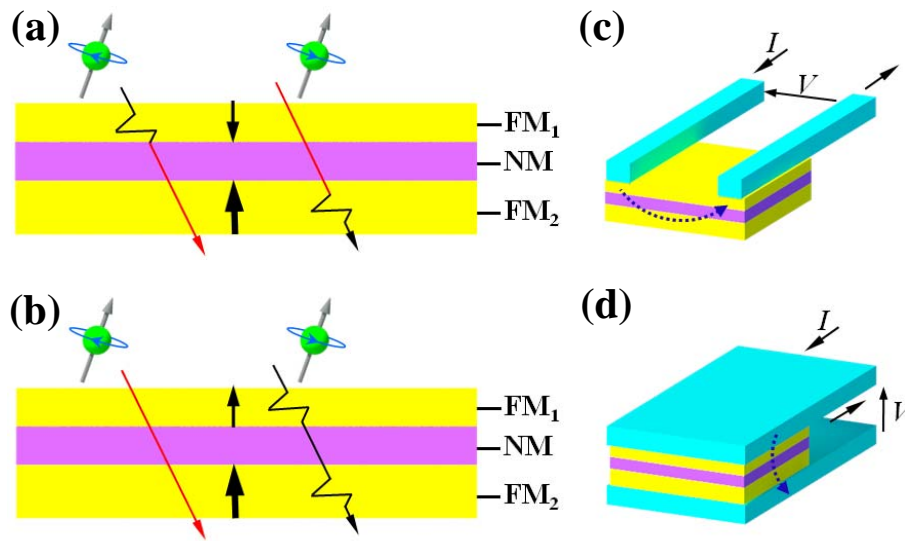


Figure 1-9 Schematic illustrations of (a) electron scattering with parallel magnetization direction, (b) electron scattering with antiparallel magnetization direction, (c) current in plane (CIP) set up of spin valve, (d) current perpendicular to plane (CPP) set up of spin valve.

### 1.7 Background of this work

Currently,  $L1_0$ -CoPt and FePt structures have attracted researchers' interests due to their high magnetocrystalline anisotropy, large coercivity and high thermal stability, which make them promising materials not only for the ultrahigh density magnetic recording media but also for the emerging spintronics technology.

On one hand, the layered  $L1_0$  structure can be used for perpendicular pseudo spin valves,<sup>[26,27]</sup> which are the core elements in magnetic sensors, hard disk read heads, and magnetic random access memories (MRAM). In spin valves, the interface diffusion and large roughness between adjacent layers are still challenging problems which affect the magnetic and magnetoresistance properties. For instance, recently, P. Ho *et al.* fabricated the  $L1_0$ -FePt pseudo spin valve with TiN spacer layer on MgO substrates; however, the giant magnetoresistance (GMR) ratio ranged only up to 0.61% due to the large roughness of the interface between FePt and TiN layers.<sup>[27]</sup> As to the substrate materials, although MgO (001) single crystalline substrate is effective to promote  $L1_0$  structure, high cost, poor mechanical properties and hydrophilic nature limit its practical application.

On the other hand,  $L1_0$  granular films can be used for the heat-assisted magnetic recording media (HAMR), which is the most promising recording media in the next 10 years. Currently, much effort has been devoted on enlarging the perpendicular coercivity, reducing the grain size, averaging the grain distribution, lowering the ordering temperature, etc.<sup>[28-37]</sup> To realize the above objectives, MgO seed layer is widely used on amorphous substrates to promote the  $L1_0$  ordering for FePt/CoPt.<sup>[29-34]</sup> Although significant progress for fabricating  $L1_0$  FePt/CoPt granular films with large perpendicular coercivity and small grain size has been made by using MgO seed layer, the small surface energy of MgO ( $1.1 \text{ J/m}^2$ ) can result in a large contact angle between FePt/CoPt and MgO, which is not favorable for the epitaxial growth. Furthermore, it will promote the formation of in-plane variants and lead to a large in-plane coercivity.<sup>[34,38]</sup> TiN has a similar structure with MgO, but owns a larger surface energy ( $1.28 \text{ J/m}^2$ ), which is more suitable for the epitaxial growth of  $L1_0$  FePt/CoPt.

However, it is difficult to fabricate highly (100) oriented TiN as a seed layer.<sup>[39]</sup> It is known that TiN (200) plane has the lowest surface energy which is the driving force for the growth in (200) orientation. However, besides surface energy, strain energy also affects the growth orientation, and TiN (111) plane has the lowest strain energy.<sup>[40]</sup> Since strain energy of the film is proportional to the film thickness,<sup>[41]</sup> TiN tends to grow in (111) orientation when the thickness is large. On the other hand, if TiN film is too thin, it will show random growth orientation on amorphous substrates.<sup>[42]</sup> Thus, to fabricate highly (100) oriented TiN as a seed layer, generally another buffer layer is needed to improve the wettability of TiN, or bias voltage is needed during the sputtering process, which increases the complicity for the practical industrial fabrication.<sup>[38,43]</sup>

### **1.8 Objectives of this work**

By considering the versatile promising applications and unsolved critical issues of L1<sub>0</sub> structure, this work focuses on achieving below objectives:

- (1) To control the crystalline growth of CoPt by using TiN layer, and obtain (001) oriented L1<sub>0</sub>-CoPt with perpendicular magnetic anisotropy on glass substrates.
- (2) To investigate the mechanism of the effect of TiN layer on the microstructure and magnetic properties of L1<sub>0</sub>-CoPt, and then obtain highly (001) oriented L1<sub>0</sub>-CoPt layered structure with strongest perpendicular magnetic anisotropy through controlling TiN layer on glass substrates.
- (3) To realize perpendicular magnetic anisotropy in L1<sub>0</sub>-CoPt single layer films with large perpendicular coercivity and narrow opening-up of in-plane hysteresis loops by

only using TiN seed layer on glass substrates from the point of view of practical application.

## **1.9 Organization of this thesis**

**Chapter 1 Introduction:** The development of magnetic recording technology is briefly introduced, especially for the current used perpendicular magnetic recording and heat-assisted magnetic recording, the next generation of magnetic recording technology. Moreover, exchange bias effect and spin valves are also briefly introduced, which can help to understand the content in the following chapters. The background, objectives and organization of this thesis are described.

**Chapter 2 Fabrication and characterization of CoPt/TiN films:** The experimental procedures for fabricating CoP/TiN films, methods for microstructure characterization and magnetic properties measurement are introduced. Typical experimental results are also ascribed through each measurement method.

**Chapter 3 Effect of period on the structure and magnetic properties of L1<sub>0</sub>-CoPt/TiN multilayer films:** Through studying the microstructure and magnetic properties of L1<sub>0</sub>-CoPt multilayer films with different periods, the enhancement of (001) texture and perpendicular magnetic anisotropy by alternate deposition of TiN and CoPt is verified.

**Chapter 4 Effect of TiN layer thickness on the structure and magnetic properties of L1<sub>0</sub>-CoPt/TiN multilayer films:** By changing the thickness of TiN layer and annealing temperatures, the effect of TiN layer on the microstructure and magnetic properties of L1<sub>0</sub>-CoPt layered structure is systematically studied. The optimum thickness of TiN layer and

annealing temperature for fabricating  $L1_0$ -CoPt with high magnetic anisotropy energy is obtained.

**Chapter 5 Perpendicular exchange-bias-like effect in CoPt/TiN multilayer films:**

Perpendicular Exchange-bias-like effect is observed in CoPt/TiN multilayer films. Origin for this exchange-bias-like effect is discussed by investigating the microstructure and conducting the micromagnetic simulation.

**Chapter 6 Realization of perpendicular magnetic anisotropy in  $L1_0$ -CoPt/TiN**

**single layer films:**  $L1_0$ -CoPt single layer films are successfully fabricated by only using one TiN seed layer on glass substrates. Effect of  $N_2$  on the microstructure and the magnetic properties of  $L1_0$ -CoPt single layer films is systematically studied. A novel method for fabricating  $L1_0$ -CoPt films with large perpendicular coercivity and small in-plane coercivity is proposed.

**Chapter 7 Conclusions:** The general conclusions of this thesis are summarized.

**Reference**

1. G. Qin, Y. Ren, N. Xiao, B. Yang, L. Zuo, and K. Oikawa, *Int. Mater. Rev.*, 54, 157 (2009).
2. R. Stamps, *et al.*, *J. Phys. D: Appl. Phys.* 47, 333001 (2014).
3. S. Iwasaki and K. Takemura, *IEEE Trans. Magn.* 11, 1173 (1975).
4. G. A. Bertero, *et al.*, *IEEE Trans. Magn.* 38, 1627 (2002).
5. N. Honda, J. Ariake, and K. Ouchi, *IEEE Trans. Magn.* 34, 1651 (1998).
6. Y. Hirayama, Y. Honda, T. Takeuchi, and M. Futamoto, *IEEE Trans. Magn.* 35 2766 (1999).
7. Y. Inaba, *et al.*, *IEEE Trans. Magn.* 41, 3130 (2005).
8. T. Oikawa, *et al.*, *IEEE Trans. Magn.* 38, 1976 (2002).
9. G. W. Qin, Y. P. Ren, N. Xiao, B. Yang, L. Zuo, and K. Oikawa, *Int. Mater. Rev.*, 54, 157 (2009).
10. M. H. Kryder, *et al.*, *Proceedings of the IEEE*, 96, 1810 (2008).
11. S. D. Granz and M. H. Kryder, *J. Magn. Magn. Mater.* 324, 287 (2012).
12. D. Weller, O. Mosendz, G. Parker, S. Pisana, and T. S. Santos, *Phys. Status Solidi A* 210, 1245 (2013).
13. M. Yan, N. Powers, and D. Sellmyer *J. Appl. Phys.* 93, 8292 (2003).
14. K. R. Coffey, M. A. Parker, and J. K. Howard, *IEEE Trans. Magn.* 31, 2737 (1995).
15. H. An, S. Takada, T. Sannomiya, S. Muraishi, J. Shi, and Y. Nakamura, *Appl Phys A.* 113, 31 (2013).

16. K. Barmak, J. Kim, L. H. Lewis, K. R. Coffey, M. F. Toney, A. J. Kellock, and J. U. Thiele, *J. Appl. Phys.* **98**, 033904 (2005).
17. Y. K. Takahashi, K. Hono, T. Shima, and K. Takanashi, *J. Magn. Magn. Mater.* **267**, 248 (2003).
18. T. Yokota, L. Gao, S. H. Liou, M. L. Yan, and D. J. Sellmyer, *J. Appl. Phys.* **95**, 7270 (2004).
19. X. Xu, Z. Yang, and H. Wu, *J. Magn. Magn. Mater.* **295**,106 (2005).
20. L. Zhang, Y. K. Takahashi, A. Perumal, and K. Hono, *J. Magn. Magn. Mater.* **322**, 2658 (2010).
21. E. Yang, S. Ratanaphan, J. Zhu, and D. Laughlin, *J. Appl. Phys.* **109**, 07B770 (2011).
22. E. Manios, V. Alexandrakis, and D. Niarchos, *J. Magn. Magn. Mater.* **316**, e166 (2007).
23. Y. Tsuji, S. Noda, and Y. Yamaguchi, *J. Vac. Sci. Technol. B* **25**, 1892 (2007).
24. M. Weisheit, L. Schultz, and S. Fahler, *J. Appl. Phys.* **95**, 7489 (2004).
25. K. Dong, H. Li, J. Hu, Y. Peng, G. Ju, G. Chow, and J. Chen, *IEEE Trans. Magn.* **49**, 668 (2013).
26. P. Ho, G. Han, K. He, G. Chow, and J. Chen, *J. Appl. Phys.* **111**, 083909 (2012).
27. P. Ho, G. Han, K. He, G. Chow, and J. Chen, *Appl. Phys. Lett.* **99**, 252503 (2011).
28. K. F. Dong, H. H. Li, Y. G. Peng, G. Ju, G. M. Chow, and J. S. Chen, *Appl. Phys. Lett.* **104**, 192404 (2014).
29. J. S. Chen, B. C. Lim, J. F. Hu, B. Liu, G. M. Chow, and G. Ju, *Appl. Phys. Lett.* **91**, 132506 (2007).
30. H. Ho, E. Yang, D. E. Laughlin, and J. G. Zhu, *Appl. Phys. Lett.* **102**, 112411 (2013).

31. S. D. Granz, K. Barmak, and M. H. Kryder, *Eur. Phys. J. B* 86, 81 (2013).
32. Y. Peng, J. G. Zhu, and D. E. Laughlin, *J. Appl. Phys.* 99, 08F907 (2006).
33. B. S. D. Ch. S. Varaprasad, Y. K. Takahashi, J. Wang, T. Ina, T. Nakamura, W. Ueno, K. Nitta, T. Uruga, and K. Hono, *Appl. Phys. Lett.* 104, 222403 (2014).
34. B. S. D. Ch. S. Varaprasad, Y. K. Takahashi, Antony Ajan, and K. Hono, *J. Appl. Phys.* 113, 203907 (2013).
35. G. R. Trichy, D. Chakraborti, J. Narayan, and J. T. Prater, *Appl. Phys. Lett.* 92, 102504 (2008).
36. J. W. Liao *et al.*, *Appl. Phys. Lett.* 102, 062420 (2013).
37. K. K. Tham, S. Hinata, S. Saito, and M. Takahashi, *J. Appl. Phys.* 115, 17B752 (2014).
38. H. H. Li, K. F. Dong, Y. G. Peng, G. Ju, G. M. Chow, and J. S. Chen, *J. Appl. Phys.* 110, 043911 (2011).
39. T. Li, S. Noda, Y. Tsuji, T. Ohsawa, and H. Komiyama, *J. Vac. Sci. Technol. A* 20, 583 (2002).
40. U. C. Oh and J. H. Je, *J. Appl. Phys.* 74, 1692 (1993).
41. J. E. Sundgren, *Thin Solid Films* 128, 21 (1985).
42. H. An, Q. Xie, J. Wang, T. Sannomiya, S. Muraishi, Z. Zhang, Y. Nakamura, and J. Shi, *J. Vac. Sci. Technol. A* 33, 021512 (2015).
43. Y. Tsuji and S. Noda, *J. Vac. Sci. Technol. B* 29, 031801 (2011).
44. W. H. Meiklejohn and C. P. Bean, *Phys. Rev.* 105, 904 (1957).
45. P. Kappenberger, S. Martin, Y. Pellmont, H. J. Hug, J. B. Kortright, O. Hellwig, and E. E. Fullerton, *Phys. Rev. Lett.* 91, 267202 (2003).

46. B. Y. Wang, *et al.*, Phys. Rev. B 83, 104417 (2011).
47. Z. Diao, D. Apalkov, M. Pakala, Y. Ding, A. Panchula, and Y. Huai, Appl. Phys. Lett. 87, 232502 (2005).
48. T. Tokunaga, M. Taguchi, T. Fukami, Y. Nakaki, and K. Tsutsumi, J. Appl. Phys. 67, 4417 (1990).
49. W. Cain, and M. Kryder, J. Appl. Phys. 67, 5722 (1990).
50. J. Sort, A. Popa, B. Rodmacq, and B. Dieny, Phys. Rev. B. 70, 174431 (2004).

## Chapter 2 Fabrication and characterization of CoPt/TiN films

Fabrication, microstructure characterization and magnetic properties measurement are the essential parts in this work, and they are ascribed in this chapter. For film fabrication, dc magnetron sputtering is used. X-ray diffraction, x-ray reflectivity, atomic force microscope and transmission electron microscopy are utilized to detect the structure. Vibrating sample magnetometer is applied to measure the magnetic properties of the films.

### 2.1 Film fabrication and heat treatment

#### 2.1.1 dc magnetron sputtering

Magnetron sputtering is a well developed technology in industry for fabricating nano-films from versatile materials. The microstructure of the nano-films can be delicately controlled by the flow rate ratio of sputtering gases, sputtering power, substrate temperature, seed layers, etc.<sup>[1]</sup> In this work, a dual facing-target dc magnetic sputtering machine was used. As shown in Fig. 2-1(a), mounted by two same targets on the surfaces, two magnets with opposite magnetic poles are facing each other. By applying a negative high voltage between the cover and the target,  $\text{Ar}^-$  is forced to bombard the surface of the target and generate electrons and target atoms. Due to the Lorentz force, electrons do spiral motion and collide with Ar atoms, then generate more  $\text{Ar}^-$  bombarding the target. Target atoms are sputtered and deposited on the substrates. Fig. 2-1(b) shows the setup of the dual facing-target dc magnetron sputtering machine similar with the actual machine (Fig. 2-1(c)). Before sputtering, the base pressure in chamber is better than  $5 \times 10^{-5}$  Pa. During sputtering, sputtering gas Ar and reactive gas  $\text{N}_2$  with an appropriate flow rate ratio are applied to keep

the sputtering pressure as 0.2 Pa. The current and voltage for depositing TiN are 60mA and 900 V, which are 30 mA and 1200 V for depositing CoPt. Substrate stage can be heated up to 400 °C, which can also be rotated by a motor. Film thickness is controlled by deposition time.

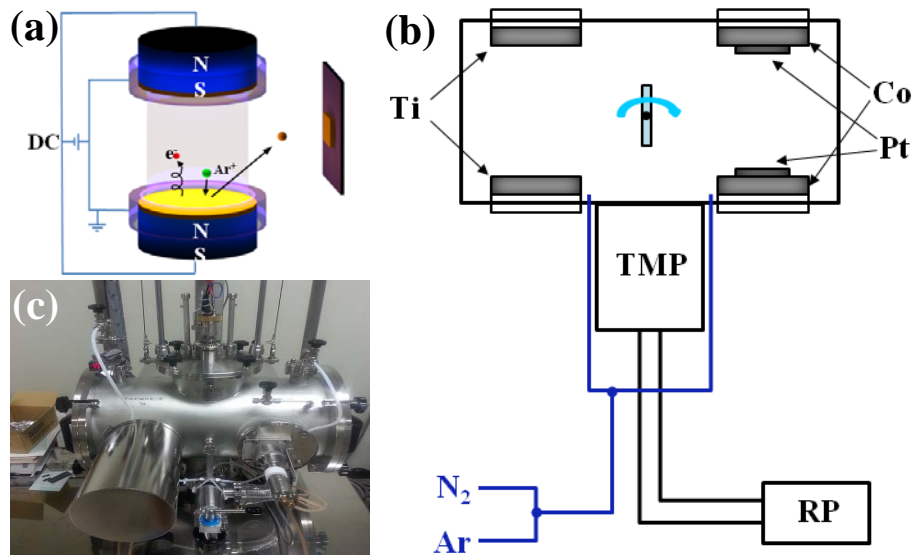


Figure 2-1 (a) Schematic illustrations of the working principle for dual facing-target dc magnetic sputtering, (b) schematic diagram of the setup of the dual facing-target dc magnetron sputtering machine, (c) the actual photo of the sputtering machine.

### 2.1.2 Heat treatment

Post-annealing process is critical for the control of microstructure and magnetic properties of nano-films. A tube furnace with a vacuum system is used, which can achieve a high vacuum of  $1 \times 10^{-5}$  Pa.

### 2.2 Structure characterization

For structure characterization, X-ray diffraction (XRD) was used to detect the crystal orientations of CoPt and TiN in multilayer films. X-ray reflectivity (XRR) was used to detect

the interface roughness in multilayer films. Atomic force microscope (AFM) was used to observe the surface structure for single layer films, and transmission electron microscopy (TEM) was used to directly observe the layered structure.

## 2.2.1 X-ray diffraction

### 2.2.1.1 Fundamentals of XRD

X-ray diffraction (XRD) is a convenient tool to identify the atom arrangement and crystal structure in a sample without any destruction. Incident X-rays are diffracted by the atoms into specific directions, and by measuring the angles and intensities, crystal structure can be identified (Fig. 2-2(a)).<sup>[2]</sup> The emergence of the XRD peaks can be explained by Bragg's law:  $2d\sin\theta=n\lambda$ . When a beam of X-rays enters the crystalline with an angle of  $\theta$ , the waves are scattered from different lattice planes with an interplanar distance  $d$ . When the difference of the traverse length is equal to an integer multiple of the wavelength, interference will be enhanced (Fig. 2-2(b)).

Illustration of conventional XRD set up is shown in Fig. 2-2(c), X-ray is in  $x$ - $z$  plane and sample surface is in  $y$ - $z$  plane. The normal line of sample surface  $z_N$  is parallel to  $z$  axis. In this work, XRD profiles were taken by Bruker D8 Discover diffractometer (Bruker AXS, Inc., Madison, WI) by using Cu  $K_\alpha$  radiation, which was operated at 35 kV, 300 mA.

In-plane XRD was also conducted to characterize the crystal structure in the in-plane direction of the films.  $\psi$  is the angle between the normal line of sample surface  $z_N$  and  $z$  axis. Theoretically, when  $\psi=90^\circ$ , in-plane XRD can be taken (Fig. 2-2(d)). In this work, we used  $\psi=89.2^\circ$ , since the thicknesses of films are only in nanometer scale, XRD peak is impossible to be detected at absolute  $90^\circ$ .

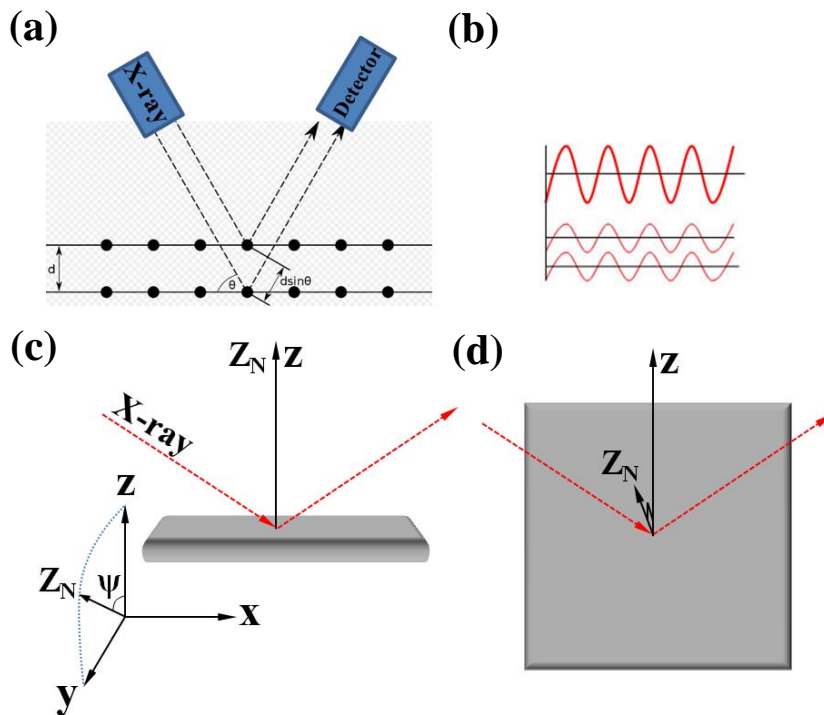


Figure 2-2 Schematic illustrations of (a) XRD work principle, (b) enhancement of two X-ray waves interference, (c) conventional XRD, (d) in-plane XRD.

### 2.2.1.2 XRD measurement of TiN single layer

Since CoPt and TiN has epitaxial growth relation, in order to fabricate (001) textured CoPt, highly (100) textured TiN should be fabricated. Therefore, the texture of TiN single layer was studied firstly by changing deposition parameters. The most important parameters, N<sub>2</sub> flow rate ratio, substrate temperature and sputtering power, were systematically studied. Figure 2-3 shows the XRD profiles of TiN single layer deposited for 1.5 hours at substrate temperature of 400 °C by changing the flow rate ratio between N<sub>2</sub> and (N<sub>2</sub>+Ar). TiN shows strongest (200) peak when N<sub>2</sub> flow rate ratio is around 9%. By further decreasing N<sub>2</sub> flow rate ratio to 4.3%, TiN (111) peak appears, which is undesirable for CoPt epitaxial growth. Therefore, N<sub>2</sub> flow rate ratio of 9% was optimum for fabrication of (100) textured TiN.

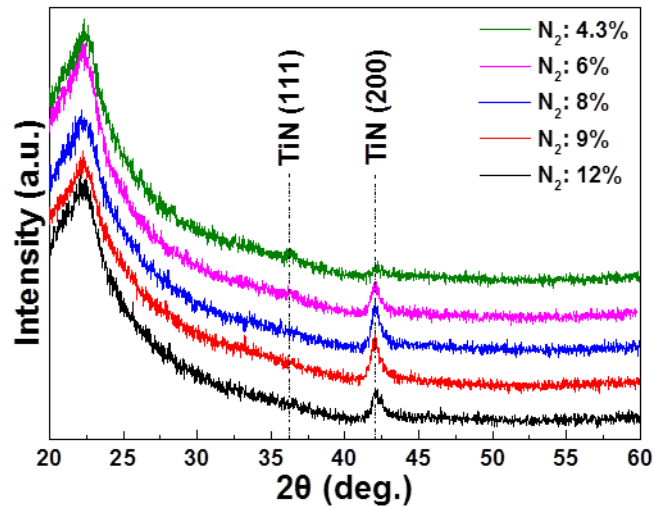


Figure 2-3 XRD profiles of TiN single layers with different N<sub>2</sub> flow rate ratios during deposition.

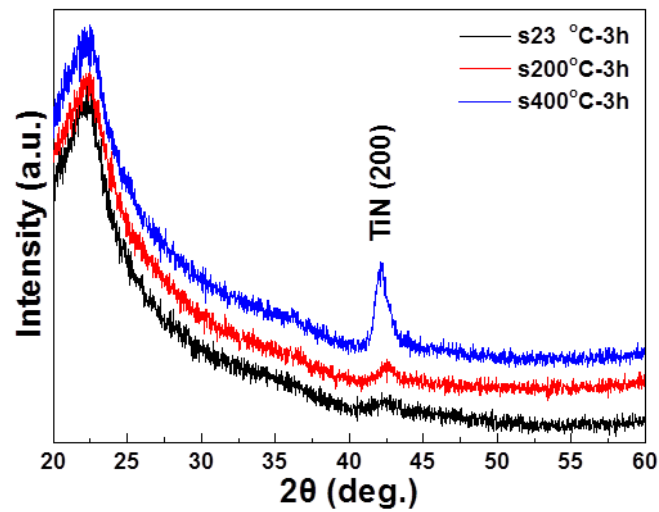


Figure 2-4 XRD profiles of TiN single layers with different substrate temperatures during deposition.

By fixing N<sub>2</sub> flow rate ratio at 9%, the effect of substrate temperature was studied (Fig. 2-4). Although the deposition period of time was kept same as 3 hours, the intensity of TiN

(200) peak becomes weaker by decreasing the substrate temperature, which indicates that 400 °C is the optimum temperature for (100) textured TiN deposition.

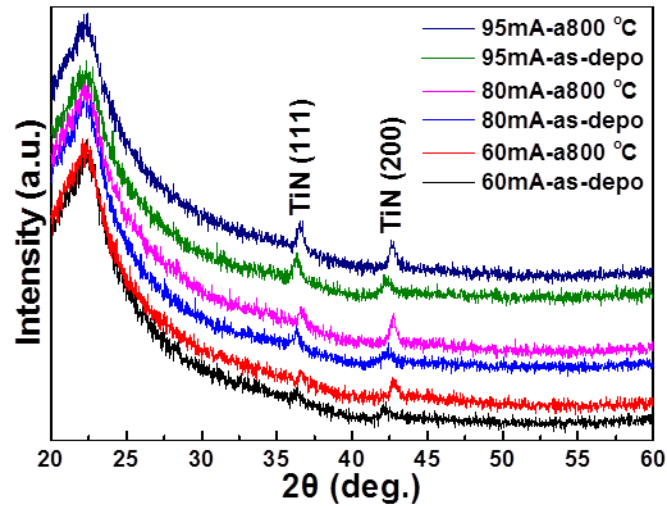


Figure 2-5 XRD profiles of TiN single layers by using different sputtering current during sputtering. Deposition period of time is 1.5 hours.

Figure 2-5 shows the XRD profiles of TiN single layer by changing the sputtering power. All samples were deposited for 1.5 hours at substrate temperature of 400 °C. Since fixed-current mode was used for the sputtering, the sputtering power was changed through changing the sputtering current. N<sub>2</sub> flow rate ratio was fixed at 4.3%, at which the change of both TiN (200) and (111) peaks can be investigated. By increasing the sputtering current, both peaks become stronger. However, the weaker TiN (111) peak with sputtering current of 60 mA becomes stronger than TiN (200) peak by increasing the sputtering current to 95 mA. Although TiN layer thickness increases with increasing the current which might be responsible for the stronger (111) peak, by considering that the maximum limitation of the current is 100 mA for the electric source in our sputtering machine, 60 mA is applied in this

work. It is noteworthy that the annealing process can increase the crystallinity but has no effect on the texture, since the proportion between (111) and (100) peaks has no obvious change before and after annealing.

From above study, the optimum deposition parameters for (100) textured TiN fabrication:  $N_2$  flow rate ratio of 9%, substrate temperature of 400 °C and sputtering current of 60 mA, are obtained and will be used in the subsequent experiments.

### 2.2.1.3 XRD measurement of CoPt/TiN multilayer films

Figure 2-6 shows the typical XRD profiles of CoPt/TiN multilayer films. TiN layer shows (200) texture. CoPt shows (100) textured A1 structure before and after annealing at 600 °C. After annealing at 700 and 800 °C,  $L1_0$  structure was obtained, which can be identified by the (001) super lattice peak and (002) fundamental peak.

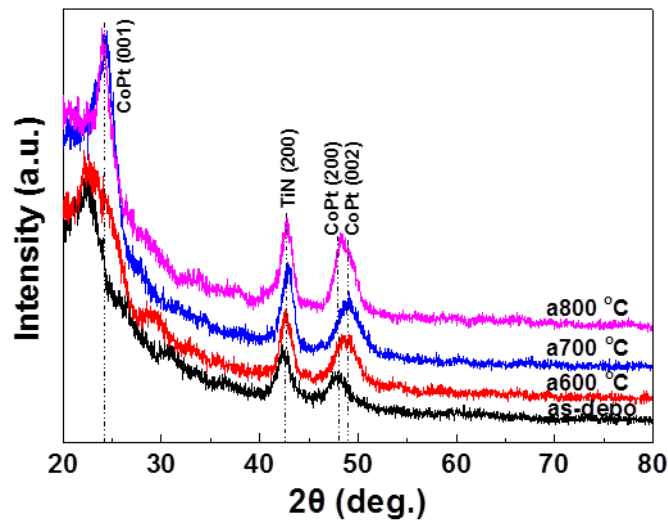


Figure 2-6 Typical XRD profiles of  $TiN(5\text{ nm})/[CoPt(4\text{ nm})/TiN(6\text{ nm})]_5$  multilayer films, before and after annealing at 600, 700 and 800°C for 3 hours.

## 2.2.2 X-ray reflectivity

### 2.2.2.1 Fundamentals of XRR

X-ray reflectivity (XRR) is a well established technique to investigate the interface conditions and measure the thicknesses of single layer and multilayer films. By measuring the intensity of X-rays reflected from the interface and surface of films in the particular angles, the interface condition can be analyzed (Fig. 2-7). If the interface is not perfectly smooth, then the reflected intensity will deviate by following the law of Fresnel reflectivity.<sup>[3]</sup>

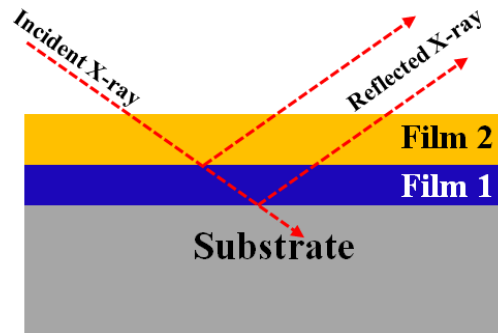


Figure 2-7 Schematic illustration of XRR work principle.

In this work, XRR measurement was taken by Bruker D8 Discover diffractometer (Bruker AXS, Inc., Madison, WI) by using Cu  $K_{\alpha}$  radiation, which was operated at 35 kV, 300 mA.

#### 2.2.2.2 XRR Measurement of CoPt/TiN multilayer films

Figure 2-8 shows the typical XRR profiles of CoPt/TiN multilayer films. Red line is the measured data and blue dashed line is the fitted data to quantify the interface roughness. Fitting process was performed by LEPTOS software. The interface roughness is calculated to

be 0.698 nm for TiN(5 nm)/[CoPt(4 nm)/TiN(2 nm)]<sub>5</sub> multilayer films after annealing at 700 °C.

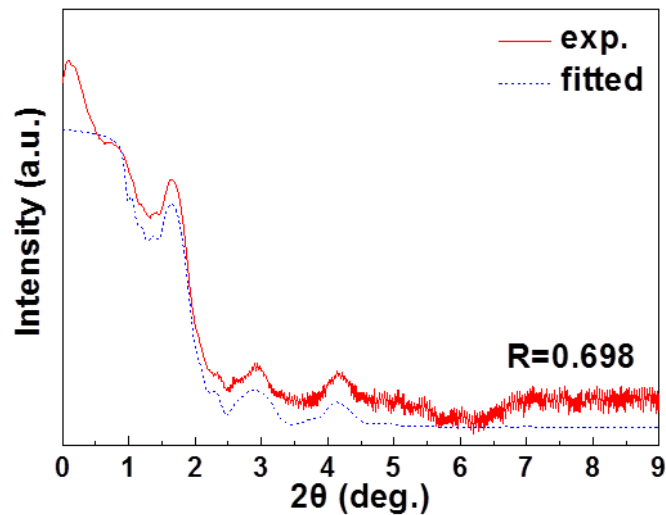


Figure 2-8 Typical XRR profiles of TiN(5 nm)/[CoPt(4 nm)/TiN(2 nm)]<sub>5</sub> multilayer films after annealing at 700°C for 3 hours.

## 2.2.3 Transmission electron microscopy

### 2.2.3.1 Fundamentals of TEM

Transmission electron microscopy (TEM) is an indispensable tool for microstructure observation which can reach a resolution up to atomic level. Accelerated electrons pass through a very thin sample and then are collected and enlarged by objective lens, intermediate lens and projector lens, and then finally projected an image on the screen. TEM generally has two work modes, which are diffraction mode and image mode, as shown in Fig. 2-9(a) and (b). The difference between these two modes is the location of the object plane.

### (1). Diffraction mode

The objective lens collects the electrons from the exit surface of the TEM specimen, disperses them to generate diffraction pattern in the back-focal plane (BFP), and then recombines them to form an image in the image plane.<sup>[4]</sup> Therefore, in diffraction mode, to see the diffraction pattern, imaging lens have to be adjusted so that the back-focal plane of the objective lens works as the object plane (Fig. 2-9(a)). Then the diffraction pattern can be projected on the screen.<sup>[4]</sup> Since sometimes particular areas instead of the whole surface of samples are needed to take the diffraction patterns, and the direct beam is generally too intense that has a high risk to damage the screen, so a selected-area aperture is generally used, which is called selected-area diffraction. By using the selected-area aperture, we can take diffraction patterns within a selected area, and investigate the structure of these areas independently.<sup>[4]</sup>

### (2). Image mode

In order to directly observe an image, the intermediate lens should be readjusted to make sure its object plane is the image plane of the objective lens (Fig. 2-9(a)).<sup>[4]</sup> Image mode includes bright-field, dark-field and high-resolution imaging.

#### a). Bright-field and dark-field imaging

The diffraction pattern created in the back-focal plane contains the direct beam electrons and diffracted beam electrons. If the direct beam is selected, a bright-field image can be formed. On the other hand, if the diffracted beam is selected a dark-field image can be obtained (Fig. 2-10). Electrons can be selected by an objective aperture, which is the most important aperture in TEM. As shown in Fig. 2-10(a), if the objective aperture blocks the

diffracted beam and only let direct beam pass through, bright-field image is formed. The contrast in bright-field image is due to the mass-thickness and diffraction, which is generally used to estimate the crystal grain size.<sup>[4]</sup>

As shown in Fig. 2-10(b), when the objective aperture blocks the direct beam and let the diffracted beam pass through, a dark-field image is formed. Because the objective aperture is displaced for the selection, the selected diffracted beam deviates from the optic center line. Therefore, such a displaced-aperture image is difficult to focus on an older TEM.<sup>[4]</sup> This problem can be solved by adjusting the diffracted beam back on the optic center line, which is called centered dark-field imaging (Fig. 2-10(c)). If the adjusted angle is equal to the diffraction angle, a clear dark-field image can be formed.<sup>[4]</sup>

#### b). High-resolution imaging

High-resolution imaging allows for the direct observation of the atomic structure of materials, which is very important for researchers. The contrast of a high-resolution image is due to the interference in the image plane of the electron wave. Thus, the coexistence of the direct beam and diffracted beam after the back-focal plane of the objective lens is needed. Therefore, it cannot be obtained by the normal bright-field and dark-field imaging. A sufficiently large objective aperture is requested to let both the direct beam and diffracted beam pass through. By adjusting the focus center, beam tilt and specimen position, high-resolution image can be obtained.

#### (3). Fabrication of TEM samples

Since thin films are studied in this work, cross-sectional image is needed for the observation. The fabrication procedure of TEM samples is as below (Fig. 2-11).

- a). Deposit two samples on 10 mm×10 mm glass/silicon substrates at same experimental condition.
- b). Mix the G2 resin with the G2 harder by using the volume ratio of 10:1 and uniformly spread it on the film surface of one sample.
- c). Attach the other sample film-to-film, clamp the two samples, and solidify them at 100 °C for 40 minutes.
- d). Cut the samples into 1.5mm×0.5 mm, fix one piece in a 3mm diameter and 0.5mm thick sample template by using the carbon paste, and then solidify it at 175 °C for 4 hours.
- e). Polish the two surfaces of the sample by using sand papers until the thickness around 50 μm.
- f). Ion mill the sample with a small angle to make a whole at the center of the samples. Finally, clean the surface by using gentle-milling machine.

In this work, TEM images were taken by JEM 3010 transmission electron microscope at a voltage of 300 kV.

### **2.2.3.2 Observations of CoPt/TiN multilayer films**

Figure 2-12 shows the cross-sectional TEM image of TiN(5 nm)/[CoPt(4 nm)/TiN(4 nm)]<sub>5</sub> multilayer film after annealing at 700 °C. The continuous dark CoPt layers sandwiched by the bright TiN layers with a sharp transition interface can be clearly identified. Due to the high mass density of CoPt, it shows darker contrast compared with TiN. The dark areas in TiN layers are due to the diffraction contrast.

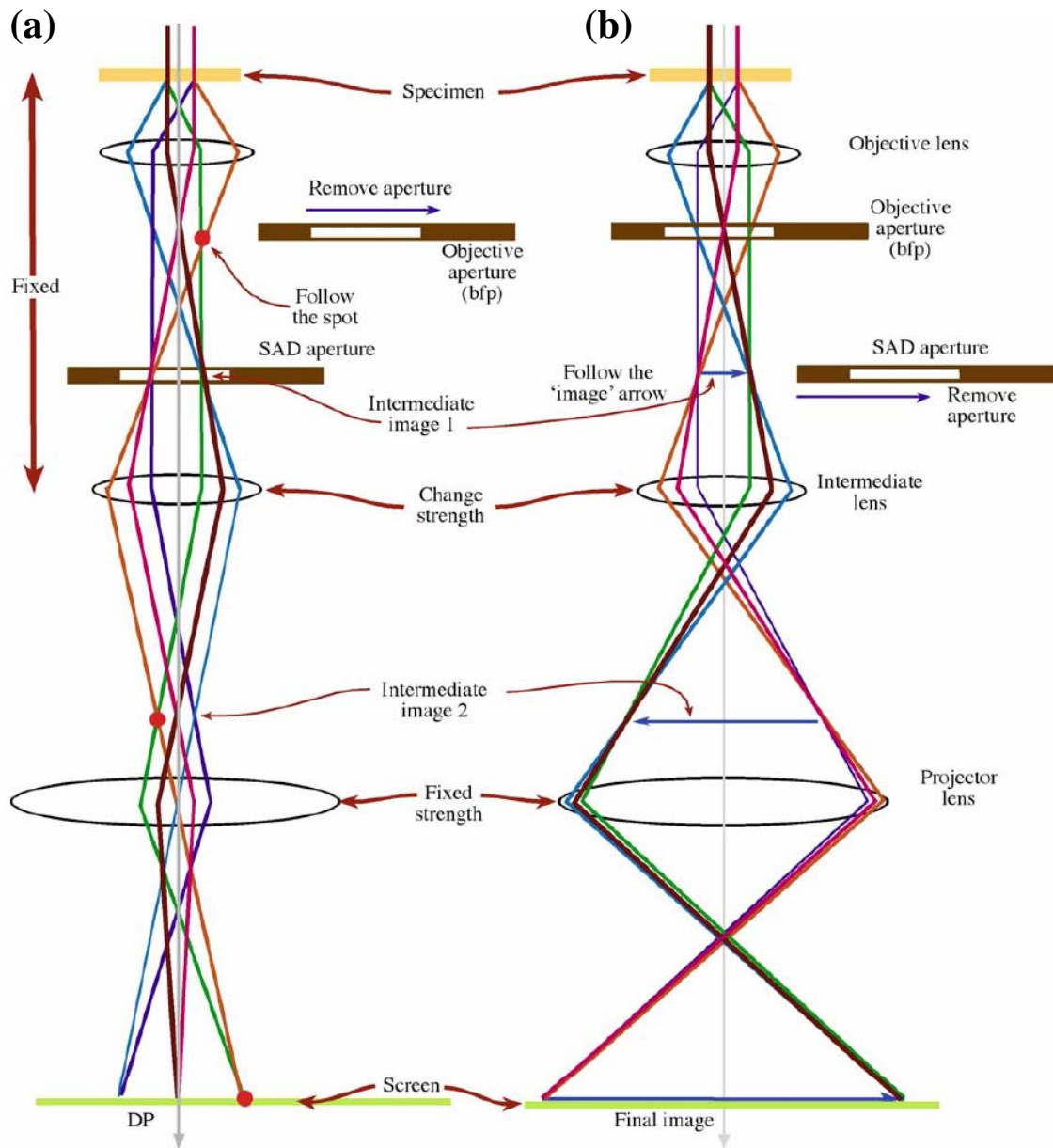


Figure 2-9 Schematic diagrams of the ray paths for the two basic operation modes of TEM:

(a) diffraction mode, (b) image mode. The figure is cited from reference [4].

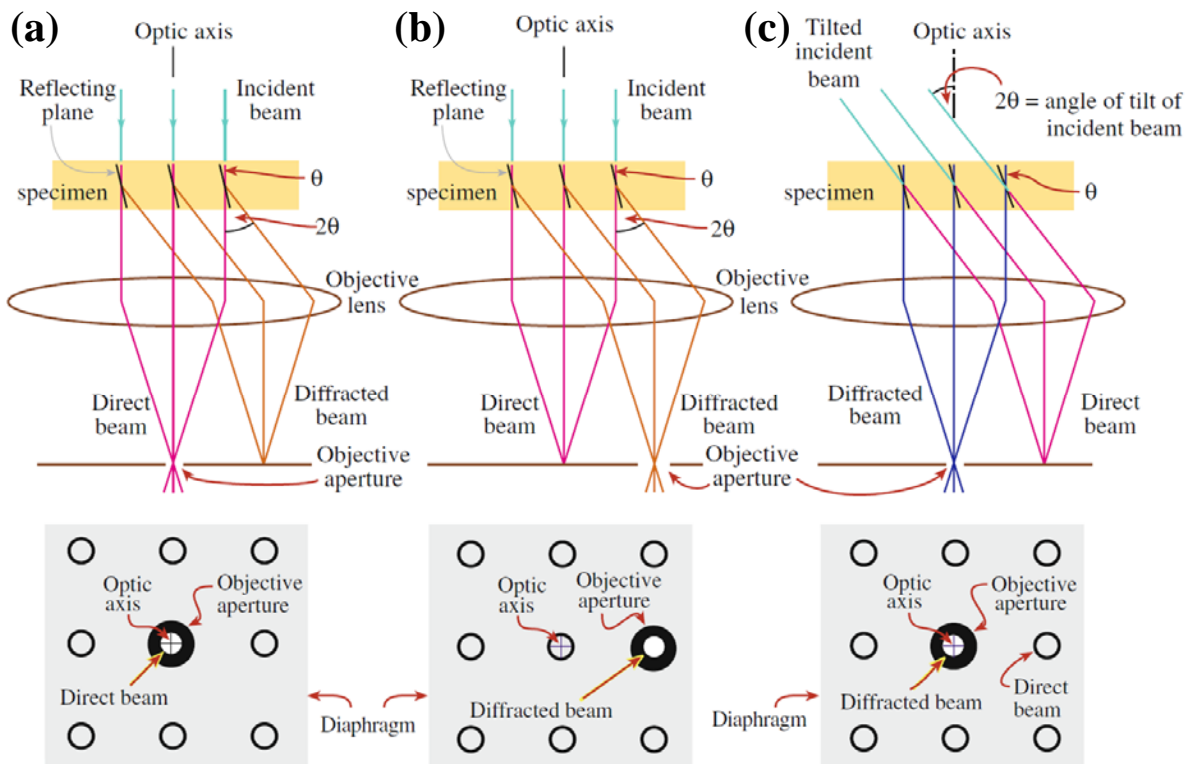


Figure 2-10 Schematic diagrams of the ray paths for producing (a) bright field image, (b) displaced-aperture dark field image, (c) centered dark-field image. The figure is cited from reference [4].

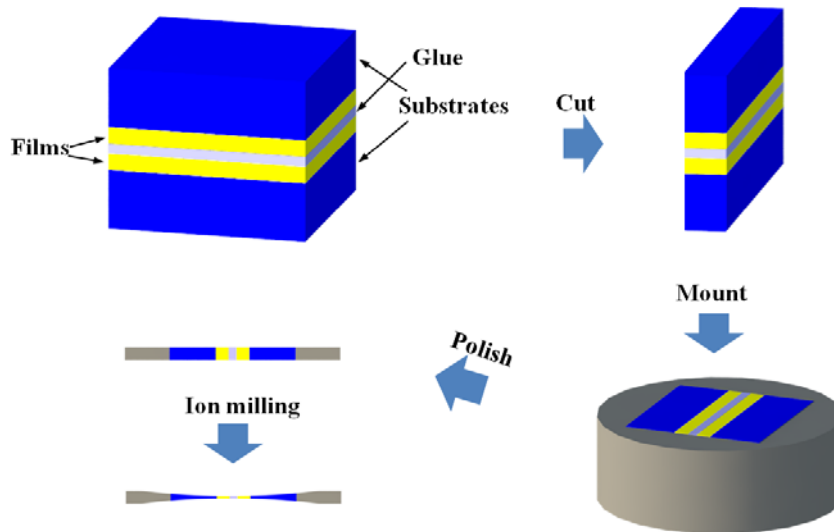


Figure 2-11 Schematic illustrations of the procedure to prepare TEM samples.

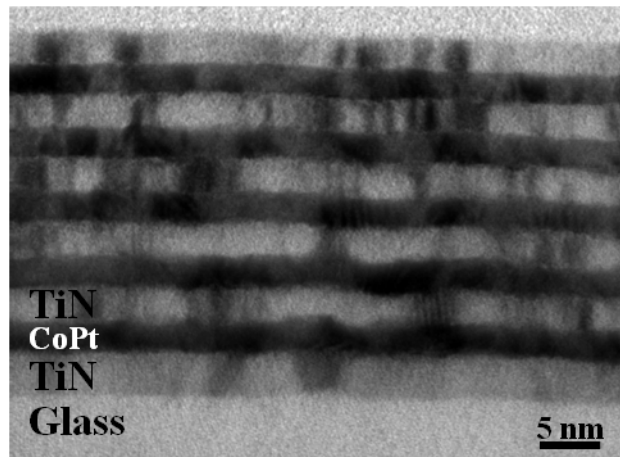


Figure 2-12 Cross-sectional TEM image of TiN(5 nm)/[CoPt(4 nm)/TiN(4 nm)]<sub>5</sub> multilayer film.

## 2.2.4 Atomic force microscopy

### 2.2.4.1 Fundamentals of AFM

Atomic force microscopy (AFM) is a type of scanning probe microscopy with resolution level of nanometers. It can measure the surface morphology and quantify the roughness of

samples. It consists of a cantilever with a sharp tip at its end. When the tip touches the sample surface, force between the tip and sample surface causes a bend of the cantilever, then transfer to image signals. AFM images directly reflect the height contrast of the sample surfaces.

In this work, AFM images were taken by HITACHI AFM 5000N with maximum laser power of 40  $\mu$ W and laser wave length of 635 nm.

#### 2.2.4.2 Surface observations of CoPt/TiN films

Figure 2-13(a) shows the AFM surface image of 30 nm thick TiN single layer deposited at 400 °C. Surface roughness is calculated to be 0.78 nm, indicating a smooth surface condition. 4 nm CoPt was deposited on TiN layer as shown in Fig. 2-13(b). CoPt formed continuous layer after the deposition. After annealing at 700 °C, it can be seen that CoPt agglomerated into small particles (Fig. 2-13(c)).

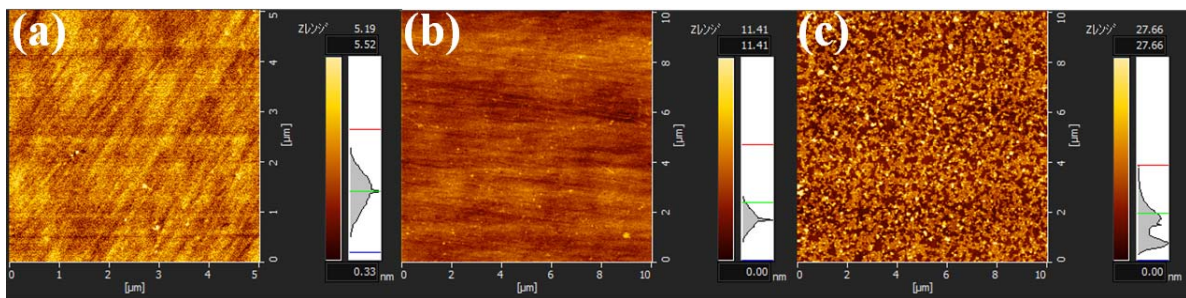


Figure 2-13 AFM surface images of (a) TiN(30 nm) single layer deposited at 400 °C, (b) TiN(30 nm)/CoPt(4 nm) deposited at 400 °C, (c) TiN(30 nm)/CoPt(4 nm) after annealing at 700 °C.

## 2.3 Magnetic properties measurement

### 2.3.1 Fundamentals of magnetic hysteresis loops

Figure 2-14(a) shows typical magnetizations of a ferromagnetic thin films  $M$  by varying the external magnetic field  $H$ , which is called magnetic hysteresis loop. Suppose a thin film sample has easy magnetization axis in the perpendicular direction of the film plane (Fig. 2-14(b)), by increasing magnetic field  $H$ , magnetization  $M$  also increases, then reach to a saturated magnetization  $M_s$ . By reducing  $H$ ,  $M$  keeps unchanged or decreases, but will have a remained magnetization  $M_r$  even  $H$  reduces to 0. In order to make the sample back to demagnetized status, an opposite  $H$  with an appropriate value is required, which is the coercivity  $H_c$ . Magnetization in in-plane direction has similar tendency, only is harder to be magnetized. The area between in-plane and out-of-plane magnetization curves is the effective anisotropy energy  $K_{\text{eff}}$ , which is defined as  $K_{\text{eff}}=H_k M_s/2$ . If the film has in-plane magnetic anisotropy, then  $K_{\text{eff}}$  is negative. Oppositely,  $K_{\text{eff}}$  is positive when perpendicular magnetic anisotropy is obtained.

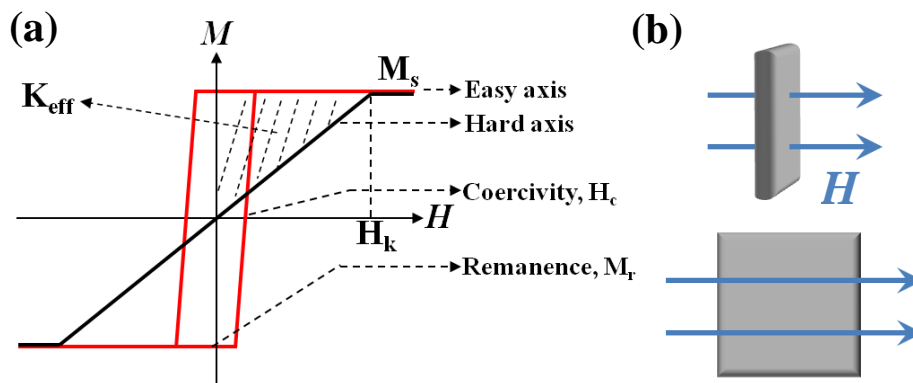


Figure 2-14 Schematic illustrations of (a) typical magnetic hysteresis loops of ferromagnetic materials, (b) Out-of-plane and in-plane magnetic measurements.

In this work, magnetic properties of the samples were measured by a vibrating sample magnetometer (RIKIN BHV-50 V) with maximum magnetization field of 15 kOe.

### 2.3.2 Magnetic properties measurement of CoPt/TiN multilayer films

Figure 2-15 shows the  $M$ - $H$  curves of TiN(5 nm)/[CoPt(4 nm)/TiN(4 nm)]<sub>5</sub> multilayer films. Before annealing, film exhibits in-plane magnetic anisotropy. After annealing at 700 °C, perpendicular magnetic anisotropy is successfully obtained.

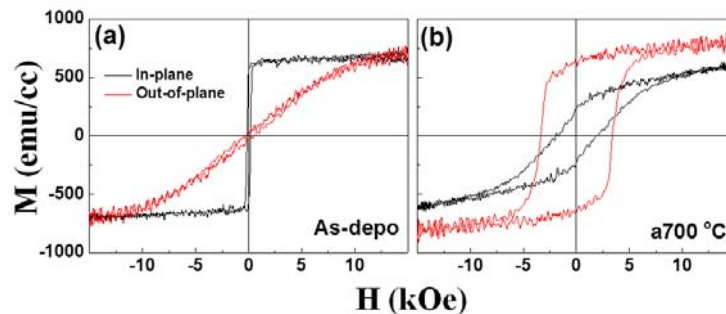


Figure 2-15  $M$ - $H$  curves of TiN(5 nm)/[CoPt(4 nm)/TiN(4 nm)]<sub>5</sub> multilayer films: (a) before annealing, (b) after annealing at 700 °C.

## 2.4 Summary

In order to fabricate (001) textured L1<sub>0</sub>-CoPt layered structure on glass substrates, the structure of TiN single layer films were investigated by changing the N<sub>2</sub> flow rate ratio, substrate temperature and sputtering power. The optimum deposition parameters: N<sub>2</sub> flow rate ratio of 9%, substrate temperature of 400 °C and sputtering current of 60 mA were obtained for fabricating highly (100) textured TiN single layer films. (001) oriented CoPt/TiN multilayer films have been fabricated on glass substrates by using above deposition

parameters. After annealing at 700 °C, multilayer films show perpendicular magnetic anisotropy.

## Reference

1. K. Seshan, Handbook of thin-film deposition processes and techniques, (William Andrew Publishing, Second edition), (2002).
2. B. D. Cullity, Elements of X-ray Diffraction, (Addison-Wesley Publishing, Inc), p 139 (1978).
3. V. Holy, J. kubena, I. Ohlidal, K. Lischka, and W. Plotz, Phys. Rev. B 47, 15896 (1993).
4. David B. Williams, C. Barry Carter. Transmission Electron Microscopy, (Springer, Second edition), (2009), p153, p183.

## **Chapter 3 Effect of period on the structure and magnetic properties of L<sub>10</sub>-CoPt/TiN multilayer films**

As described in chapter 2, (001) textured L<sub>10</sub>-CoPt/TiN multilayer films with Perpendicular magnetic anisotropy (PMA) was successfully fabricated, but the mechanism of the effect of TiN on CoPt is not clear. In our previous studies on CoPt/AlN multilayer films, we found that by alternate depositing AlN and CoPt, the AlN under layer promoted the crystallinity of the CoPt layer above it, and conversely, the CoPt layer also contributed to better crystallinity of the subsequent AlN layer.<sup>[1]</sup> In this way, highly (111) textured CoPt and (001) textured AlN layers were fabricated in the form of CoPt/AlN multilayer films. Such films show strong PMA after thermal annealing at elevated temperatures. However, the strong PMA originates from the interface effect and elastomagnetic effect. It is considered that the above enhancing effect also exists in CoPt/TiN multilayer films which can promote (001) preferred orientation of both CoPt and TiN, making it possible to take advantage of the high magnetocrystalline anisotropy energy of the L<sub>10</sub> structure to obtain PMA. This interpretation is confirmed in this chapter by investigating the microstructure and the interface condition of CoPt/TiN multilayer films through TEM images, XRD and XRR profiles.

### **3.1 Deposition of CoPt/TiN multilayer films**

Sub/TiN(5 nm)[CoPt(4 nm)/TiN(2 nm)]<sub>x</sub> multilayer (x=5,10,15 periods) films were deposited on fused quartz substrates at 400 °C by dc magnetron sputtering. The base pressure in the chamber before deposition was better than 5×10<sup>-5</sup> Pa, and the deposition pressure was

0.2 Pa. Co and Pt atom ratio was confirmed to be 44:56 by inductively coupled plasma-optical emission spectrometer. During the deposition, nitrogen and argon gases with a fixed flow rate ratio of 1:8.7 were supplied. After deposition, samples were annealed at 600, 700 and 800 °C for 3 hours in vacuum.

### **3.2 Experimental results of TiN(5 nm)[CoPt(4 nm)/TiN(2 nm)]<sub>5</sub>**

#### **3.2.1 Structure characterization**

Figure 3-1 shows the XRD profiles of TiN(5 nm)/[CoPt(4 nm)/TiN(2 nm)]<sub>5</sub> multilayer films. The as-deposited film was composed of disordered fcc CoPt phase, and only (200) peaks were detected, implying that (100) texture was formed during the deposition. This is different from the previously reported studies of multilayer films. For example, in Stavroyiannis's study of L1<sub>0</sub>-CoPt/Ag multilayer films,<sup>[2]</sup> a strong (111) CoPt peak was observed in the as-deposited film, the peak becoming even stronger after annealing. The same phenomenon was observed in Yokota's study of L1<sub>0</sub>-CoPt/Au multilayer films<sup>[3]</sup> and Zhang's study of L1<sub>0</sub>-FePt/C multilayer films.<sup>[4]</sup> The existence of (111) oriented grains severely decreases the PMA of L1<sub>0</sub> structures. However, it is difficult to control the fcc metallic crystal growth, as the (111) plane has the lowest surface energy and tends to form (111) oriented columnar texture during deposition.<sup>[5,6]</sup> Therefore, in CoPt/TiN multilayer films, it is evident that the (100) oriented TiN layers strongly promote CoPt (100) texture growth, and local epitaxial growth occurred between TiN and CoPt in the multilayer films.

L1<sub>0</sub> structure transformation begins with annealing temperature of 600 °C, but film still shows CoPt (200) peak. After annealing at 700 °C, CoPt disordered fcc structure transformed to L1<sub>0</sub> structure, which is characterized by the (001) super lattice peak and (002) fundamental

peak. It is noteworthy that after annealing, CoPt (200) peak shifts to the high angle (48.4°), which is larger than the standard angle (47.6°) (PDF No. 43-1358) indicating the existence of in-plane tensile stress. TiN shows weak (200) peak, which may be due to the much lower structure factor of TiN versus CoPt. The structure factor of the TiN (200) plane is calculated to be 71.4, versus 153 for the CoPt (002) plane.<sup>[7]</sup> Diffraction intensity is proportional to the square of the structure factor, which may lead to the much weaker intensity of the TiN (200) peak. After annealing at 800 °C, CoPt (200) peak appears again. The reason for the appearance of this peak will be investigated in the chapter 5.

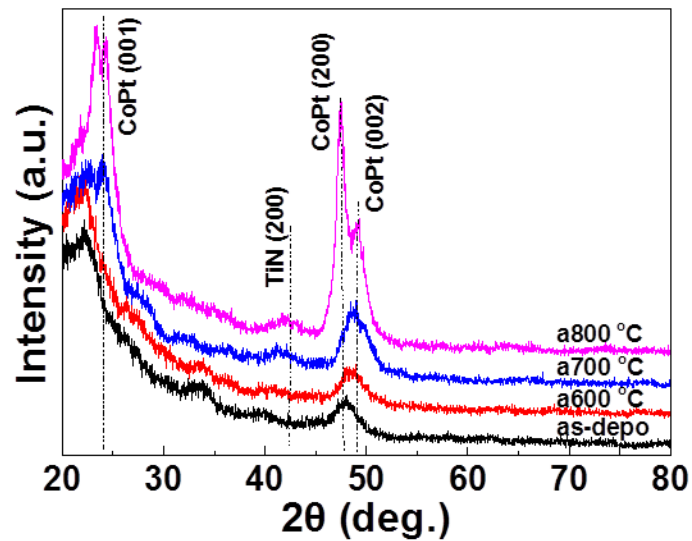


Figure 3-1 XRD profiles of TiN(5 nm)/[CoPt(4 nm)/TiN(2 nm)]<sub>5</sub> multilayer films, before and after annealing at 600, 700 and 800 °C for 3 hours.

### 3.2.2 Magnetic properties measurement

Figure 3-2 shows the  $M$ - $H$  curves of TiN(5 nm)/[CoPt(4 nm)/TiN(2 nm)]<sub>5</sub> multilayer films. The as-deposited sample exhibits a soft magnetic property and strong in-plane

magnetic anisotropy due to the shape anisotropy effect of continuous thin films. Film still shows in-plane magnetic anisotropy after annealing at 600 °C. PMA is obtained after annealing at 700 °C, which is well consistent with the XRD profiles. After annealing at 800 °C, film shows magnetic isotropy.

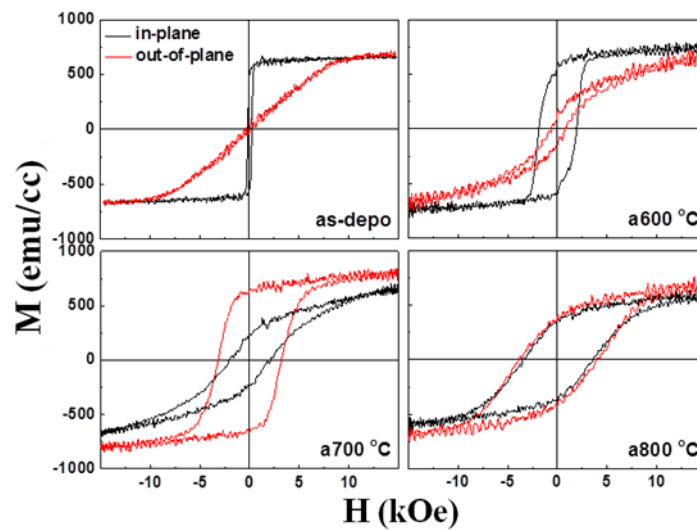


Figure 3-2  $M$ - $H$  curves of TiN(5 nm)/[CoPt(4 nm)/TiN(2 nm)]<sub>5</sub> multilayer films, before and after annealing at 600, 700 and 800 °C for 3 hours.<sup>[20]</sup>

### 3.3 Experimental results by increasing multilayer periods

#### 3.3.1 Structure characterization

Figure 3-3 shows the cross-sectional TEM images of TiN(5 nm)[CoPt(4 nm)/TiN(2 nm)]<sub>15</sub> multilayer films. The continuous dark CoPt layers sandwiched by the bright TiN layers with a sharp transition interface can be clearly identified (Fig. 3-3(a)). The average thicknesses for CoPt and TiN layers measured from Fig. 3-3(a) were about 3.78 nm and 2.2 nm, which were close to the designed values of CoPt (4 nm)/TiN (2 nm). It is noteworthy that the first 5 nm TiN seed layer exhibits random growth orientation because of the amorphous

nature of the fused quartz substrate<sup>[8]</sup> (Fig. 3-3(c)). This is also confirmed from the FFT result in Fig. 3-3(h), as it is seen that there is no preferred orientation for TiN. The random growth indicates the difficulty in controlling the crystalline orientation of the first TiN seed layer, which is the reason that another buffer layer is typically needed between the TiN and substrate in previous studies to obtain (100) preferred orientation.<sup>[9-11]</sup> On the other hand, TiN layers near the top surface of the multilayer film show much better crystallinity and (100) preferred orientation. This trend is apparent when comparing the high resolution images taken at the bottom and near the top surface (Fig. 3-3(b) and (c)), and the corresponding FFT results (Fig. 3-3(f) and (h)). CoPt layers also show similar trend (Fig. 3-3(e) and (g)). These results confirm the crystallinity and preferred orientation enhancing effect by alternate deposition of TiN and CoPt layers in CoPt/TiN multilayer films. It can also be seen that the interface between CoPt and TiN layer is much sharper in the top portion than the bottom. The magnified TEM image of the epitaxial growth interface between CoPt and TiN layers is shown in Fig. 3-3(d). It is well reported that, with a misfit of 10.4% between CoPt ( $a=0.38$  nm) and TiN ( $a=0.424$  nm), which is beyond the critical strain (7%-8%) for epitaxial growth, conventional lattice matching growth is barely maintained.<sup>[12]</sup> To reduce such large strain energy, edge dislocations formed periodically during epitaxial growth at the interface between the CoPt and TiN layers. The edge dislocation occurred on the CoPt side close to the interface (indicated by the white dashed lines), and after nine layers of atoms were grown ( $10 \times a_{\text{CoPt}} \approx 9 \times a_{\text{TiN}}$ ), another edge dislocation was observed. This phenomenon is consistent with the strain energy release mechanism.

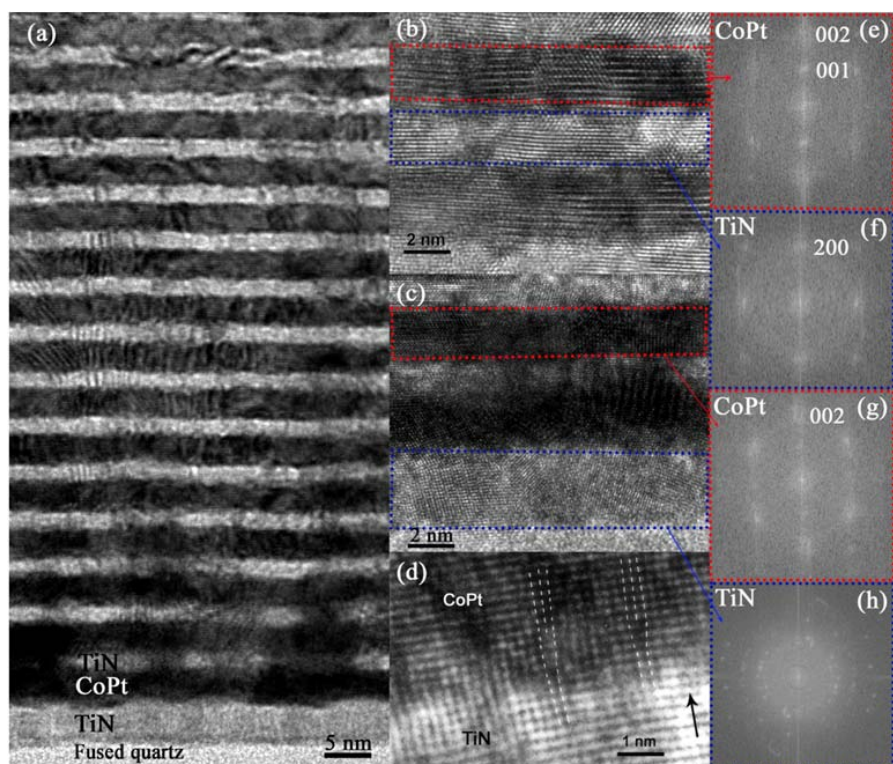


Figure 3-3 TiN(5 nm)[CoPt(4 nm)/TiN(2 nm)]<sub>15</sub> multilayer film after annealing at 700 °C: (a) TEM image of the layered structure; (b) HR-TEM image of the top portion; (c) HR-TEM image of the bottom portion; (d) HR-TEM image of the interface between the CoPt and TiN layers (the black arrow indicates the c-axis direction); (e), (f), (g) and (h) FFT results of TiN and CoPt in the selected areas.<sup>[20]</sup>

To quantitatively investigate the change of the interface roughness, XRR profiles were taken for  $\text{TiN}(5 \text{ nm})[\text{CoPt}(4 \text{ nm})/\text{TiN}(2 \text{ nm})]_x$  multilayer films ( $x=5,10,15$ ) after annealing at  $700 \text{ }^\circ\text{C}$  as shown in Fig. 3-4. By fitting the experimental curves, the root-mean square roughness was obtained. As the period increases, interface roughness decreases, which is well consistent with the TEM image (Fig. 3-3(a)).

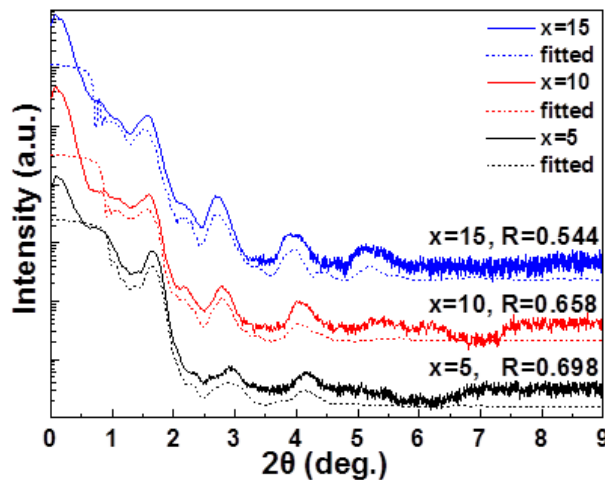


Figure 3-4 XRR profiles of  $\text{TiN}(5 \text{ nm})[\text{CoPt}(4 \text{ nm})/\text{TiN}(2 \text{ nm})]_x$  multilayer films ( $x=5,10,15$ ) after annealing at  $700 \text{ }^\circ\text{C}$ .

From the above study, one can see that the alternate deposition of TiN and CoPt layers promoted the (001) preferred orientation of CoPt layers. In order to further investigate the variation of (001) orientation, the XRD profiles of  $\text{TiN}(5 \text{ nm})[\text{CoPt}(4 \text{ nm})/\text{TiN}(2 \text{ nm})]_{15}$  multilayer films at different  $\psi$  angles were taken (Fig. 3-5).  $\psi$  is the tilt angle of the sample during measurement. In the conventional XRD profiles ( $\psi=0^\circ$ ) (Fig. 3-5(a)), only (001) and (002) peaks are observed, indicating that the c-axis is in the perpendicular direction of the film plane. When  $\psi=44.2^\circ$  (Fig. 3-5(b)), the (101) peak is observed, indicating the ordered

transformation and (001) preferred orientation of the CoPt layers. Moreover, it was found that no (001) and (002) peaks were observed in the in-plane XRD results ( $\psi=89.2^\circ$ ). Only strong (200), (220) and weak (130) peaks were detected. The absence of (002) peaks in the in-plane direction was further confirmed by using a scintillation counter, which can detect weak peaks (Fig. 3-5(c)). This result indicates that there were no L1<sub>0</sub>-CoPt grains with c-axis lying in the in-plane direction. Therefore, the polycrystalline ordered fct grains were neatly organized in the [001] direction parallel with the normal direction of the film plane, but without preferred orientation in the in-plane directions. Since c-axis is the direction of the crystalline anisotropy in L1<sub>0</sub>-CoPt, this film texture contributes to PMA in the multilayer films.

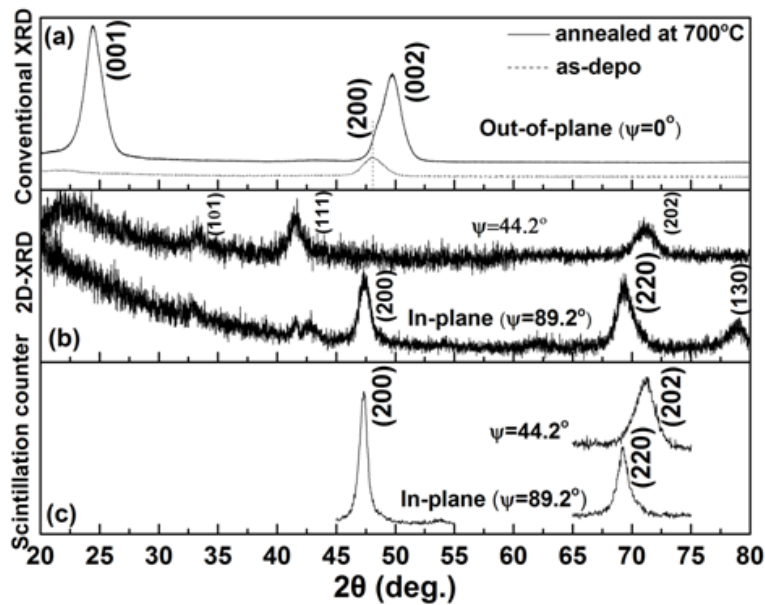


Figure 3-5 XRD profiles of TiN(5 nm)[CoPt(4 nm)/TiN(2 nm)]<sub>15</sub> multilayer film after annealing at 700 °C: (a) Conventional XRD profiles, (b) XRD profiles at different  $\psi$  angles taken by 2D detector, (c) narrow scans around peak positions taken by scintillation counter.<sup>[20]</sup>

### 3.3.2 Magnetic properties measurement

Figure 3-6 shows the  $M$ - $H$  curves of TiN(5 nm)[CoPt(4 nm)/TiN(2 nm)] <sub>$x$</sub>  multilayer films ( $x=5,10,15$ ) after annealing at 700 °C. Apparently, PMA is markedly enhanced by increasing the number of periods. It is noteworthy that the in-plane coercivity reduces as period increases, which also indicates the enhancement of PMA with periods.

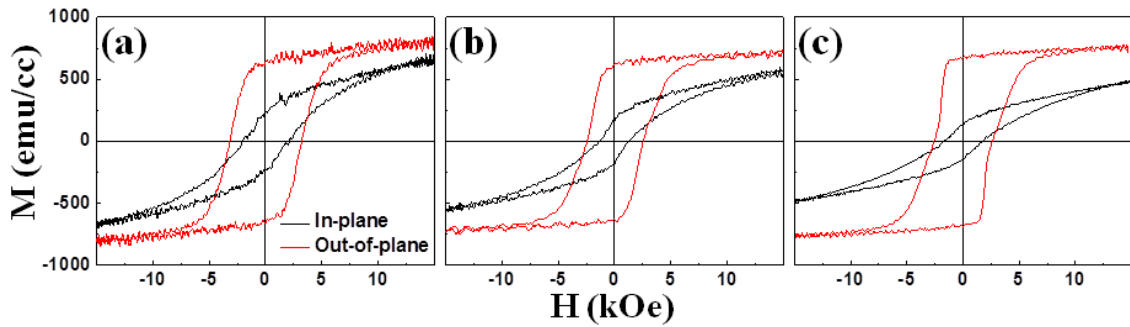


Figure 3-6  $M$ - $H$  curves of TiN(5 nm)[CoPt(4 nm)/TiN(2 nm)] <sub>$x$</sub>  multilayer films ( $x=5,10,15$ ) after annealing at 700 °C.<sup>[20]</sup>

In order to quantitatively evaluate the change of the magnetic properties, the effective anisotropy energy density  $K_{eff}$  and square ratio  $M_r/M_s$  were calculated and plotted in Fig. 3-7.  $K_{eff}$  is defined as  $K_{eff}=H_k M_s/2$ ,<sup>[13]</sup> where  $H_k$  is the anisotropy field and estimated from the hard-axis saturation field.  $M_s$  is the saturation magnetization and  $M_r$  is the remnant magnetization normalized by the CoPt volume, respectively. As shown in Fig. 3-7, the anisotropy energy  $K_{eff}$  increases with the multilayer period. When the period is 15,  $K_{eff}$  increased to  $12.7 \times 10^6$  erg/cm<sup>3</sup> and  $M_r/M_s$  increased to near unity, which confirms the enhancing effect of TiN layers for achieving (001) preferred orientation and improving PMA of L1<sub>0</sub>-CoPt layered structure.

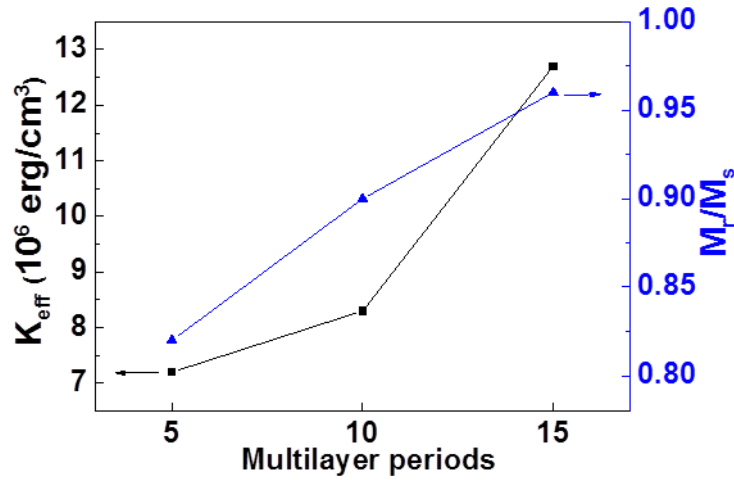


Figure 3-7 Anisotropy energy  $K_{\text{eff}}$ , and  $M_r/M_s$  vs multilayer periods.<sup>[20]</sup>

### 3.3.3 In-plane residual stress and magnetoelastic anisotropy

It should be noted that the in-plane stress plays an important role to make the c-axis perpendicular to the film plane. In the L1<sub>0</sub>-CoPt lattice,  $c$  is smaller than  $a$ , and during cooling down from high annealing temperature, in-plane tensile stress due to the different coefficient of thermal expansion between substrates and films, will be introduced in the film. It has been reported in FePt/B<sub>2</sub>O<sub>3</sub> multilayer films by Ichitsubo that tensile stress rotates the L1<sub>0</sub> FePt particles to make the c-axis perpendicular to the film plane.<sup>[14]</sup> Furthermore, the in-plane stress generates magnetoelastic anisotropy in the films also affects PMA.<sup>[15]</sup> Magnetoelastic energy is expressed as:  $K_{me} = -(3/2)\lambda\sigma_{//}$ , where  $\lambda$  is the magnetostriction constant, and  $\sigma_{//}$  is the in-plane stress. In contrast to FePt, because CoPt has negative magnetostriction constant along [001] direction,<sup>[16]</sup> the tensile stress generates positive magnetoelastic energy and favors PMA.

In order to correctly calculate the stress, we measured the peak angle from the in-plane

and out-of-plane XRD in Fig. 3-5(c), and calculated the actual lattice parameter  $a$  and  $c$ . The actual  $a$  is 0.384 nm, which is larger than 0.380 nm (PDF No. 43-1358), and  $c$  is 0.367 nm, smaller than 0.370 nm. Thus, there is no doubt that in-plane tensile stress is introduced in the multilayer film. By using the generalized Hook's law,<sup>[14]</sup> in-plane stresses  $\sigma_1$  and  $\sigma_2$  are given by:

$$\sigma_1 = \sigma_2 = (c_{11} + c_{12})\varepsilon_a + c_{12}\varepsilon_c$$

Where  $\varepsilon_a$  and  $\varepsilon_c$  are the elastic strains along  $a$  and  $c$  axis. The elastic constants are  $c_{11}=289.7$ ,  $c_{12}=178.5$  GPa.<sup>[17,18]</sup> The stress is calculated to be 2.21 GPa, then magnetoelastic energy is calculated to be  $7 \times 10^5$  erg/cm<sup>3</sup>. The ratio between magnetoelastic energy and total magnetic energy is about 6%, indicating that magnetocrystalline energy is the foremost source for the L1<sub>0</sub>-CoPt/TiN multilayer structure. Thermal stress is also estimated by assuming no stress in the films at 700 °C,<sup>[19]</sup> which is 1.96 GPa. The merely minor difference suggests that the thermal stress is dominant for the residual stress in the film. Although the lattice parameter misfit between CoPt and TiN is more than 10%, relatively little stress in the CoPt layer is generated by the epitaxial growth between them, which may be due to the formation of the edge dislocation as mentioned in Fig. 3-3(d).

### 3.4 Summary

Highly (001) oriented L1<sub>0</sub>-CoPt/TiN multilayer films with strong PMA have been successfully deposited on glass substrates. After annealing at 700 °C, the film exhibits PMA, and CoPt (001) super lattice and (002) fundamental peak are detected from the XRD profiles indicating the ordering transformation of CoPt layers from A1 to L1<sub>0</sub> structure. It is found that the alternate deposition of TiN and CoPt effectively improves the crystallinity and (001)

preferred orientation of CoPt layers. By increasing the multilayer period, anisotropy energy and  $M_r/M_s$  are greatly enhanced.

**Reference**

1. Y. Hodumi, J. Shi, and Y. Nakamura, *Appl. Phys. Lett.* **90**, 212506 (2007).
2. S. Stavroyiannis, I. Panagiotopoulos, D. Niarchos, J. A. Christodoulides, Y. Zhang, and G. C. Hadjipanayis, *Appl. Phys. Lett.* **73**, 3453 (1998).
3. T. Yokota, L. Gao, S. H. Liou, M. L. Yan, and D. J. Sellmyer, *J. Appl. Phys.* **95**, 7270 (2004).
4. Y. Zhang, J. Wan, M. J. Bonder, and G. C. Hadjipanayis, *J. Appl. Phys.* **93**, 7175 (2003).
5. K. R. Coffey, M. A. Parker, and J. K. Howard, *IEEE Trans. Magn.* **31**, 2737 (1995).
6. H. An, S. Takada, T. Sannomiya, S. Muraishi, J. Shi, and Y. Nakamura, *Appl. Phys. A* **113**, 31 (2013).
7. B. D. Cullity, *Elements of X-ray Diffraction*, Addison-Wesley Publishing, Inc, p.124, (1978).
8. T. Li, S. Noda, Y. Tsuji, T. Ohsawa, and H. Komiyama, *J. Vac. Sci. Technol. A* **20**, 583 (2002).
9. Y. Tsuji and S. Noda, *J. Vac. Sci. Technol. B* **29**, 031801 (2011).
10. H. H. Li, K. F. Dong, Y. G. Peng, G. Ju, G. M. Chow, and J. S. Chen, *J. Appl. Phys.* **110**, 043911 (2011).
11. K. F. Dong, H. H. Li, J. F. Hu, Y. G. Peng, G. Ju, G. M. Chow, and J. S. Chen, *IEEE Trans. Magn.* **49**, 668 (2013).
12. J. Narayan and B. C. Larson, *J. Appl. Phys.* **93**, 278 (2003).
13. S. Emori and G. D. Beach, *J. Appl. Phys.* **110**, 033919 (2011).

14. T. Ichitsubo, S. Tojo, T. Uchihara, E. Matsubara, A. Fujita, K. Takahashi, and k. Watanabe, *Phys. Rev. B* 77, 094114, (2008).
15. M. Johnson, P. Bloemen, F. Broeder, and J Vries, *Rep. Prog. Phys.* 59, 1409 (1996).
16. H. Takahashi, S. Tsunashima, and S. Uchiyama, *J. Magn. Magn. Mater.* 126, 282 (1993).
17. J. Touchy, E. du Tremolet de Lacheisserie, J. C. Genna, and A. Waintal, *J. Magn. Magn. Mater.* 21, 69 (1980).
18. J. Rouchy and A. Waintal, *Solid State Commun.* 17, 1227 (1975).
19. P. Rasmussen, X. Rui, and J. E. Shield, *Appl. Phys. Lett.* 86, 191915, (2005).
20. Hongyu An, Qian Xie, Jian Wang, Takumi Sannomiya, Shinji Muraishi, Zhengjun Zhang, Yoshio Nakamura, and Ji Shi, *Journal of Vacuum Science and Technology A*, 33, 021512, (2015).

## Chapter 4 Effect of TiN layer thickness on the structure and magnetic properties of L1<sub>0</sub>-CoPt/TiN multilayer films

Due to the epitaxial growth relation between TiN and CoPt, TiN layer has a very significant effect on the interface microstructure and the magnetic properties of L1<sub>0</sub>-CoPt/TiN multilayer films. Thus, controlling the growth orientation, interface structure of TiN and CoPt layers in L1<sub>0</sub>-CoPt/TiN multilayer films becomes important to study. In this chapter, L1<sub>0</sub>-CoPt/TiN multilayer films were fabricated on quartz glass substrates. The magnetic anisotropy, ordering degree, microstructure and interface roughness have been systematically investigated by changing the thicknesses of TiN layers.

### 4.1 Deposition of CoPt/TiN multilayer films

Substrate/TiN(5 nm)[CoPt(4 nm)/TiN( $x$  nm)]<sub>5</sub> multilayer films ( $x=1,2,4,6,8,10,14$  nm) were deposited on fused quartz substrates at 400 °C by dc magnetron sputtering. The base pressure in the chamber before deposition was better than  $5 \times 10^{-5}$  Pa, and the deposition pressure was 0.2 Pa. Co<sub>0.44</sub>Pt<sub>0.56</sub> was deposited from a 2-inch composite Co-Pt target. Nitrogen and argon gases with fixed flow rate ratio of 1:8.7 were supplied during sputtering. After deposition, samples were annealed at 600, 700, 800 °C for 3 hours in vacuum (better than  $1 \times 10^{-5}$  Pa).

### 4.2 Magnetic properties measurement

Fig. 4-1 shows the  $M-H$  curves of CoPt/TiN multilayer films with different thickness of TiN layer before annealing. All the films exhibit in-plane magnetic anisotropy due to the shape anisotropy effect.

After annealing at 600 °C, partial of A1 CoPt grains transformed to L1<sub>0</sub>-CoPt structure, leading to the easier magnetization in the out-of-plane direction (Fig. 4-2). However, samples still show in-plane anisotropy, indicating that the annealing temperature of 600 °C is not sufficiently high for the most A1 CoPt grains transformation.

When increasing the annealing temperature to 700 °C, PMA is shown in all the samples (Fig. 4-3). It can be seen that TiN layer thickness has significant effect on the magnetic properties of the multilayer films. PMA becomes stronger by increasing the TiN layer thickness from 1 nm. Strongest PMA is obtained with TiN thickness of 4 nm, and thereafter, PMA becomes weaker.

As shown in Fig. 4-4, after annealing at 800 °C, films show similar tendency with which annealed at 700 °C, except for the optimum TiN thickness of 8 nm to obtain strongest PMA.

The above study indicates that both TiN layer thickness and annealing temperature have strong effect on the magnetic properties of L1<sub>0</sub>-CoPt layers. In order to quantitatively study the effect of the TiN layer thickness and the annealing temperature on the magnetic anisotropy of CoPt/TiN multilayer films, the effective magnetic anisotropy energy  $K_{\text{eff}}$  was calculated and plotted in Fig. 4-5.  $K_{\text{eff}}$  equals to the area between the in-plane and perpendicular magnetization curves. Positive  $K_{\text{eff}}$  represents perpendicular magnetic anisotropy and negative  $K_{\text{eff}}$  represents in-plane magnetic anisotropy.<sup>[1]</sup> Since some hard axis loops cannot be saturated by the maximum 15 kOe external magnetic field, those loops were carefully extrapolated to obtain the crossover point of the easy and the hard axis of the magnetization curves. As shown in Fig. 4-5, all the films annealed at 600 °C have a negative

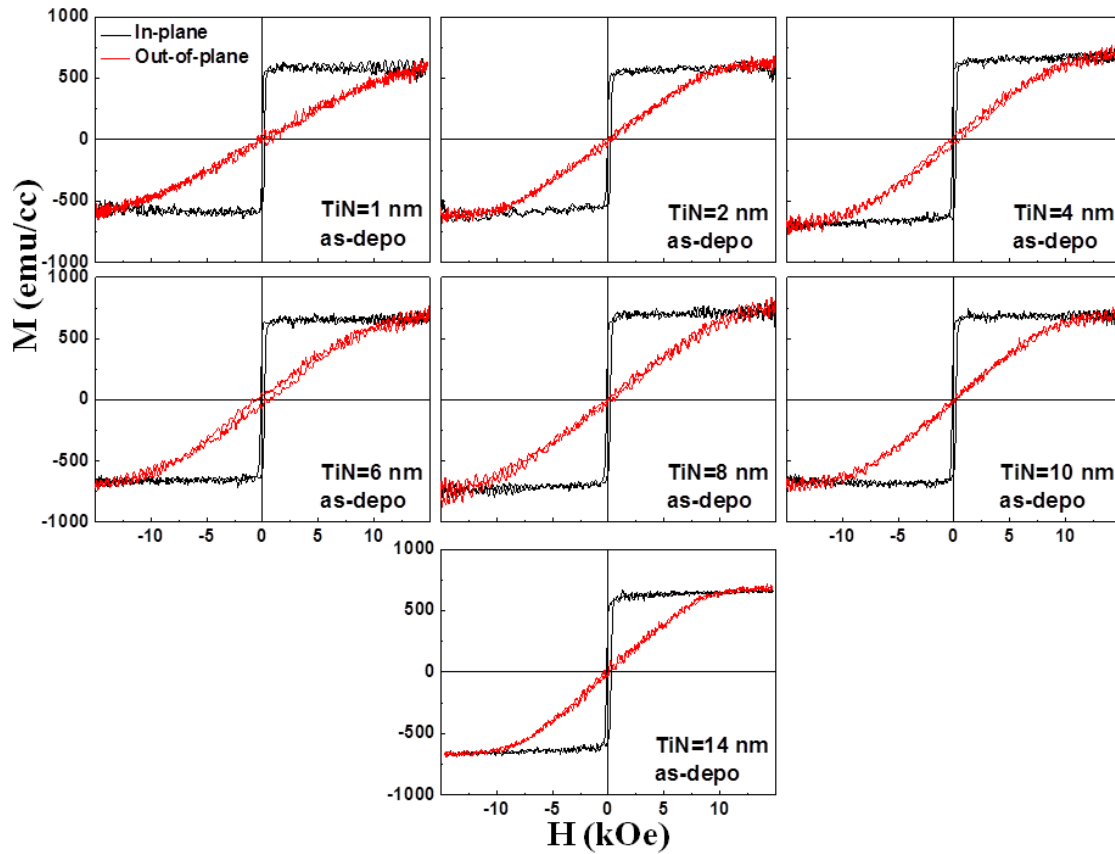


Figure 4-1  $M$ - $H$  curves of as-deposited TiN(5 nm)[CoPt(4 nm)/TiN( $x$  nm)]<sub>5</sub> multilayer films ( $x=1,2,4,6,8,10,14$ ).

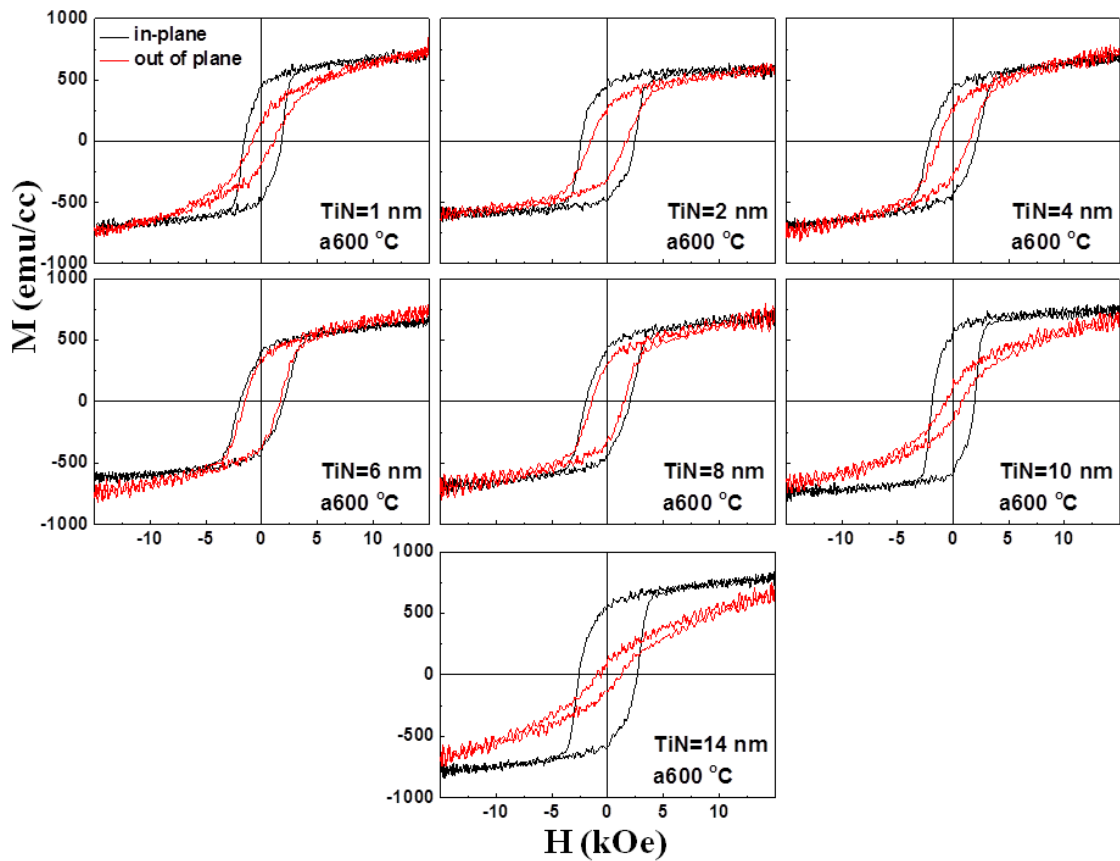


Figure 4-2  $M$ - $H$  curves of  $\text{TiN}(5 \text{ nm})[\text{CoPt}(4 \text{ nm})/\text{TiN}(x \text{ nm})]_5$  multilayer films ( $x=1,2,4,6,8,10,14$ ) annealed at  $600 \text{ }^\circ\text{C}$  for 3 hours.

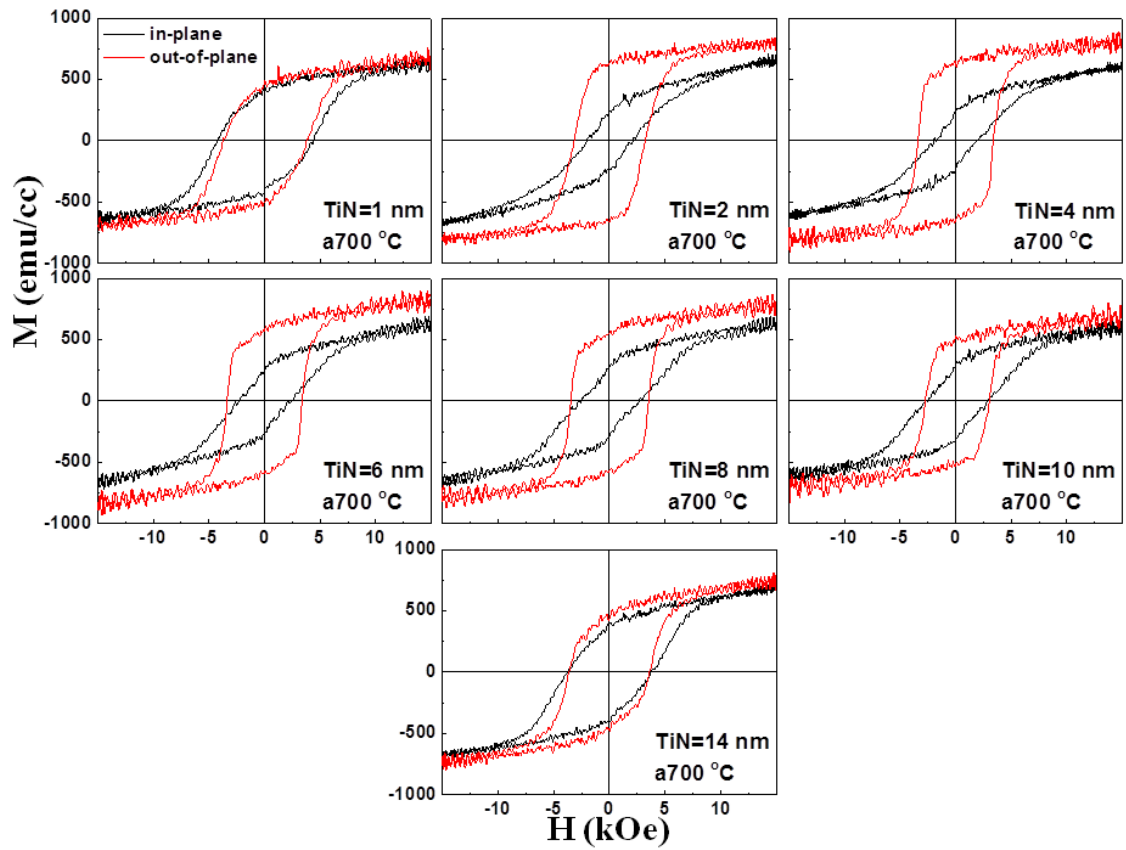


Figure 4-3  $M$ - $H$  curves of  $\text{TiN}(5 \text{ nm})[\text{CoPt}(4 \text{ nm})/\text{TiN}(x \text{ nm})]_5$  multilayer films ( $x=1,2,4,6,8,10,14$ ) annealed at  $700 \text{ }^\circ\text{C}$  for 3 hours.

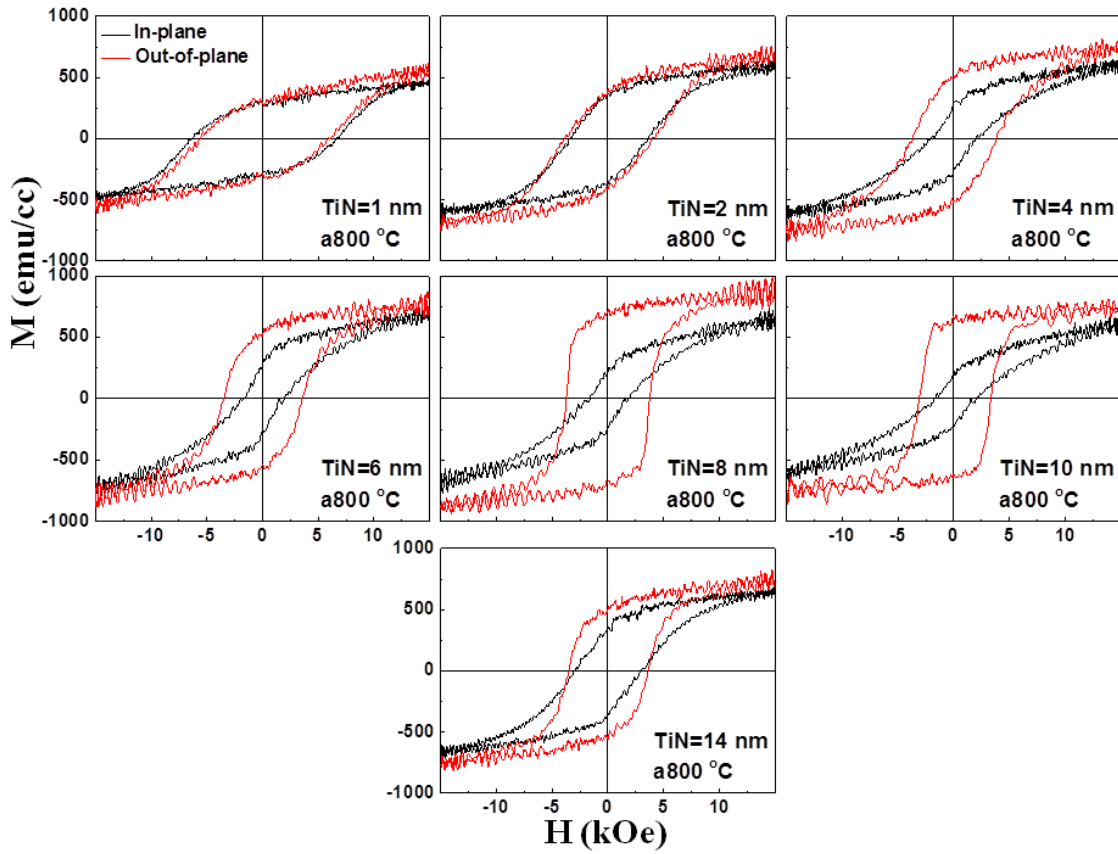


Figure 4-4  $M$ - $H$  curves of  $\text{TiN}(5 \text{ nm})[\text{CoPt}(4 \text{ nm})/\text{TiN}(x \text{ nm})]_5$  multilayer films ( $x=1,2,4,6,8,10,14$ ) annealed at  $800 \text{ }^\circ\text{C}$  for 3 hours.

$K_{\text{eff}}$ , indicating that 600 °C is not sufficient to make most disordered CoPt structure transform to L1<sub>0</sub> structure in CoPt/TiN multilayer films on glass substrates, although it is considered that L1<sub>0</sub> structure transformation has already been triggered at 600 °C. After annealing at 700 °C, positive  $K_{\text{eff}}$  is obtained, which increases with increasing the TiN layer thickness up to 4 nm, reaching the maximum, and then decreases by the further increase of the TiN layer thickness. Similar tendency is observed for samples annealed at 800 °C, except for the optimal TiN thickness of 8 nm for the maximum  $K_{\text{eff}}$ . The existence of the optimal thickness may be related to the growth orientation of TiN or the interface roughness between TiN and CoPt layers, since these two factors can directly influence the crystalline orientation of CoPt layer through the epitaxial growth between CoPt and TiN layers.

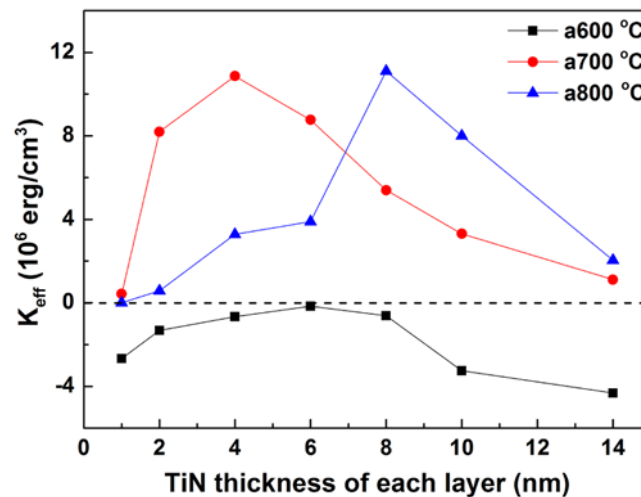


Figure 4-5 Effective magnetic anisotropy energy  $K_{\text{eff}}$  vs the thickness of each TiN layer in CoPt/TiN multilayer films after annealing at 600, 700 and 800 °C for 3 hours.<sup>[14]</sup>

## 4.3 Structure characterization

### 4.3.1 XRD measurement

In order to clarify the growth orientation and crystallinity, XRD measurement was conducted. Figure 4-6(a) shows the XRD profiles of TiN(5 nm)[CoPt(4 nm)/TiN(4 nm)]<sub>5</sub> multilayer films. The as-deposited sample only exhibits TiN (200) and CoPt (200) peak indicating the formation of the disordered fcc CoPt structure in the film. It is noted that no CoPt (111) peak has been detected, which suggests the epitaxial growth between TiN and CoPt layers. L1<sub>0</sub> structure transformation begins with annealing temperature of 600 °C. After annealing at 700 °C, most disordered fcc CoPt phase has transformed to L1<sub>0</sub>-CoPt phase which is confirmed by the strong CoPt (001) and (002) peaks. It is known that fcc metals deposited on amorphous substrates, tend to form (111) oriented columnar texture due to the lowest surface energy of (111) plane.<sup>[2]</sup> In such a case, for fcc-CoPt films, even ordering process occurs, the c-axis ([001] direction) of L1<sub>0</sub> structure is not aligned to the normal of the film plane. Therefore, in order to obtain (001) texture, costly single crystalline substrates are generally used for the L1<sub>0</sub>-CoPt epitaxial growth. In our CoPt/TiN multilayer films, with annealing at 700 °C, the (100) oriented TiN layer promotes CoPt (001) texture growth, and the alternate deposition between TiN and CoPt also enhances the (001) preferred orientation for both TiN and CoPt layers. After annealing at 800 °C, for the film with 4 nm thick TiN layers, CoPt (200) peak becomes stronger, which indicates that 800 °C may be too high to maintain the layered structure, leading to the coalescence of the adjacent CoPt layers.. Thicker TiN layers are needed to prevent the coalescence of CoPt layers, which can be

verified in Fig. 4-6(b). Different from the sample with TiN layer of 4 nm, the sample with TiN layer of 8 nm still shows strong CoPt (002) peak even after annealing at 800 °C.

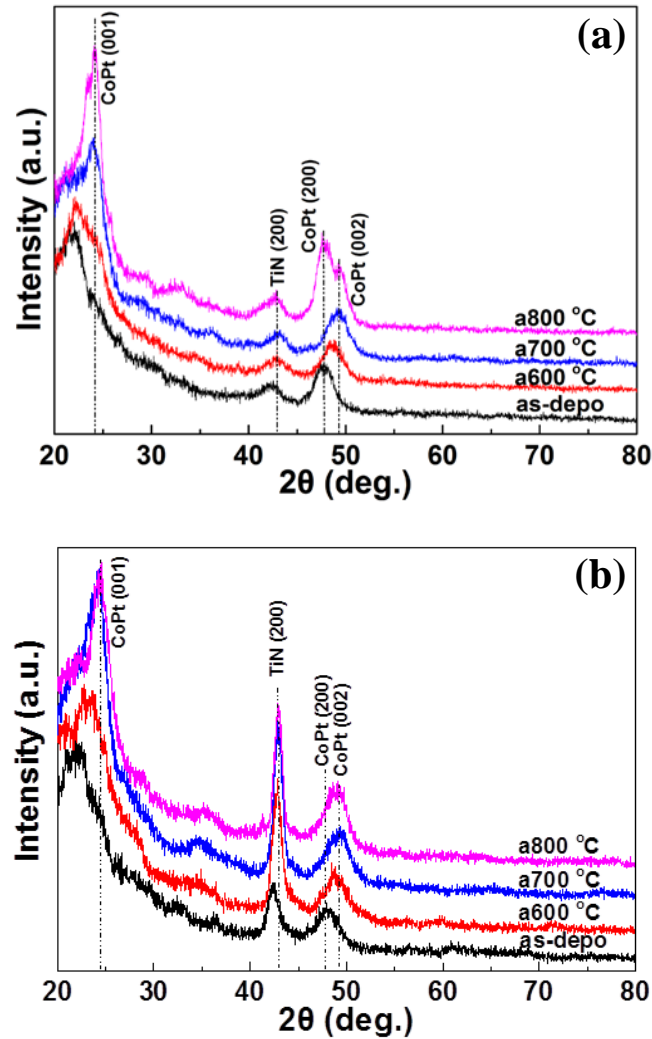


Figure 4-6 XRD profiles of  $\text{TiN}(5 \text{ nm})[\text{CoPt}(4 \text{ nm})/\text{TiN}(x \text{ nm})]_5$  multilayer films: as-deposited, annealed at 600, 700 and 800 °C for 3 hours, respectively. (a)  $x=4$ , (b)  $x=8$ .<sup>[14]</sup>

### 4.3.2 Calculation of chemical ordering parameter

Chemical ordering parameter  $S$  is an important factor which reflects the ordering degree and magnetic anisotropy in L1<sub>0</sub> structure. It is given by the following Eq. (4-1):

$$S^2 = (I_{001} / I_{002})_{meas} / (I_{001} / I_{002})_{calc} \quad (4-1)$$

Where,  $I_{001}$  and  $I_{002}$  are the integrated intensity of (001) super lattice peak and (002) fundamental peak from the XRD profiles.  $(I_{001} / I_{002})_{meas}$  and  $(I_{001} / I_{002})_{calc}$  are the measured and calculated diffraction intensity ratio, respectively.  $I_{calc}$  is given in Eq. (4-2):

$$I_{calc} = |F|^2 p(LP)e^{-2M} \quad (4-2)$$

$$LP = \frac{1 + \cos^2 2\theta}{\sin^2 \theta \cos \theta} \quad (4-3)$$

Where  $F$  is the structure factor,  $p$  is the multiplicity factor,  $LP$  is the Lorentz-polarization factor,  $e^{-2M}$  is the temperature factor.<sup>[3]</sup> Since few previous studies have given the value of  $(I_{001} / I_{002})_{calc}$ ,<sup>[4-6]</sup> some studies even applied  $c/a$  ( $L1_0$  lattice parameter ratio),<sup>[7,8]</sup> which is not precise due to the residual stress existing in the films, therefore, we summarized the parameters in table 4-1, and  $(I_{001} / I_{002})_{calc}$  is calculated to be 1.893. This value is close to Okamoto's calculation of FePt, which is 2.0.<sup>[9]</sup>

Table 4-1 Parameters to calculate the ordering parameter S of L1<sub>0</sub>-CoPt.<sup>[14]</sup>

Peak	$\theta$	$f_{Co}$	$M_{Co}$	$f_{Pt}$	$M_{Pt}$	$p$	$ F ^2$	$e^{-2M}$
001	12	22.81	0.006185	70.02	0.00574	2	8915	0.988
002	24.6	17.6	0.0257	58.93	0.0239	2	23427	0.9516

Figure 4-7 shows the dependence of the ordering parameter S on the TiN layer thickness. The dependence of S on TiN thickness is similar to that of  $K_{eff}$ , which indicates that the magnetocrystalline anisotropy is the foremost source of the magnetic anisotropy in L1<sub>0</sub>-CoP/TiN multilayer films. The largest S in our L1<sub>0</sub>-CoPt/TiN multilayer films is about 0.85, and to obtain maximum L1<sub>0</sub>-CoPt structure, the optimum thickness of TiN layer is

around 4 and 8 nm, with annealing at 700 and 800 °C, respectively.

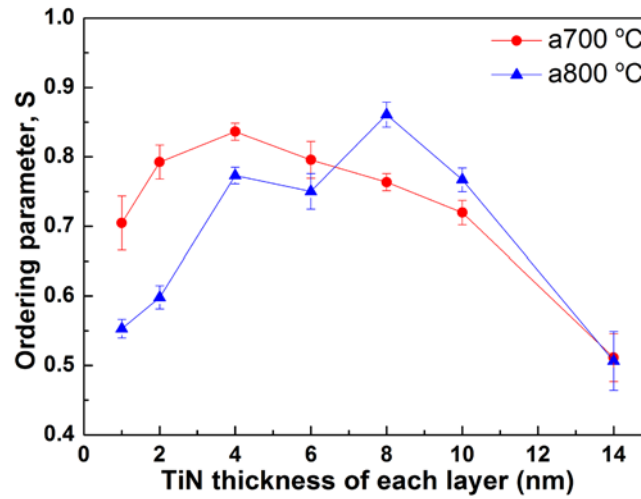


Figure 4-7 The ordering parameter  $S$  vs the thickness of each TiN layer in CoPt/TiN multilayer films after annealing at 700 and 800 °C.<sup>[14]</sup>

### 4.3.3 Mechanism for the change of magnetic anisotropy and ordering parameter

In order to investigate the mechanism that  $K_{\text{eff}}$  and  $S$  increases by increasing the TiN layer thickness when it is below 4 nm, cross-sectional TEM images of the films with TiN layer thickness of 2 and 4 nm annealed at 700 °C were taken as shown in Fig. 4-8. It is clearly seen that when the TiN layer thickness is 2 nm (Fig. 4-8(a)), TiN layers are discontinuous in some parts. By increasing the TiN layer thickness to 4 nm, it becomes continuous and the composition transition at the interface is much sharper (Fig. 4-8(b)). In Roquiny's study on TiN growth,<sup>[10]</sup> traditional island growth of Volmer-Weber mode is verified, which is, by increasing the TiN thickness, island nucleation is formed at the initial growth, then followed by coalescence and finally by a continuous growth. Similar result has also been obtained in Li's study.<sup>[11]</sup> This growth mode seemingly works in our multilayer films. In Fig. 4-8(a), due

to the discontinuity of the TiN layers, two adjacent CoPt layers have coalesced with each other and formed larger grains (shown by the arrows). It is considered that this coalescence affects the (001) crystalline orientation of CoPt.

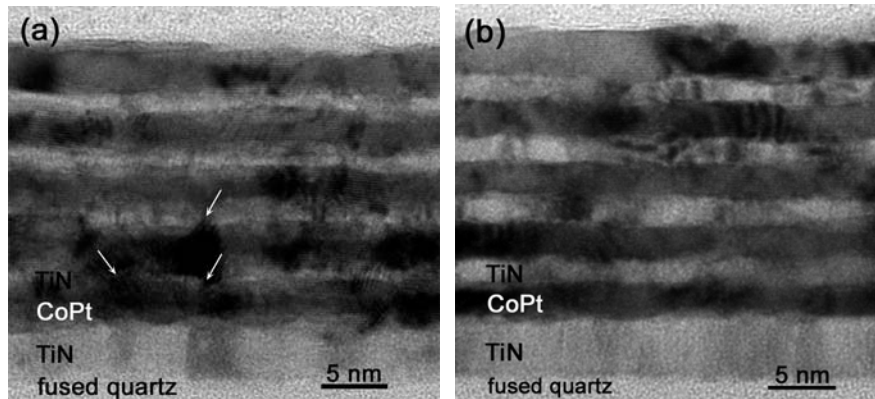


Figure 4-8 Cross-sectional TEM images of TiN(5 nm)[CoPt(4 nm)/TiN(x nm)]<sub>5</sub> multilayer films after annealing at 700 °C: (a)  $x=2$  nm, (b)  $x=4$  nm. The arrows represent the coalescence of two CoPt layers.<sup>[14]</sup>

Another interesting phenomenon is that after annealing at 700 °C,  $K_{\text{eff}}$  decreases gradually when increasing the thickness of TiN layers beyond 4 nm. It is known that TiN (200) plane has the lowest surface energy which is the driving force for (200) orientation growth. However, besides surface energy, strain energy is another energetic condition that affects the growth orientation of TiN films, and TiN (111) plane has the lowest strain energy.<sup>[12]</sup> Since the strain energy of the film is proportional to the film thickness,<sup>[13]</sup> TiN tends to grow with (111) crystalline orientation when the TiN thickness is large.<sup>[11]</sup> On the other hand, when the TiN layer is too thick, the roughness of the interface between TiN and CoPt layers increases, which also prevents the c-axis of L1<sub>0</sub>-CoPt from orienting to the

normal of the film plane.

Figure 4-9 shows the x-ray reflectivity (XRR) profiles of the multilayer films with TiN layer thickness of 1, 2, 4, 8 and 14 nm. When the TiN layer thickness is 1 nm (Fig. 4-9(a)), the profile decays fast after annealing at 700 °C, indicating the bad interface quality due to the coalescence of the adjacent CoPt layers, and after annealing at 800 °C, the interface quality becomes even worse. It is considered that no periodic structure remains with TiN layer thickness of 1 nm. When the TiN layer thickness is 2 nm (Fig. 4-9(b)), the periodic structure remains after annealing at 700 °C. However, the periodicity is greatly impaired after annealing at 800 °C, as the profile decays faster than it does in the case of annealing at 700 °C. This result indicates the coalescence of the layers and the roughening of the interfaces. This reveals that the annealing process at 800 °C coarsens the interface when the TiN layer is thin. The sample with 4 nm thick TiN layer shows better interface quality than the one with 2 nm thick TiN layer, but the annealing process at 800 °C also slightly impairs the interface quality (Fig. 4-9(c)). When the TiN layer thickness is 8 nm (Fig. 4-9(d)), the interface quality of the films annealed at 800 °C becomes better than annealed at 700 °C. As one can see high-order peaks become stronger for annealing at 800 °C. When the TiN layer thickness is 14 nm (Fig. 4-9(e)), the interface quality becomes worse again, since the profiles decay fast again. This is due to the roughening of the interface between TiN and CoPt layers when TiN layer thickness is too thick. From the above discussion, it is seen that the interface condition between TiN and CoPt layers is strongly interrelated with  $K_{\text{eff}}$  and  $S$ , and the interface condition is directly determined by the TiN layer thickness and annealing temperature.

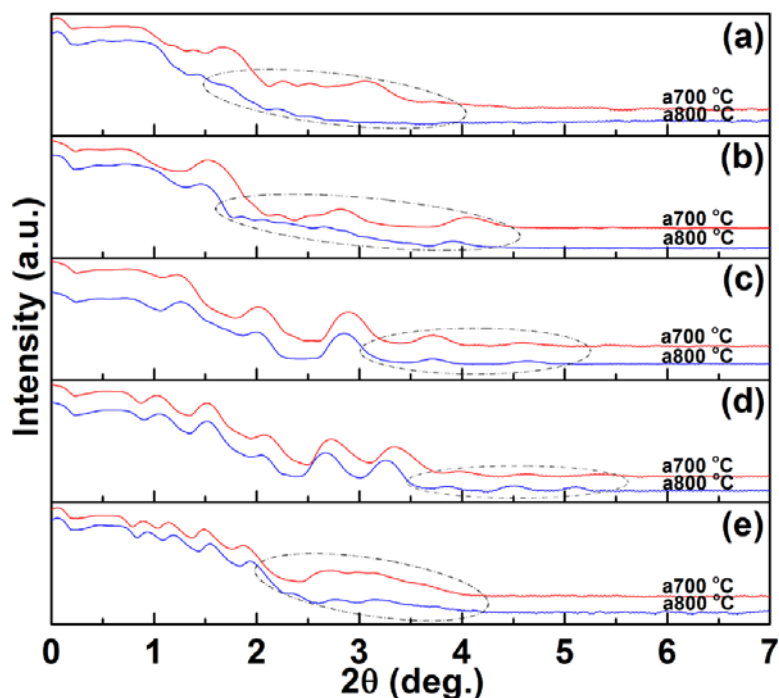


Figure 4-9 XRR profiles of TiN(5 nm)[CoPt(4 nm)/TiN( $x$  nm)]<sub>5</sub> multilayer films after annealing at 700 °C and 800 °C: (a)  $x=1$  nm, (b)  $x=2$  nm, (c)  $x=4$  nm, (d)  $x=8$  nm, (e)  $x=14$  nm.<sup>[14]</sup>

#### 4.4 Summary

L1<sub>0</sub>-CoPt/TiN multilayer films with perpendicular magnetic anisotropy have been successfully deposited on the glass substrates. It is found that by changing the TiN layer thickness and annealing temperature, the ordering degree and magnetic anisotropy energy of the L1<sub>0</sub>-CoPt/TiN multilayer films can be controlled. To obtain the maximum value of the anisotropy energy and ordering degree, the optimum thickness of TiN layer is about 4 and 8 nm for the multilayer films annealed at 700 and 800 °C, respectively. When TiN layer is below 2 nm, after annealing, TiN tends to be discontinuous and this results in the coalescence of the adjacent CoPt layers. When TiN layer is above 8 nm, the interface roughness becomes

larger. The above interface microstructures severely affect the (001) crystalline orientation of L1<sub>0</sub>-CoPt layer, and reduce the anisotropy energy.

**Reference**

1. M. Johnson, P. Bloemen, F. Broeder, and J. Vries, *Rep. Prog. Phys.* 59, 1409 (1996).
2. K. R. Coffey, M. A. Parker, and J. K. Howard, *IEEE Trans. Magn.* 31, 2737 (1995).
3. B. D. Cullity, *Elements of X-ray Diffraction*, (Addison-Wesley Publishing, Inc), p 139 (1978).
4. G. Giannopoulos, T. Speliotis, W. Li, G. Hadjipanayis, and D. Niarchos, *J. Magn. Magn. Mater.* 325, 75 (2013).
5. H. Yang, C. Chung, and J. Ding, *J. Magn. Magn. Mater.* 312, 239 (2006).
6. Y. Takahashi, K. Hono, T. Shima, and K. Takanashi, *J. Magn. Magn. Mater.* 267, 248 (2003).
7. H. Wang, B. Hu, L. Zhang, M. Li, E. Ja, and Z. Liu, *J. Magn. Magn. Mater.* 362, 47 (2014).
8. Y. Endo, N. Kikuchi, O. Kitakami, and Y. Shimada, *J. Appl. Phys.* 89, 7065 (2001).
9. S. Okamoto, N. Kikuchi, O. Kitakami, T. Miyazaki, and Y. Shimada, *Phys. Rev. B.* 66, 024413 (2002).
10. Ph. Roquiny, G. Mathot, G. Terwagne, F. Bodart, and P. van den Brande, *Nucl. Instrum. Methods Phys. Res. B.* 161-163, 600 (2000).
11. T. Li, S. Noda, Y. Tsuji, T. Ohsawa, and H. Komiyama, *J. Vac. Sci. Technol. A.* 20, 583 (2002).
12. U. C. Oh, and J. H. Je, *J. Appl. Phys.* 74, 1692 (1993).
13. J. E. Sundgren, *Thin Solid Films.* 128, 21 (1985).
14. Hongyu An, Jian Wang, Takumi Sannomiya, Shinji Muraishi, Yoshio Nakamura, and Ji Shi. *Journal of Physics D: Applied Physics*, 48, 155001, (2015).

## Chapter 5 Perpendicular exchange-bias-like effect in CoPt/TiN multilayer films

Since Meiklejohn *et al.* discovered the exchange bias (EB) effect in cobalt fine particles (~20 nm) with the shell of cobaltous oxide,<sup>[1]</sup> it has been extensively studied in the last decades due to its promising application in spin valves, tunnel junctions, etc. Generally, EB effect can be obtained in ferromagnetic/antiferromagnetic (FM/AFM) material systems, such as Fe/CoO,<sup>[2]</sup> FeNi/FeMn,<sup>[3]</sup> Co/CoN,<sup>[4]</sup> etc. Recently, EB effect in materials with perpendicular magnetic anisotropy (PMA) has also attracted researchers' interests and perpendicular exchange bias (PEB) has been observed in CoPt/CoO,<sup>[5]</sup> [Co/Pt]/IrMn,<sup>[6]</sup> [Co/Pd]/FeMn,<sup>[7]</sup> [Co/Pt]NiO,<sup>[8]</sup> etc. In these FM/AFM material systems, by applying external magnetic field cooling (FC) through the Néel temperature of the AFM material, hysteresis loop is shifted along the magnetic field axis with coercivity enhancement. It is noteworthy that such phenomenon exists not only in FM/AFM material systems, but also in ferrimagnetic/ferrimagnetic (Ferri/Ferri),<sup>[9]</sup> ferri/FM,<sup>[10]</sup> and FM/FM<sup>[11]</sup> material systems, where it is called exchange-bias-like (EB-like) effect. For instance, Cain *et al.*<sup>[10]</sup> reported the in-plane EB-like effect in an exchange coupled NiFe/TbCo bilayer thin film, and interpreted that the magnetization in the TbCo layer varies from in-plane at the interface to perpendicular at the top surface leading to this EB-like effect. Sort *et al.*<sup>[11]</sup> also observed in-plane EB-like effect by depositing permalloy (with in-plane anisotropy) on Pt/Co multilayer (with perpendicular anisotropy). They explained that this effect originates from the coupling between the permalloy layer and uncompensated in-plane magnetic moment in the Pt/Co

multilayer.

In this chapter, we present successful observation of the perpendicular EB-like effect in L1<sub>0</sub>-CoPt/TiN multilayer films deposited on glass substrates after annealing and discuss the origin of this effect.

### 5.1 Fabrication of L1<sub>0</sub>-CoPt/TiN multilayer films

Substrate/TiN(5 nm)[CoPt(4 nm)/TiN(2 nm)]<sub>15</sub> multilayer films were deposited on fused quartz substrates at 400 °C by dc magnetron sputtering. The base pressure in the chamber before deposition was better than  $5 \times 10^{-5}$  Pa, and the deposition pressure was 0.2 Pa. Co<sub>0.44</sub>Pt<sub>0.56</sub> was deposited from a 2-inch composite CoPt target. Nitrogen and argon gases with fixed flow rate ratio of 1:8.7 were applied during sputtering. After deposition, samples were annealed at 700, 800 °C for 3 hours in vacuum (better than  $1 \times 10^{-5}$  Pa).

Magnetic properties were measured by a vibrating sample magnetometer (RIKIN BHV-50 V), and all the measurements were conducted in perpendicular to the film plane direction at room temperature except for the noted figures. To investigate the structure of the films, x-ray diffraction (XRD) profiles were taken on Bruker D8 Discover diffractometer by applying Cu K $\alpha$  radiation. Micromagnetic simulations were performed by using the OOMMF code.<sup>[21]</sup> The parameters used for the L1<sub>0</sub>-CoPt layer were the saturation magnetization  $M_s = 800 \text{ emu/cm}^3$  and the perpendicular uniaxial magnetocrystalline anisotropy constant  $K_u = 3 \times 10^7 \text{ erg/cm}^3$ .<sup>[23]</sup> The parameters used for the A1-CoPt layer were the saturation magnetization  $M_s = 800 \text{ emu/cm}^3$  without magnetocrystalline anisotropy. The exchange constant  $A_{\text{ex}} = 3 \times 10^{-7} \text{ erg/cm}$  was used for both A1 and L1<sub>0</sub>-CoPt layers.<sup>[24]</sup>

## 5.2 Observation of perpendicular exchange-bias-like effect

Figure 5-1(a) shows the  $M$ - $H$  curves of the TiN (5 nm)[CoPt(4 nm)/TiN(2 nm)]<sub>15</sub> multilayer film measured at room temperature after applying a 5 kOe perpendicular field cooling (FC) from 350 °C. The sample was annealed at 800 °C to obtain L1<sub>0</sub>-CoPt structure and PMA before applying FC. Compared with the zero field cooling (ZFC) loop, both shifts along with the field axis (horizontal) and magnetization axis (vertical) are observed after FC process. Furthermore, the direction of horizontal shift is opposite with the positive FC direction; however the vertical shift is same with the positive FC direction. It is vice versa for the sample applied in a negative cooling field (the inset of Fig. 5-1(a)). As it is known, in FM/AFM material system, EB effect originates from the coupling effect between the spins in FM material and the uncompensated interfacial spins pinned in the AFM material which is hardly to be switched by the external field.<sup>[12]</sup> Therefore, theoretically, the uncompensated interfacial spins should generate a vertical shift. However, only few vertical shifts can be observed in FM/AFM material systems, since the magnetization of the uncompensated interfacial spins is too weak compared with the FM material.<sup>[13,14]</sup> In our L1<sub>0</sub>-CoPt/TiN multilayer film, the hysteresis loop is not saturated yet, and the uncompensated perpendicular magnetic moment generated by a 5 kOe FC from 350 °C, cannot be offset even in a 10 kOe field at room temperature. The percentage of this uncompensated perpendicular magnetic moment generated by FC is calculated to be about 17% after correcting the vertical shift (centering the hysteresis loop along the magnetization axis<sup>[11]</sup>), as shown in Fig. 5-1(b). After correcting the vertical shift, a horizontal shift still can be observed in the opposite direction of the external field, and vice versa for the negative field (inset of Fig. 5-1(b)). This horizontal

shift phenomenon is completely same as the shift in FM/AFM material system indicating the existence of FM/AFM-like coupling effect in the film. The value of the EB,  $H_{ex}$  is about 290 Oe here. Due to the multilayer structure, this value is four times larger than Sort *et al.* reported in [Pt/Co]/NiFe film (70 Oe),<sup>[11]</sup> and eight times larger than Navas *et al.* reported in CoCrPt/Ni film (33 Oe).<sup>[15]</sup>

To investigate the effect of FC temperature, the dependence of  $H_{ex}$  and  $H_c$  on different FC temperatures is plotted in Fig. 5-2 before and after correcting the vertical shift. Two samples were annealed at 700 and 800 °C before applying FC, respectively. By increasing the FC temperature,  $H_{ex}$  increases, and the sample annealed at 800 °C has much larger value than 700 °C (Fig. 5-2(a)). The coercivity  $H_c$  also increases (Fig. 5-2(b)), which is a typical phenomenon resulted from the coupling effect in the film. The insets of Fig. 5-2 show the dependence of  $H_{ex}$  and  $H_c$  on FC temperatures after correcting the vertical shift. Compared with the measurements before correcting the vertical shift,  $H_{ex}$  and  $H_c$  exhibit similar tendency except for the relatively smaller value of  $H_{ex}$ . The maximum value of  $H_{ex}$  is about 400 Oe. It is noteworthy that even after correcting the vertical shift,  $H_{ex}$  annealed at 800 °C is still much larger than 700 °C at the same FC condition. This implies that much amount of uncompensated perpendicular magnetic moment exists in the film after annealing at 800 °C, which induces much stronger coupling effect and generate a larger value of  $H_{ex}$ .

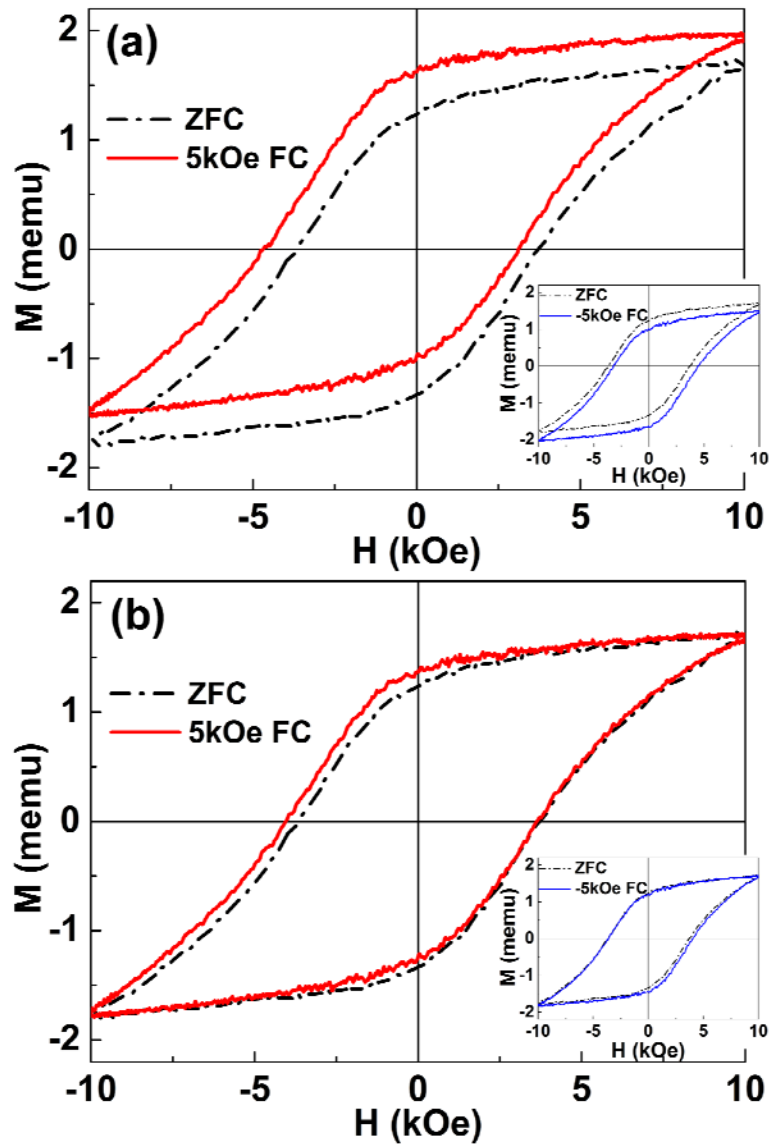


Figure 5-1 Perpendicular  $M$ - $H$  curves of  $\text{TiN}(5 \text{ nm})[\text{CoPt}(4 \text{ nm})/\text{TiN}(2 \text{ nm})]_{15}$  multilayer film after 5 kOe field cooling from 350 °C to room temperature (sample was annealed at 800 °C before applying FC). (a) before correcting the vertical shift (inset: -5 kOe FC was applied). (b) after correcting the vertical shift (inset: -5 kOe FC was applied).

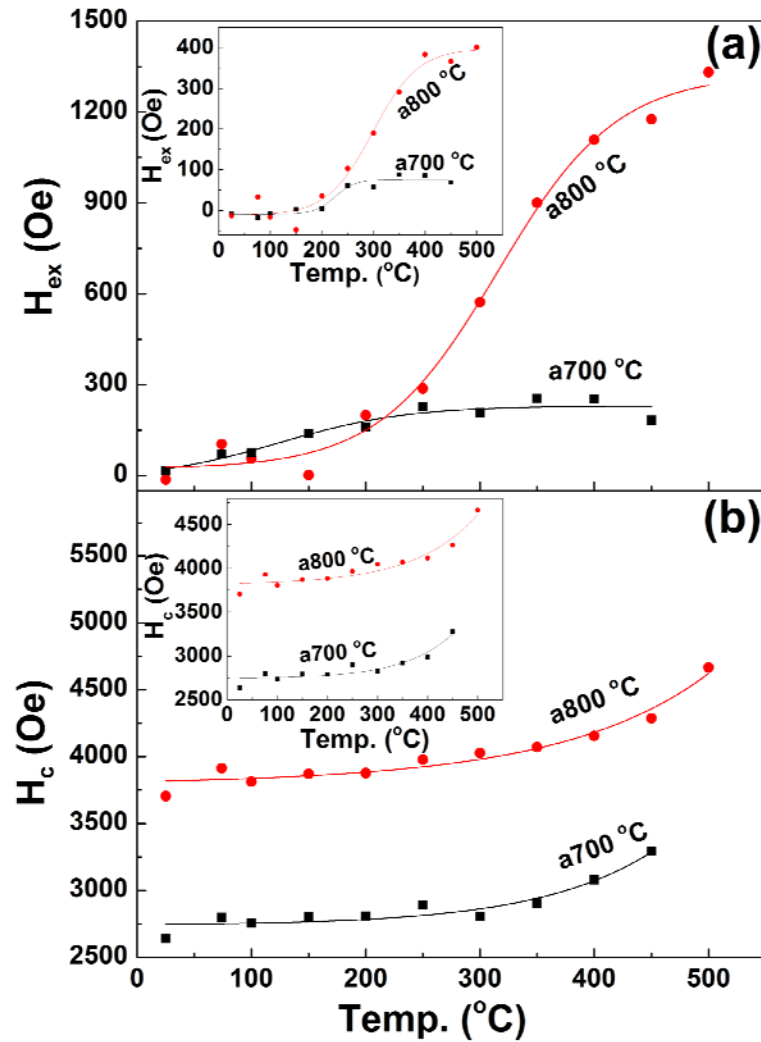


Figure 5-2 Dependence of  $H_{ex}$  and  $H_c$  on FC temperatures before correcting the vertical shift. Insets of Fig. 6-2(a) and (b) show the dependence of  $H_{ex}$  and  $H_c$  on FC temperatures after correcting the vertical shift, respectively. FC is kept as 5 kOe from different temperatures cooling down to room temperature and samples were annealed at 700 and 800  $^{\circ}$ C before applying FC. The lines are guides to eyes.

Training effects are sometimes observed in FM/AFM material systems, i.e.,  $H_{ex}$  and  $H_c$  vary with repeated hysteresis loop numbers.<sup>[16]</sup> This effect has also been observed in Sort's study of NiFe/[Co/Pt] system.<sup>[11]</sup> The CoPt/TiN multilayer films also exhibit the training effect. Figure 5-3 shows the dependence of  $H_{ex}$  and  $H_c$  on the loop number. Both  $H_{ex}$  and  $H_c$  decrease abruptly at the beginning, and then tend to be constant.  $H_{ex}$  is larger than 1000 Oe even after one hundred loop numbers indicating the quite stable coupling condition in the film.

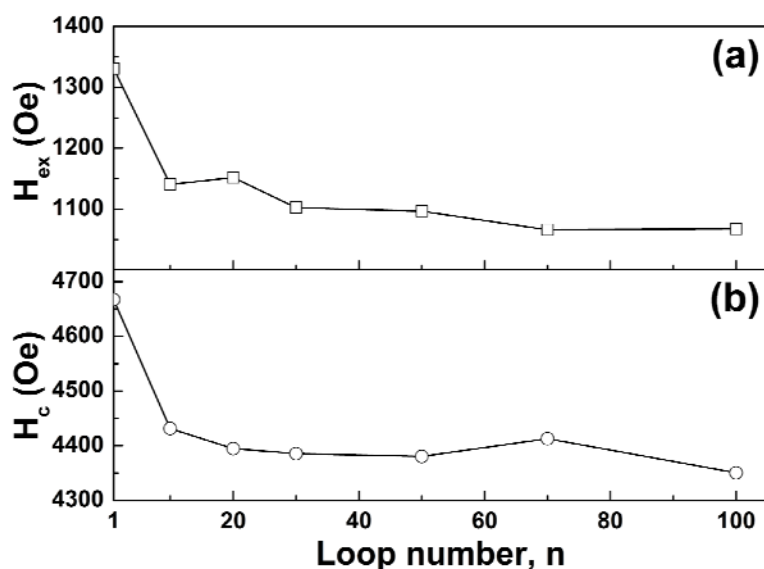


Figure 5-3 Dependence of  $H_{ex}$  and  $H_c$  on the loop number (without correcting the vertical shift). Sample was annealed at 800 °C before applying FC. FC is kept as 5 kOe from 500 °C cooling down to room temperature, and then applied a maximum 10 kOe magnetic field.

### 5.3 The origin of exchange-bias-like effect

To investigate the origin of the EB-like effect, XRD profiles were measured as shown in Fig. 5-4. After annealing at 700 °C, the film shows strong CoPt (001) and (002) peaks

indicating the existence of the highly (001) oriented L<sub>10</sub>-CoPt phase in the film. After annealing at 800 °C, the L<sub>10</sub>-CoPt grain size increases, since both peaks become stronger and sharper. However, CoPt (200) peak appears showing much stronger intensity than (002) peak. This (200) peak might indicate some L<sub>10</sub>-CoPt grains with (001) orientation aligning parallel to the in-plane direction of the film. However, by measuring the in-plane XRD profile, no (001) and (002) peaks are detected. This means that all L<sub>10</sub>-CoPt grains have (001) orientation aligning to the normal of the film plane, and the strong (200) peak is contributed by the A1-CoPt grains. In our CoPt films, the atomic ratio of Co and Pt is 44:56, and according to the Co-Pt binary phase diagram,<sup>[22]</sup> the equilibrium phase of CoPt is A1 at 800 °C. It is reasonable that after annealing at 800 °C, samples cooling through the L<sub>10</sub> phase transformation temperature range (600 °C < T < 800 °C) at a relatively fast cooling speed (about 20 °C/min in our case) can partially retain quenched A1 phase grains and result in the coexistence of A1 and L<sub>10</sub> phase in the films. Since A1-CoPt has soft magnetic property and L<sub>10</sub>-CoPt has hard magnetic property, the spin coupling between A1 and L<sub>10</sub>-CoPt phase may be responsible for the observed EB-like effect.

To further investigate the coupling mechanism, we focused on the influence of the TiN layer on the CoPt layer. Fig. 5-5(a) shows the *M-H* curve of the bilayer TiN(50 nm)/CoPt(4 nm) film after annealing at 700 °C. The film exhibits strong PMA and large perpendicular coercivity (about 9 kOe). However, after depositing a 2 nm thick TiN layer on the film, PMA of the film becomes drastically weaker and the perpendicular coercivity decreases down to about 5 kOe (Fig. 5-5(b)). Moreover, after depositing another 4 nm thick CoPt layer, PMA becomes stronger again and perpendicular coercivity increases to about 6 kOe (Fig. 5-5(c)).

The above phenomenon clearly shows that TiN layer impedes the  $L1_0$  transformation of the adjacent CoPt layer underneath, but promotes the  $L1_0$  transformation of the adjacent CoPt layer above it. Therefore, a single CoPt layer sandwiched by two TiN layers results in the remaining of the A1 phase in the upper portion and the formation of the  $L1_0$  phase in the lower portion after annealing, as illustrated in Fig. 5-5(d). Since the lattice parameter of CoPt ( $a = 0.38$  nm) is smaller than TiN ( $a = 0.424$  nm), according to our previous study,<sup>[17]</sup> for CoPt deposited on TiN layer, tensile stress exists in CoPt layer. Similar result was also reported in Li's study on FePt deposited on TiN layer.<sup>[18]</sup> For TiN deposited on CoPt layer, TiN induces compressive stress in CoPt layer.<sup>[19]</sup> It is well reported that tensile stress promotes the  $L1_0$  transformation and compressive stress has the opposite effect,<sup>[20]</sup> which is consistent with our above analysis. Therefore, after annealing at 700 °C, CoPt/TiN multilayer film remains a small amount of A1-CoPt phase due to the effect of the TiN layer. After annealing at 800 °C, the amount of A1-CoPt phase further increases due to both the effect of the TiN layer and the quenching effect when cooling down from 800 °C.

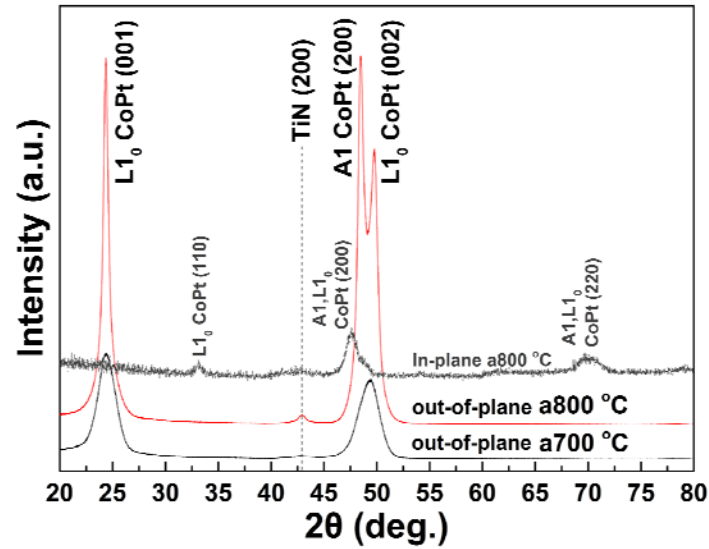


Figure 5-4 Conventional out-of-plane XRD profiles of  $[\text{CoPt}(4 \text{ nm})/\text{TiN}(2 \text{ nm})]_{15}$  multilayer films after annealing at  $700 \text{ }^\circ\text{C}$  and  $800 \text{ }^\circ\text{C}$ , respectively. The gray dash line shows the in-plane XRD of the sample after annealing at  $800 \text{ }^\circ\text{C}$ .

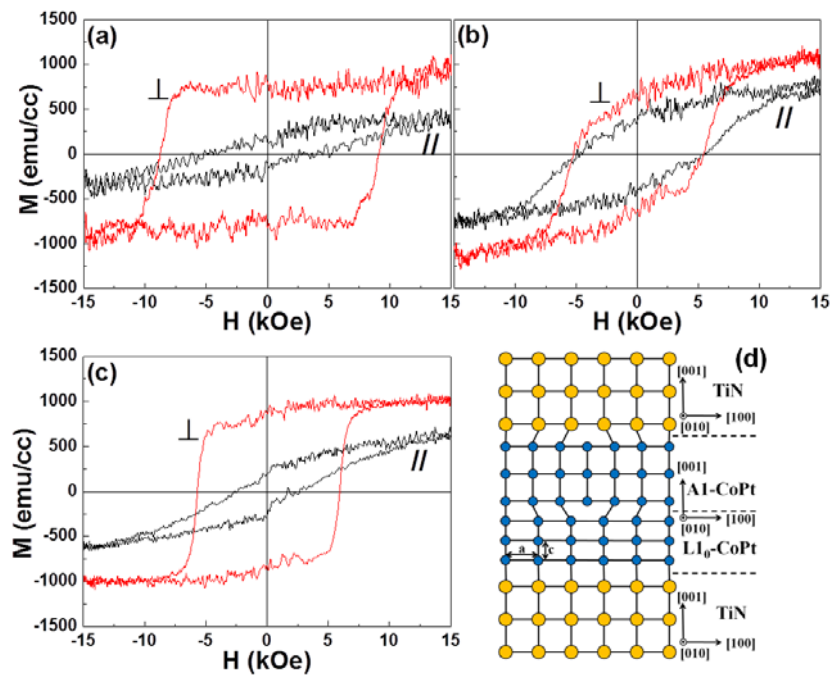


Figure 5-5  $M$ - $H$  curves after annealing at  $700 \text{ }^\circ\text{C}$ : (a)  $\text{TiN}(50 \text{ nm})/\text{CoPt}(4 \text{ nm})$ , (b)  $\text{TiN}(50 \text{ nm})/\text{CoPt}(4 \text{ nm})/\text{TiN}(2 \text{ nm})$ , (c)  $\text{TiN}(50 \text{ nm})/\text{CoPt}(4 \text{ nm})/\text{TiN}(2 \text{ nm})/\text{CoPt}(4 \text{ nm})$ , (d) schematic illustration of the interfaces between TiN and CoPt layers.

## 5.4 2D micromagnetic simulations

Based on the above study, 2D micromagnetic simulations were performed to illustrate the dynamical magnetization process as shown in Fig. 6-6. To simplify the model, we used a large magnetic saturation field instead of the FC from high temperature, and assume that one single 4 nm thick CoPt layer is composed of 1.5 nm A1-CoPt layer and 2.5 nm L1<sub>0</sub>-CoPt layer, respectively. Fig. 6-6(a) shows the cross-sectional image before applying external magnetic field. The spins in A1-CoPt layer are coupled with the spins in L1<sub>0</sub>-CoPt layer, and present a semi-circle distribution. After the saturation in the perpendicular direction (+y direction), all the spins in the L1<sub>0</sub>-CoPt layer are switched to the +y direction (Fig. 6-6(b)). Then, a smaller magnetic field  $H_t$  is applied in -y direction. As  $H_t$  increases, the spins in the A1-CoPt layer are switched to -y direction firstly, and it can be seen from Fig. 6-6(c) that the spins in the A1-CoPt layer near the interface are pinned by the spins in L1<sub>0</sub>-CoPt layer, which is similar to the pinning effect of the AFM layer. This pinning effect would cost additional energy for the reversal of the spins in A1-CoPt layer, and then generate a shift in the hysteresis loops, which is responsible for the EB-like effect. Furthermore, in the center of the A1-CoPt layer, a small domain with spins in +y direction is formed due to the coupling effect from the spins in L1<sub>0</sub>-CoPt layer. This domain also retards the spin switching in A1-CoPt layer. As  $H_t$  increases to the maximum value, some spins in the L1<sub>0</sub>-CoPt layer are also switched together with the spins in A1-CoPt layer (Fig. 6-6(d)). It is worth to mention that this simple model cannot fully reflect the practical spin switching process in the CoPt/TiN films. In the model, the magnetization condition in Fig. 6-6(d) is unstable, which means that if a few parts of spins in the L1<sub>0</sub>-CoPt layer are switched, then all other spins in the L1<sub>0</sub>-CoPt

layer would be switched together. However, in the practical condition, defects and the subgrain boundaries in the  $L1_0$ -CoPt layer can be the pinning points to stop the continuously switching and more energy is needed for the subsequent spin switching.

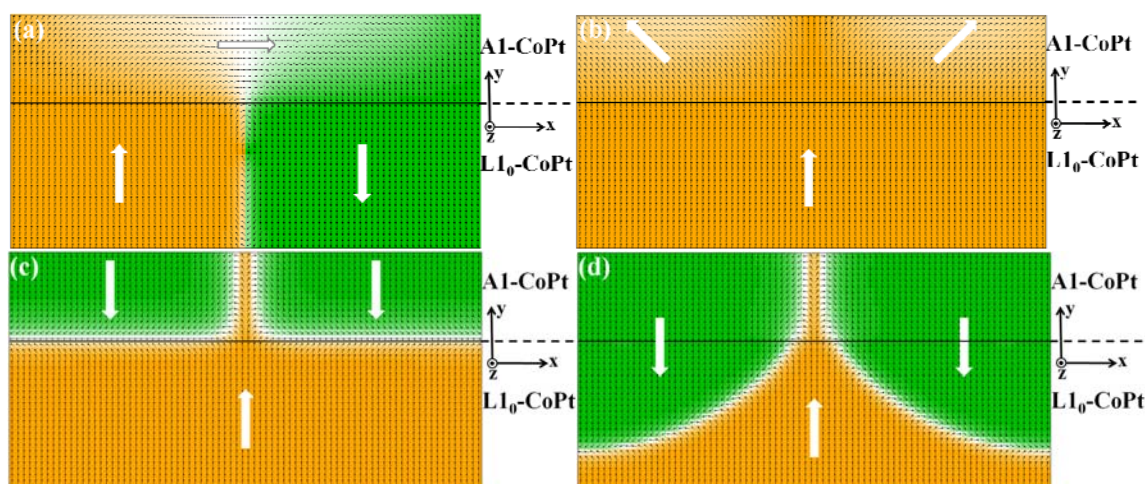


Figure 6-6 Cross-sectional images of the magnetization distribution simulated for one 4 nm thick CoPt layer with  $L1_0$ -CoPt of 2.5 nm and Al-CoPt of 1.5 nm: (a) before applying magnetic field (assuming as ZFC state). (b) after saturation in +y direction. (c) applying a small magnetic field  $H_t$  in -y direction. (d)  $H_t$  increases to the negative maximum value and switches some spins in  $L1_0$ -CoPt layer. The y axis is the direction normal to the film plane.

## 5.5 Summary

We have successfully observed the perpendicular exchange-bias-like effect in CoPt/TiN multilayer films after annealing at 700 and 800 °C. It is found that the TiN layer promotes the  $L1_0$  transformation of the CoPt layer above it, but impedes the  $L1_0$  transformation of the CoPt layer below it. This effect generates the coexistence of the Al-CoPt phase and  $L1_0$ -CoPt phase in one CoPt layer sandwiched by two TiN layers. The coupling effect between Al and

$L1_0$ -CoPt phases has been illustrated by the 2D micromagnetic simulations. After the magnetic saturation, all the spins in the  $L1_0$ -CoPt phase are switched to the direction of the magnetic field. Since A1-CoPt is soft magnetic phase, the spins in the A1-CoPt phase can be easily switched by a smaller magnetic field. Therefore, near the interface of the A1 and  $L1_0$ -CoPt phases, the spins in A1-CoPt phase are pinned by the spins in the  $L1_0$ -CoPt phase. This pinning effect costs additional energy for the spin switching in the A1-CoPt phase, and generates exchange-bias-like effect.

**Reference**

- <sup>1</sup>W. H. Meiklejohn, and C. P. Bean, *Phys. Rev.* 102, 1413 (1956).
- <sup>2</sup>S. P. Pati, A. Roychowdhury, S. Kumar, and D. Das, *J. Appl. Phys.* 113, 17D708 (2013).
- <sup>3</sup>B. Dieny, V. S. Speriosu, S. S. P. Parkin, B. A. Gurney, D. R. Wilhoit, D. Mauri, *Phys. Rev. B.* 43, 1297 (1991).
- <sup>4</sup>H. Lin, C. Hsu, Y. Yao, Y. Chen, T. Kuan, F. Kuan, F. Yang, C. Tung, *NanoStruct. Mater.* 6, 977 (1995).
- <sup>5</sup>J. Wang, T. Omi, T. Sannomiya, S. Muraishi, J. Shi, and Y. Nakamura, *Appl. Phys. Lett.* 103, 042401 (2013).
- <sup>6</sup>J. Sort, V. Baltz, F. Garcia, B. Rodmacq, and B. Dieny, *Phys. Rev. B.* 71, 054411 (2005).
- <sup>7</sup>L. Lin, N. Thiyagarajah, H. Joo, J. Heo, K. Lee, and S. Bae, *Appl. Phys. Lett.* 97, 242514 (2010).
- <sup>8</sup>Z. Liu and S. Adenwalla, *J. Appl. Phys.* 94, 1105 (2003).
- <sup>9</sup>T. Tokunaga, M. Taguchi, T. Fukami, Y. Nakaki, and K. Tsutsumi, *J. Appl. Phys.* 67, 4417 (1990).
- <sup>10</sup>W. Cain, and M. Kryder, *J. Appl. Phys.* 67, 5722 (1990).
- <sup>11</sup>J. Sort, A. Popa, B. Rodmacq, and B. Dieny, *Phys. Rev. B.* 70, 174431 (2004).
- <sup>12</sup>J. Nogués, and I. Schuller, *J. Magn. Magn. Mater.* 192, 203 (1999).
- <sup>13</sup>H. Ohldag, A. Scholl, F. Nolting, E. Arenholz, S. Maat, A. T. Young, M. Carey, and J. Stohr, *Phys. Rev. Lett.* 91, 017203 (2003).
- <sup>14</sup>P. Huang, H. Huang, and C. Lai, *Appl. Phys. Lett.* 90, 062509 (2007).
- <sup>15</sup>D. Navas, J. Torrejon, F. Béron, C. Redondo, F. Batallan, B. Toperverg, A. Devishvili, B.

Sierra, F. Castano, K. Pirota, and C. Ross, *New. J. Phys.* 14, 113001 (2012).

<sup>16</sup>A. Hochstrat, C. Binek, and W. Kleemann. *Phys. Rev. B.* 66, 092409 (2002).

<sup>17</sup>H. An, Q. Xie, J. Wang, T. Sannomiya, S. Muraishi, Z. Zhang, Y. Nakamura, and J. Shi, *J. Vac. Sci. Technol. A* 33, 021512 (2015).

<sup>18</sup>H. Li, K. Dong, J. Hu, T. Zhou, G. Chow, and J. Chen, *J. Phys. D: Appl. Phys.* 46, 015002 (2013).

<sup>19</sup>D. Paskiewicz, D. Savage, M. Holt, P. Evans, and M. Lagally, *Scientific Reports*, 4, 4218 (2014).

<sup>20</sup>T. Ichitsubo, S. Tojo, T. Uchihara, E. Matsubara, A. Fujita, K. Takahashi, and K. Watanabe, *Phys. Rev. B.* 77, 094114 (2008).

<sup>21</sup>Micromagnetic simulations were performed using the OOMMF code, available at <http://math.nist.gov/oommf/>

<sup>22</sup>The Co-Pt binary phase diagram is available at

<http://www.crct.polymtl.ca/fact/documentation/BINARY/Co-Pt.jpg>

<sup>23</sup>H. Shima, K. Oikawa, A. Fujita, K. Fukamichi, and K. Ishida, *Appl. Phys. Lett.* 86, 112515 (2005).

<sup>24</sup>A. Bollero, L. D. Buda-Prejbeanu, V. Baltz, J. Sort, B. Rodmacq, and B. Dieny, *Phys. Rev. B.* 73, 144407 (2006).

## Chapter 6 Realization of PMA in L1<sub>0</sub>-CoPt/TiN single layer films

Heat-assisted magnetic recording (HAMR), which can drastically increase the areal recording density of the hard disc drive (HDD), has been considered to be the next generation of the magnetic recording technology.<sup>[1,2]</sup> As a promising candidate for HAMR materials, L1<sub>0</sub> FePt and CoPt structure have attracted researchers' interests due to their high magnetocrystalline anisotropy and large coercivity.<sup>[3-5]</sup> Much effort has been devoted on enlarging the perpendicular coercivity, reducing the grain size, averaging the grain distribution, lowering the ordering temperature, etc.<sup>[6-15]</sup> To realize the above objectives, MgO seed layer is widely used on amorphous substrates to promote the L1<sub>0</sub> ordering for FePt/CoPt.<sup>[7-12]</sup> Although significant progress for fabricating L1<sub>0</sub> FePt/CoPt granular films with large perpendicular coercivity and small grain size has been made by using MgO seed layer, the small surface energy of MgO (1.1 J/m<sup>2</sup>) can result in a large contact angle between FePt/CoPt and MgO, which is not favorable for the epitaxial growth. Furthermore, it will promote the formation of in-plane variants and lead to a large in-plane coercivity.<sup>[12,16]</sup> Recently, Li *et al.* reported a successful fabrication of L1<sub>0</sub> FePt with very narrow opening-up of in-plane hysteresis loop by using TiN intermediate layer instead of MgO.<sup>[16]</sup> TiN has a similar structure with MgO, but owns a larger surface energy (1.28 J/m<sup>2</sup>), which is more suitable for the epitaxial growth of L1<sub>0</sub> FePt/CoPt. However, it is difficult to fabricate highly (100) oriented TiN as a seed layer.<sup>[17]</sup> It is known that TiN (200) plane has the lowest surface energy which is the driving force for the growth in (200) orientation. However, besides surface energy, strain energy also affects the growth orientation, and TiN (111) plane has the

lowest strain energy.<sup>[18]</sup> Since strain energy of the film is proportional to the film thickness,<sup>[19]</sup> TiN tends to grow in (111) orientation when the thickness is large. On the other hand, if TiN film is too thin, it will show random growth orientation on amorphous substrates.<sup>[20]</sup> Thus, to fabricate highly (100) oriented TiN as a seed layer, generally another buffer layer is needed to improve the wettability of TiN, or bias voltage is needed during the sputtering process, which increases the complicacy for the practical industrial fabrication.<sup>[16,21]</sup> In this chapter, we present the successful fabrication of L1<sub>0</sub> CoPt with narrow opening-up of in-plane hysteresis loop by only using TiN on glass substrates. Furthermore, we show that during the deposition of CoPt, introducing an appropriate amount of N<sub>2</sub> can reduce the grain size, uniform the grain distribution and enhance the perpendicular coercivity without enlarging the opening-up of in-plane hysteresis loop.

### 6.1 Fabrication of L1<sub>0</sub>-CoPt/TiN single layer films

Firstly, substrate/TiN( $x$  nm)/CoPt(4 nm) ( $x=10,30,50,100$  nm) were deposited on fused quartz substrates at 400 °C by dc magnetron sputtering. The base pressure in the chamber before deposition was better than  $5 \times 10^{-5}$  Pa, and the deposition pressure was 0.2 Pa. Co<sub>0.44</sub>Pt<sub>0.56</sub> was deposited from a 2-inch composite Co-Pt target. N<sub>2</sub> and Ar gases with fixed flow rate ratio of 1:8.7 were supplied during the whole deposition process. After deposition, samples were annealed at 600, 700°C for 1 hour in vacuum (better than  $1 \times 10^{-5}$  Pa). Secondly, another group of samples substrate/TiN(30 nm)/CoPt(4 nm) were deposited by changing the N<sub>2</sub> flow rate ratio. For the TiN deposition, the flow rate ratio between N<sub>2</sub> and (N<sub>2</sub>+Ar) was fixed as 10%. For the subsequent CoPt deposition, the flow rate ratio between N<sub>2</sub> and (N<sub>2</sub>+Ar) was changed as 0%, 10%, 20% and 30%. The samples of this group were annealed

at 700 °C for 1 hour in vacuum. All the measurements were conducted at room temperature.

## 6.2 structure characterization of TiN single layer

TiN single layer films with different thicknesses were firstly deposited on fused quartz substrates and then investigated by AFM and XRD to obtain the optimum condition for CoPt epitaxial growth. Figure 6-1(a), (b), (c) and (d) show the surface AFM images of TiN single layer with different thickness. All TiN layers are continuous with smooth surfaces. The surface root mean squared roughness  $R_{\text{RMS}}$  of films with different thicknesses were calculated by AFM. To fabricate highly (100) oriented TiN layer with small surface roughness, we used substrate temperature of 400 °C. It can be seen that all the samples have surface roughness lower than 1.0 nm, and TiN with 50 nm shows smallest roughness of 0.6 nm. The corresponding XRD profiles are shown in Fig. 6-1(b). All the films exhibit TiN (200) peak, which increases with TiN thickness. TiN (111) peak appears when TiN thickness is 50 nm and becomes stronger with TiN thickness of 100 nm. This is consistent with our interpretation in chapter 3. Although TiN (200) plane has the lowest surface energy to drive crystal grow in (100) orientation, TiN (111) plane has the lowest strain energy, which also affects the growth orientation. As the thickness increases, crystal tends to grow in (111) orientation.

## 6.3 Magnetic properties measurement of CoPt/TiN films

Figure 6-2 shows the  $M-H$  curves of the TiN( $x$  nm)/CoPt(4 nm) ( $x=10,30,50,100$  nm) after annealing at 600 and 700 °C. Compared with which annealed at 600 °C, the samples annealed at 700 °C show much stronger PMA and larger perpendicular coercivity. Especially, the film with TiN thickness of 30 nm shows largest perpendicular coercivity of 12 kOe after annealing at 700 °C. When TiN thickness is 10 nm, it is too thin for TiN to have a highly

(100) texture due to the non-epitaxial growth relation between TiN and glass substrate, leading to a weak PMA. Oppositely, when TiN thickness is above 50 nm, the perpendicular coercivity decreases with increasing TiN thickness. Nevertheless, due to the very low surface roughness of TiN seed layer, all samples annealed at 700 °C with TiN thickness above 30 nm exhibit very narrow opening-up in the in-plane hysteresis loops.

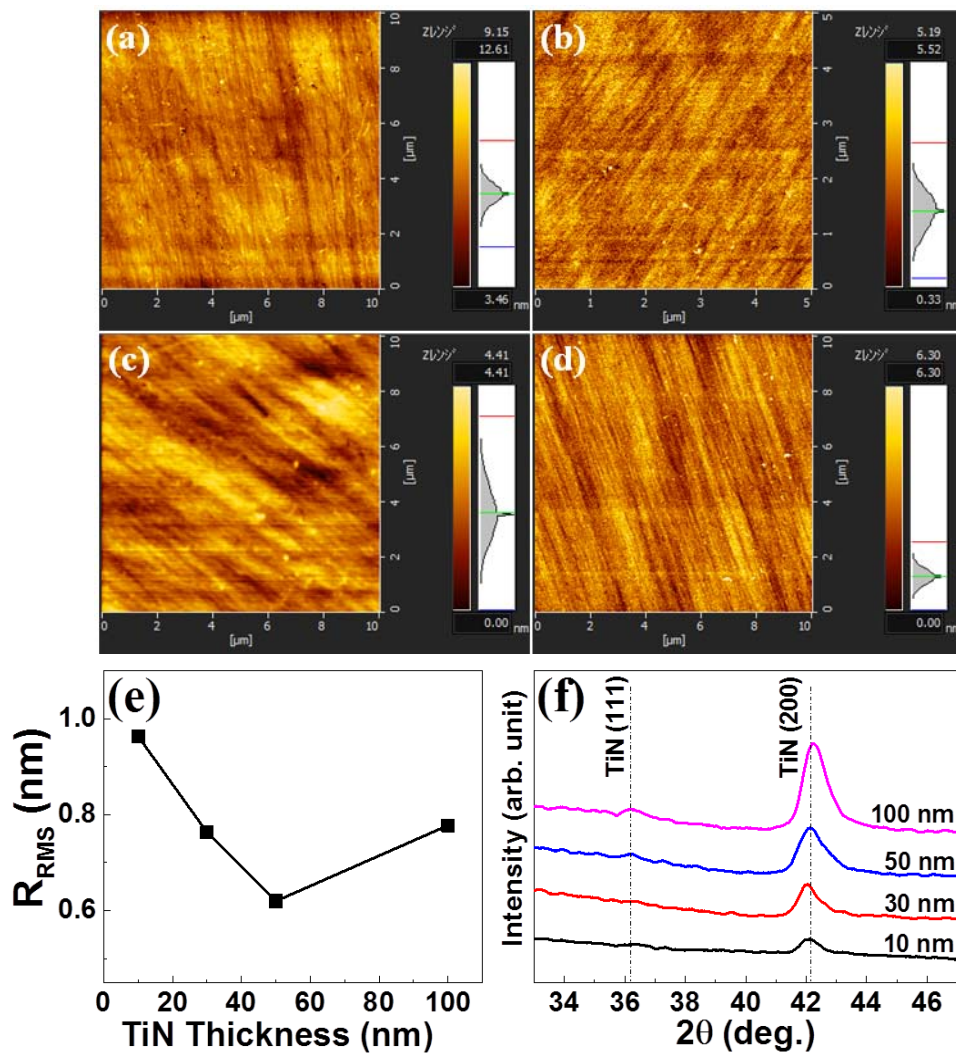


Figure 6-1 AFM surface images of TiN single layer with different thickness: (a) 10 nm, (b) 30 nm, (c) 50 nm and (d) 100 nm. (e) The surface roughness vs TiN single layer thickness. (f) XRD profiles of TiN single layer with different thickness.

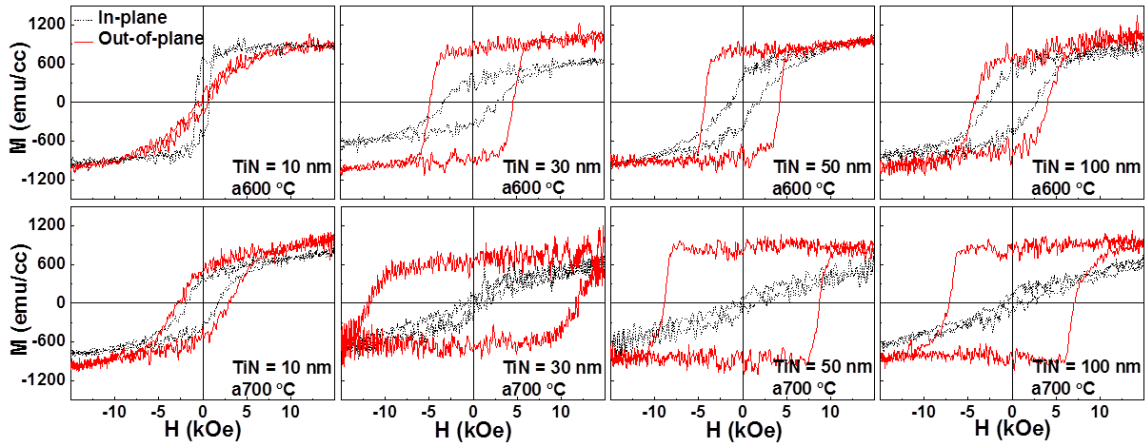


Figure 6-2  $M$ - $H$  curves of TiN( $x$  nm)/CoPt(4 nm) films ( $x=10,30,50,100$ ) after annealing at 600 and 700 °C, respectively.

#### 6.4 Effect of N<sub>2</sub> doping during deposition

Since the sample with TiN seed layer thickness of 30 nm shows best magnetic property, we further fabricated a set of TiN(30 nm)/CoPt(4 nm) films with different N<sub>2</sub> flow rate ratio during the deposition of CoPt to investigate the effect of N<sub>2</sub> (N<sub>2</sub> flow rate ratio was fixed for TiN deposition). Fig. 6-3(a), (b), (c) and (d) show the AFM images of the samples before annealing. For all the samples, continuous CoPt layers were formed on the surfaces of TiN seed layers. After annealing, continuous CoPt layers become discontinuous maze and granular shapes (Fig. 6-3(e), (f), (g) and (h)). From the AFM images shown in Fig. 6-3(e), (f), (g) and (h), it can be seen that CoPt grain size decreases with increasing N<sub>2</sub> flow rate ratio up to 20%, above which, CoPt grain size increases again. The sample deposited with N<sub>2</sub> flow rate ratio of 20% shows smallest grain size and narrowest grain distribution. The corresponding  $M$ - $H$  curves are shown in Fig. 6-3(i), (j), (k) and (l). Perpendicular coercivity increases with N<sub>2</sub> flow rate ratio up to 20% (out-of-plane hysteresis loop in Fig. 6-3(k) is not

saturated), then decreases by further increasing N<sub>2</sub> flow rate ratio. The above phenomenon indicates that introducing N<sub>2</sub> with different flow rate ratio during CoPt deposition has significant effect on the microstructure and magnetic properties of L1<sub>0</sub> CoPt films.

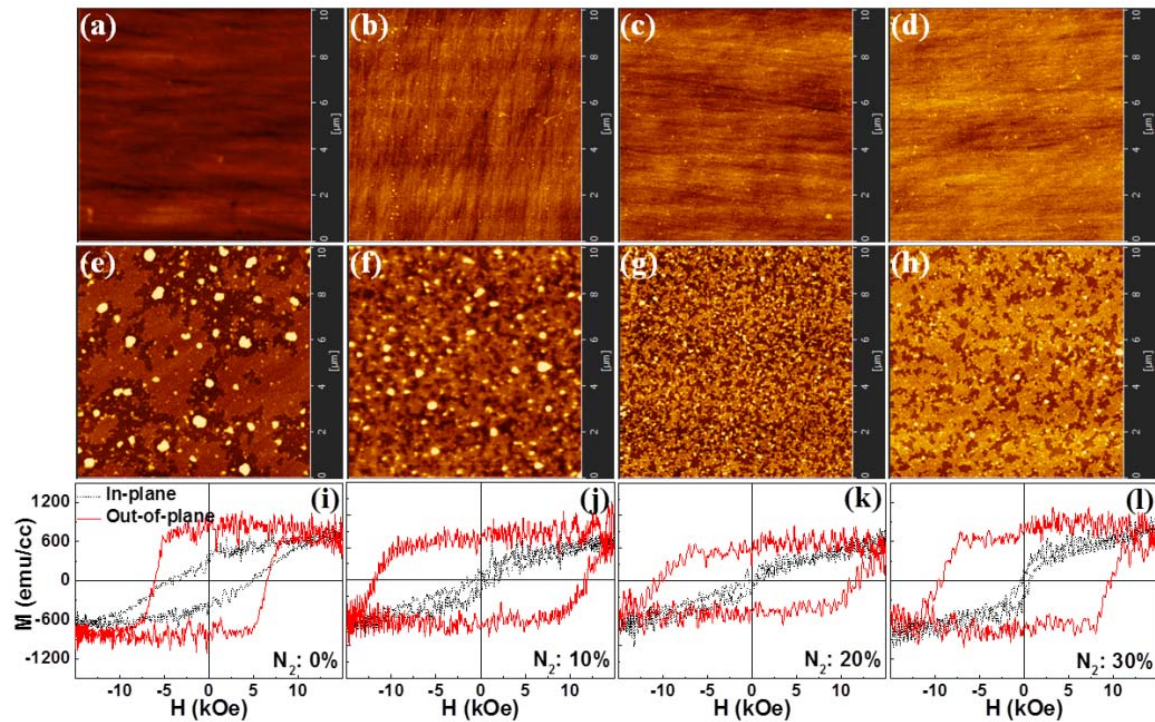


Figure 6-3 (a), (b), (c) and (d) The AFM images of TiN(30 nm)/CoPt(4 nm) films before annealing with different flow rate ratio between N<sub>2</sub> and (N<sub>2</sub>+Ar) during the deposition of CoPt. (a) 0%, (b) 10%, (c) 20%, (d) 30%. (e), (f), (g) and (h) the corresponding AFM images after annealing at 700 °C. (i), (j), (k) and (l) the corresponding *M-H* curves after annealing at 700 °C.

Since AFM images only reflect the contrast of the height difference, to further confirm the distribution of the elements in the films, FE-AES mappings were conducted and the results are shown in Fig. 6-4. Yellow color denotes the element distribution in each figure.

Fig. 6-4(a) and (c) exhibit Co and Ti distributions for the sample with N<sub>2</sub> flow rate ratio of 0% after annealing at 700 °C. The discontinuous plate and particle shapes are well consistent with the AFM image in Fig. 6-3(e). For instance, the brighter parts in Fig. 6-3(e) correspond to Co distribution in Fig. 6-4(a), and the darker parts in Fig. 6-3(e) correspond to Ti distribution in Fig. 6-4(c). The brightest particles shown in Fig. 6-3(e) turn out to be CoPt grains (indicated by white arrows in Fig. 6-4(a)), which deplete other CoPt around them and abnormally grow during the annealing process. This phenomenon does not happen for the sample with N<sub>2</sub> flow rate ratio of 20% (Fig. 6-4(b) and (d)). In Fig. 6-4(b), Co shows much more uniform distribution compared with Co distribution in Fig. 6-4(a), which is also well consistent with the AFM image in Fig. 6-3(g).

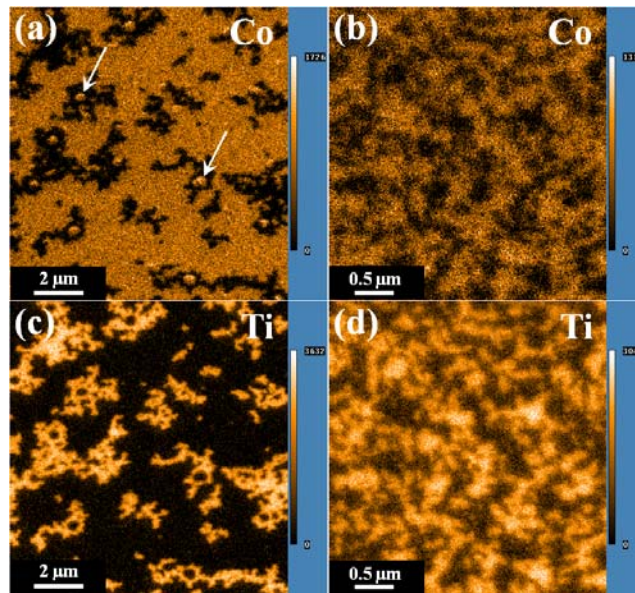


Figure 6-4 FE-AES mappings of (a) Co and (c) Ti for TiN(30 nm)/CoPt(4 nm) with N<sub>2</sub> flow rate ratio of 0% during the deposition of CoPt. FE-AES mappings of (b) Co and (d) Ti for TiN(30 nm)/CoPt(4 nm) with N<sub>2</sub> flow rate ratio of 20% during the deposition of CoPt. Samples were post annealed at 700 °C in vacuum. White arrows show the coalescence of CoPt grains.

From the above study, one can see that during the deposition of CoPt, compared with only using Ar gas atmosphere, applying an appropriate amount of N<sub>2</sub> into Ar gas can reduce L1<sub>0</sub>-CoPt grain size and enhance the perpendicular coercivity. However, the mechanism of the microstructure formation and the resultant magnetic properties of CoPt is not clear. A previous study by Wang *et al.* reported that the in-plane coercivity of Fe<sub>56</sub>Pt<sub>44</sub> (Fe rich) films can be enhanced after annealing by depositing the films in an Ar and N<sub>2</sub> atmosphere.<sup>[22]</sup> They interpreted that the formation of iron nitride was responsible. However, we used Co<sub>44</sub>Pt<sub>56</sub> (Pt rich) target, and no cobalt nitride peak was observed from the XRD profiles. Furthermore, in current work, the perpendicular coercivity is enhanced without enlarging the in-plane coercivity, which is different from their results. In order to investigate the mechanism of the effect of N<sub>2</sub>, we fabricated TiN(30 nm)/CoPt(10 nm) films with N<sub>2</sub> flow rate ratio of 20% during the deposition of CoPt and quantified N changes in CoPt layer before and after annealing. Interestingly, as shown in the depth profiles in Fig. 6-5, the amount of dissolved N drastically reduced after annealing (highlighted by red squares), which indicates that N effused from CoPt layer during the annealing process.

Figure 6-6 shows the XRD profiles of TiN(30 nm)/CoPt(10 nm) with 0% and 20% N<sub>2</sub> during deposition. As shown in Fig. 6-6(a), before annealing, compared with the barely observed peak of the film deposited with 0% N<sub>2</sub>, the film deposited with 20% N<sub>2</sub> exhibits strong CoPt (200) peak, which indicates the better crystallinity of the latter condition. After annealing (Fig. 6-6(b)), the film deposited with 20% N<sub>2</sub> shows strong CoPt (002) peak, indicating the transformation of L1<sub>0</sub> structure. While the film deposited with 0% N<sub>2</sub> exhibits weak CoPt (002) peak.

Considering above phenomenon, a practical model of N<sub>2</sub> effect is proposed as shown in Fig. 6-7. During the deposition of CoPt on TiN seed layer, local epitaxial growth between CoPt and TiN occurs. However, with a misfit of 10.4% between CoPt ( $a=0.38$  nm) and TiN ( $a=0.424$  nm), large in-plane tensile stress will be generated in CoPt layer. It is considered that an appropriate amount of dissolved N in CoPt can relieve the stress and benefit the epitaxial growth of CoPt on TiN. During the annealing process, N effuses from CoPt layer. The effusion of N promotes the diffusion mobility of Co and Pt atoms, which promotes the L<sub>10</sub> transformation degree.

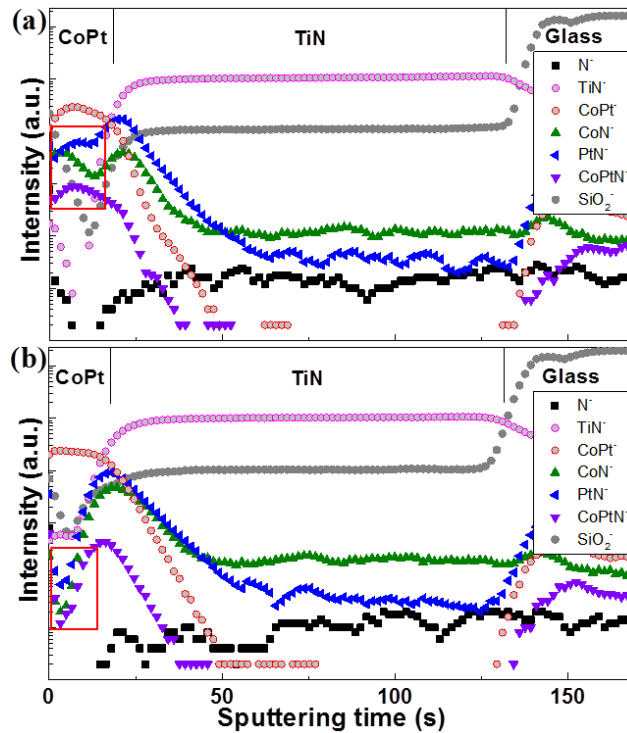


Figure 6-5 TOF-SIMS depth profiles of TiN(30 nm)/CoPt(10 nm) with N<sub>2</sub> flow rate ratio of 20% during the deposition of CoPt: (a) as-deposited condition, (b) after annealing at 700 °C in vacuum. Red squares indicate N change before and after annealing.

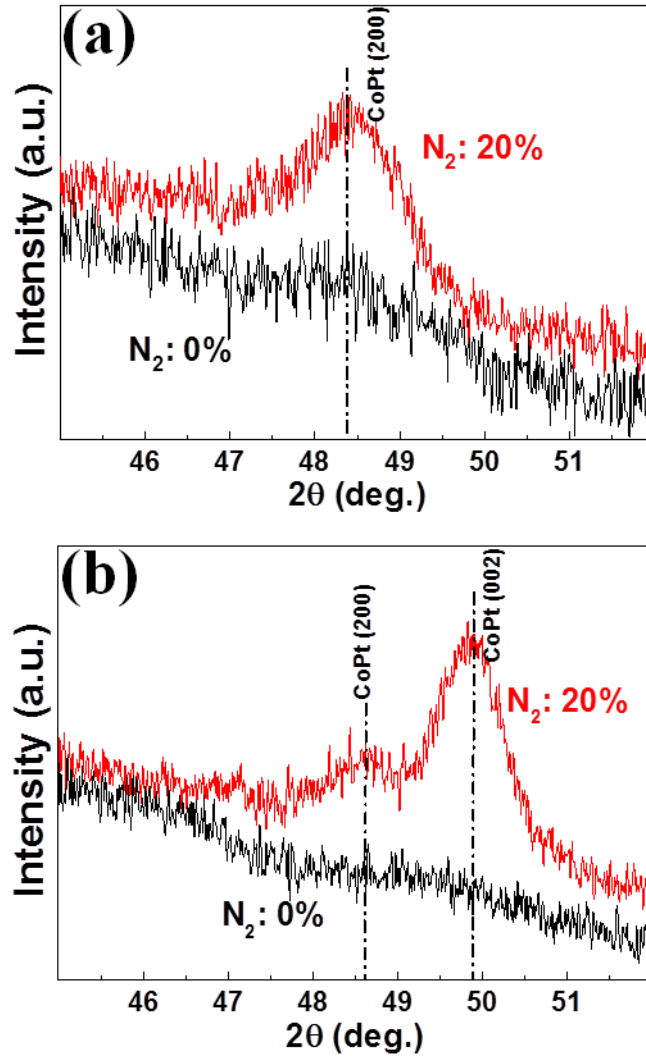


Figure 6-6 XRD profiles of TiN(30 nm)/CoPt(10 nm): (a) before annealing, (b) after annealing at 700 °C.

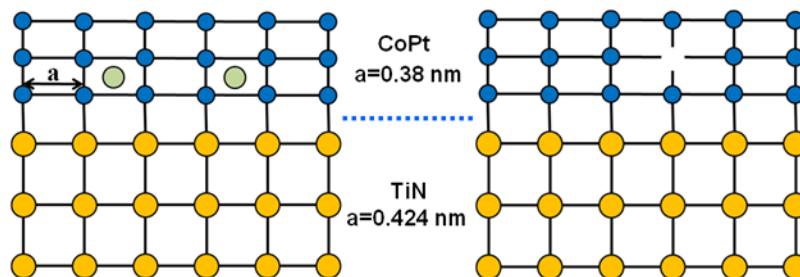


Figure 6-7 Schematic illustrations of (a) soluted N in CoPt during deposition, (b) N effused from CoPt after annealing. The missing of the atom represents the vacancy in CoPt layer.

To further investigate the effect of N, in-situ XRD was taken by changing the measuring temperature for the sample deposited with N<sub>2</sub>. As shown in Fig. 6-8, the temperature of the sample was increased and then decreased twice to observe CoPt (200) peak position shift. As indicated by the dashed line in Fig. 6-8(a), by increasing the temperature up to 500 °C, peak shifts to lower angle, which indicates the thermal expansion of the lattice parameter. However, above 500 °C, despite of the thermal expansion, peak begins to shift to higher angle, indicating the shrinkage of the lattice parameter. Two possible reasons may be responsible for this phenomenon, which are L1<sub>0</sub> ordering transformation (lattice parameter *c* is smaller than *a* in L1<sub>0</sub> structure) and N release. However, since the peak starts to shift to higher angle around 500 °C, which is much lower than the L1<sub>0</sub> ordering transformation temperature (above 600 °C), L1<sub>0</sub> ordering transformation can be excluded. Furthermore, by the following measurements in the temperature decrease of the first cycle and the subsequent increase-decrease of temperatures, the peak only shifts by following the effect of the thermal expansion. Therefore, the peak shift to higher angle in Fig.6-8(a) is caused by N release.

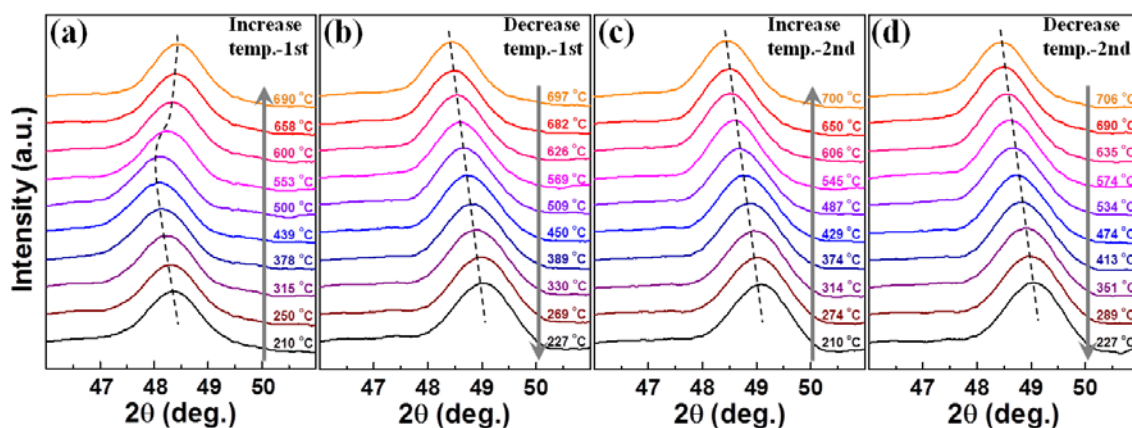


Fig. 6-8 In-situ XRD profiles of TiN(30 nm)/CoPt(10 nm) with N<sub>2</sub> flow rate ratio of 20% during the deposition of CoPt: (a) Increasing temperature in the first cycle, (b) decreasing

temperature in the first cycle, (c) increasing temperature in the second cycle, (d) decreasing temperature in the second cycle. The peak is CoPt (200) peak, and all XRD profiles are smoothed without changing the shapes and the peak positions.

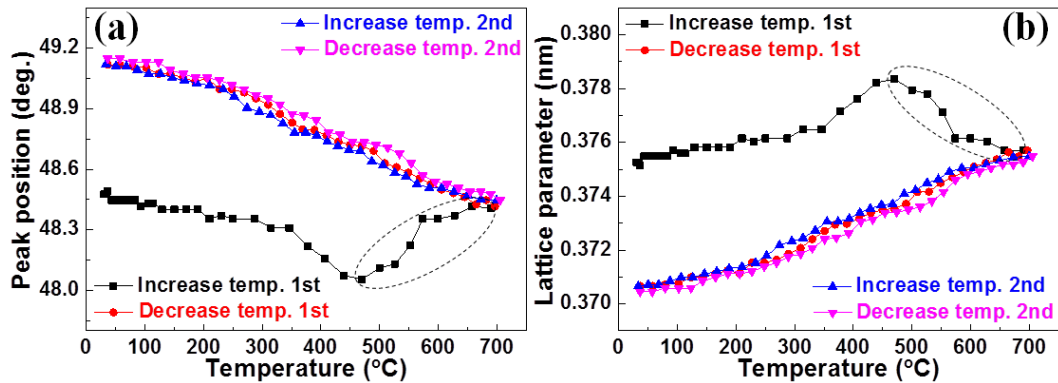


Fig. 6-9 (a) CoPt (200) peak position dependence on in-situ XRD temperatures, (b) CoPt perpendicular lattice parameter dependence on in-situ XRD temperatures. Dashed circle indicates the drastic change due to N release.

The dependence of CoPt (200) peak position and calculated CoPt lattice parameter on measuring temperatures are summarized and plotted in Fig. 6-9. As shown in Fig. 6-9(a), the measurement with increasing the temperature in the first cycle has a large deviation from the subsequent measurements. This indicates that N released during the temperature increase process in the first cycle and thermal expansion is responsible for the peak position changes in the subsequent measurements. As shown in Fig. 6-9(b), CoPt lattice parameter increases with measuring temperature up to 470 °C due to thermal expansion. Above 470 °C, the lattice parameter drastically decreases by further increasing the measuring temperature due to N release. By comparing the lattice parameter measured at room temperature before (~0.3753

nm) and after N release (~0.3707 nm), it is found that CoPt lattice parameter is 1.24% larger in the as-deposited status. The above in-situ XRD results are well consistent with our interpretation. N incorporation can expand the lattice parameter of CoPt and benefit the epitaxial growth between CoPt and TiN. Through post-annealing process, the release of N can promote the mobility of Co and Pt atoms and favor the L1<sub>0</sub> ordering transformation of CoPt.

### **6.5 Summary**

L1<sub>0</sub>-CoPt films with large perpendicular coercivity and narrow opening-up of in-plane hysteresis loops have been successfully fabricated by using a TiN seed layer on glass substrates. Furthermore, by controlling N<sub>2</sub> flow rate ratio during the deposition of CoPt, L1<sub>0</sub> CoPt grain size can be drastically reduced and perpendicular cocercivity can be further enhanced without enlarging the opening-up of the in-plane hysteresis loop. Since only Ar gas was used for L1<sub>0</sub>-CoPt/FePt granular films deposition in most previous reported studies, this study can be a new method for fabricating L1<sub>0</sub>-CoPt/FePt films.

**Reference**

- <sup>1</sup>R. L. Stamps *et al.*, J. Phys. D: Appl. Phys. 47, 333001 (2014).
- <sup>2</sup>R. E. Rottmayer *et al.*, IEEE Trans. Magn. 42, 2417 (2006).
- <sup>3</sup>M. H. Kryder *et al.*, Proc. IEEE 96, 1810 (2008).
- <sup>4</sup>S. D. Granz and M. H. Kryder, J. Magn. Magn. Mater. 324, 287 (2012).
- <sup>5</sup>D. Weller, O. Mosendz, G. Parker, S. Pisana, and T. S. Santos, Phys. Status Solidi A 210, 1245 (2013).
- <sup>6</sup>K. F. Dong, H. H. Li, Y. G. Peng, G. Ju, G. M. Chow, and J. S. Chen, Appl. Phys. Lett. 104, 192404 (2014).
- <sup>7</sup>J. S. Chen, B. C. Lim, J. F. Hu, B. Liu, G. M. Chow, and G. Ju, Appl. Phys. Lett. 91, 132506 (2007).
- <sup>8</sup>H. Ho, E. Yang, D. E. Laughlin, and J. G. Zhu, Appl. Phys. Lett. 102, 112411 (2013).
- <sup>9</sup>S. D. Granz, K. Barmak, and M. H. Kryder, Eur. Phys. J. B 86, 81 (2013).
- <sup>10</sup>Y. Peng, J. G. Zhu, and D. E. Laughlin, J. Appl. Phys. 99, 08F907 (2006).
- <sup>11</sup>B. S. D. Ch. S. Varaprasad, Y. K. Takahashi, J. Wang, T. Ina, T. Nakamura, W. Ueno, K. Nitta, T. Uruga, and K. Hono, Appl. Phys. Lett. 104, 222403 (2014).
- <sup>12</sup>B. S. D. Ch. S. Varaprasad, Y. K. Takahashi, Antony Ajan, and K. Hono, J. Appl. Phys. 113, 203907 (2013).
- <sup>13</sup>G. R. Trichy, D. Chakraborti, J. Narayan, and J. T. Prater, Appl. Phys. Lett. 92, 102504 (2008).
- <sup>14</sup>J. W. Liao *et al.*, Appl. Phys. Lett. 102, 062420 (2013).
- <sup>15</sup>K. K. Tham, S. Hinata, S. Saito, and M. Takahashi, J. Appl. Phys. 115, 17B752 (2014).

- <sup>16</sup>H. H. Li, K. F. Dong, Y. G. Peng, G. Ju, G. M. Chow, and J. S. Chen, *J. Appl. Phys.* 110, 043911 (2011).
- <sup>17</sup>T. Li, S. Noda, Y. Tsuji, T. Ohsawa, and H. Komiyama, *J. Vac. Sci. Technol. A* 20, 583 (2002).
- <sup>18</sup>U. C. Oh and J. H. Je, *J. Appl. Phys.* 74, 1692 (1993).
- <sup>19</sup>J. E. Sundgren, *Thin Solid Films* 128, 21 (1985).
- <sup>20</sup>H. An, Q. Xie, J. Wang, T. Sannomiya, S. Muraishi, Z. Zhang, Y. Nakamura, and J. Shi, *J. Vac. Sci. Technol. A* 33, 021512 (2015).
- <sup>21</sup>Y. Tsuji and S. Noda, *J. Vac. Sci. Technol. B* 29, 031801 (2011).
- <sup>22</sup>H. Y. Wang, W. H. Mao, X. K. Ma, H. Y. Zhang, Y. B. Chen, Y. J. He, and E. Y. jiang, *J. Appl. Phys.* 95, 2564 (2004).

## Chapter 7 Conclusions

The structure and Magnetic properties of CoPt/TiN thin films deposited on glass substrates by dc magnetron sputtering have been studied in this thesis. The effect of annealing temperature, TiN layer thickness and N<sub>2</sub> flow rate ratio have been systematically investigated in both CoPt/TiN multilayer films and single layer films. (001) oriented L1<sub>0</sub>-CoPt structure with perpendicular magnetic anisotropy has been successfully obtained on glass substrates by controlling TiN crystal orientation and annealing temperature.

Due to the epitaxial growth between CoPt and TiN, in order to obtain (001) oriented CoPt, (100) oriented TiN has to be fabricated. The orientation of TiN single layer has been investigated by changing N<sub>2</sub> flow rate ratio, substrate temperature and sputtering power. Through XRD measurement, N<sub>2</sub> flow rate ratio of 9%, substrate temperature of 400 °C and sputtering current of 60 mA (Voltage of 900 V) are the optimized condition to obtain highly (100) oriented TiN single layer films.

By using above deposition parameters, CoPt/TiN multilayer films were fabricated and PMA was obtained. It is found that by increasing the multilayer period, the crystallinity and crystal orientation of CoPt and TiN becomes better. As period increases, interface roughness also reduces. XRD profiles indicate that most L1<sub>0</sub>-CoPt grains have (001) orientation normal to the film plane for the sample with 15 periods after annealing at 700 °C. Alternate deposition of TiN and CoPt promotes the (001) orientation of CoPt, and due to which, magnetic anisotropy energy was drastically enhanced with period.

The effect of TiN layer thickness on the structure and magnetic properties of CoPt in CoPt/TiN multilayer films has been systematically investigated by changing TiN layer thickness from 1 nm to 14 nm. CoPt/TiN multilayer films exhibit best magnetic properties with TiN layer thickness of 4 nm and 8 nm after annealing at 700 °C and 800 °C, respectively. When TiN layer thickness is below 2 nm, multilayer films show magnetic isotropy due to the partially discontinuous condition of TiN layer. When TiN layer thickness is 14 nm, the interface roughness increases causing the large variants in CoPt layers, and leads to the reduction of PMA.

Perpendicular exchange-bias-like (EB-like) effect has been observed in CoPt/TiN multilayer films. It is found that TiN layer plays an important role for generating EB-like effect. TiN layer promotes the  $L1_0$  transformation of the adjacent CoPt layer above it, but impedes the  $L1_0$  transformation of the CoPt layer below it. This phenomenon generates the coexistence of the A1-CoPt phase and  $L1_0$ -CoPt phase in one CoPt layer sandwiched by two TiN layers after annealing. The coupling effect between A1 and  $L1_0$ -CoPt phases has been investigated. The 2D micromagnetic simulations show that after the magnetic saturation, all the spins in the  $L1_0$ -CoPt phase are switched to the direction of the magnetic field and ‘cooled down’ as a hardly magnetized phase. On the other hand, A1-CoPt is a soft magnetic phase and the spins in A1-CoPt phase can be easily switched by a smaller magnetic field. Therefore, near the interface between the A1 and  $L1_0$ -CoPt phases, the spins in A1-CoPt phase are pinned by the spins in  $L1_0$ -CoPt phase. This pinning effect costs additional energy for the spins switching in A1-CoPt phase, and responsible for the EB-like phenomenon.

Finally,  $L1_0$ -CoPt single layer films have been fabricated by using one TiN seed layer on

glass substrates from the point of view of practical application. When TiN seed layer is above 30 nm, films show large perpendicular magnetic anisotropy and narrow opening-up of in-plane hysteresis loops. Furthermore, by controlling N<sub>2</sub> flow rate ratio during the deposition of CoPt, L1<sub>0</sub>-CoPt grain size can be reduced and perpendicular cocercivity can be further enhanced without enlarging the opening-up of the in-plane hysteresis loop. Since only Ar gas was used for L1<sub>0</sub>-CoPt/FePt granular films deposition in most previous reported studies, our study can be a good method for fabricating L1<sub>0</sub>-CoPt/FePt granular films with better magnetic properties.

## Publications

### List of Papers

[1] “Effect of substrate temperature on the magnetic properties and internal stresses of CoPt/AlN multilayer deposited by dc magnetron sputtering”

Hongyu An, Susumu Takada, Takumi Sannomiya, Shinji Muraishi, Ji Shi, and Yoshio Nakamura, *Applied Physics A*, 113, 31-35, (2013). *Rapid Communication*.

[2] “Highly (001) oriented L<sub>10</sub>-CoPt/TiN multilayer films on glass substrates with perpendicular magnetic anisotropy”

Hongyu An, Qian Xie, Jian Wang, Takumi Sannomiya, Shinji Muraishi, Zhengjun Zhang, Yoshio Nakamura, and Ji Shi, *Journal of Vacuum Science and Technology A*, 33, 021512, (2015).

[3] “Control of the perpendicular magnetic anisotropy and microstructure of L<sub>10</sub>-CoPt/TiN multilayer films with the TiN layer”

Hongyu An, Jian Wang, Takumi Sannomiya, Shinji Muraishi, Yoshio Nakamura, and Ji Shi. *Journal of Physics D: Applied Physics*, 48, 155001, (2015).

[4] “Perpendicular coercivity enhancement of CoPt/TiN films by nitrogen incorporation during deposition”

Hongyu An, Jian Wang, Takashi Harumoto, Takumi Sannomiya, Shinji Muraishi, Yoshio Nakamura, and Ji Shi, *Journal of Applied Physics*, submitted on 5<sup>th</sup> Aug, (2015).

[5] “Perpendicular exchange-bias-like effect in ferromagnetic CoPt/TiN multilayer films”

Hongyu An, Takumi Sannomiya, Shinji Muraishi, Yoshio Nakamura, and Ji Shi, in preparation, (2015).

[6] “Effect of substrate temperature on the structure and magnetic properties of CoPt/AlN multilayer films”

Hongyu An, Takashi Harumoto, Takumi Sannomiya, Shinji Muraishi, Yoshio Nakamura, and Ji Shi, in preparation, (2015).

[7] “Continuous L1<sub>0</sub> CoPt thin film with narrow opening-up of in-plane hysteresis loop deposited on TiN seed layer”

Hongyu An, Takashi Harumoto, Takumi Sannomiya, Shinji Muraishi, Yoshio Nakamura, and Ji Shi, in preparation, (2015).

[8] “Magnetic coupling between A1 and L1<sub>0</sub> CoPt layers”

Hongyu An, Jian Wang, Takumi Sannomiya, Shinji Muraishi, Yoshio Nakamura, and Ji Shi, in preparation, (2015).

### **List of Oral Presentations**

[1] “Effect of Deposition and Annealing Temperature on the Magnetic Properties and Internal Stresses of CoPt/AlN Layered Films”

Hongyu An, Susumu Takada, Takumi Sannomiya, Shinji Muraishi, Ji Shi, and Yoshio Nakamura. The 2nd International Education Forum on Environment and Energy Science, 13-17 December, 2013, Huntington Beach, California, USA.

[2] “Enhancement of (001) preferred orientation in L1<sub>0</sub>-CoPt/TiN multilayer films”

Hongyu An, Qian Xie, Jian Wang, Takumi Sannomiya, Shinji Muraishi, Zhengjun Zhang, Yoshio Nakamura, and Ji Shi. 2014 Dalian University of Technology-Tokyo Institute of Technology Joint Workshop. 24-25 October 2014, Dalian, China.

[3] “Enhanced (001) preferred orientation and perpendicular magnetic anisotropy of  $L1_0$ -CoPt/TiN multilayer films on glass substrates”

H. An, Q. Xie, J. Wang, T. Sannomiya, S. Muraishi, Z. Zhang, Y. Nakamura, and J. Shi. 59th Annual Conference on Magnetism and Magnetic Materials, 3-7 November 2014, Hawaii, USA.

[4] “Highly (001) textured  $L1_0$ -CoPt/TiN multilayer films with perpendicular magnetic anisotropy”

H. An, Q. Xie, J. Wang, T. Sannomiya, S. Muraishi, Z. Zhang, Y. Nakamura, and J. Shi. The 62nd Japan Society of Applied Physics Spring Meeting, 11-14 March 2015, Kanagawa, Japan.

## **Acknowledgements**

I would like to give my deep gratitude to my advisor, Prof. Shi at the beginning. Without him, I wouldn't have chance to come to this academic university to pursue my PhD degree. In the last three years, during my difficult times no matter in research or in life, he always supported me. When I was stuck in my research, his deep insights on the essential problems and experimental intuition have helped me to get rid of the difficulties and keep me on track while his non-interference education approach has trained my research abilities to solve research issues and judge the correct research directions. When I had living trouble in Tokyo, he also gave me support and helped me to focus on the research. Without him, I couldn't finish my PhD course.

I would also like to give my deep gratitude to my advisor, Prof. Nakamura. His professional knowledge on crystal microstructure analysis and kindness to students have always helped me to overcome many obstacles and move forward. Every time I had troubles to verify my experimental results, he would analyze with me, go through the detail, and try to find the best analysis tools to clearly identify my experimental results. He also always tries to give me various temporary work opportunities to relieve my living stress as a student. I have learned that he is not only a professional scientist in research but also a gracious and compassionate person in life.

I would also like to sincerely thank Associate Prof. Muraishi. During the last three years, he has helped me not only on my research but also on solving my troubles. He has wide knowledge on the fundamental of each equipments. Every time equipment problems

happened during measurement or in normal research life, I came to him for help, and he immediately put down his work to solve the problems with me. I'm very grateful that he spent much of his precious time to help me.

I would also like to give my sincere thanks to Assistant Prof. Sannomiya. He has a wide research background based on his professional research experiences. Every time I discuss with him, his sensitive and accurate judgments on the problems always give me inspiration. Furthermore, he always helps me to review my paper, and gives me invaluable comments and suggestions even he is very busy or during the weekends. His passion and enthusiasm on research makes him the model that I would like to be in the future.

I greatly appreciate Prof. Nakagawa for being on my thesis committee. He is a great scientist in magnetic research field in Tokyo Tech and always very kind to give precious suggestions.

I would like to thank Assistant Prof. Harumoto to share his professional technique on TEM with me. He is at the same age with me, but a person that I admire.

I want to thank Dr. Jian Wang, who constantly gives me support on my research, reviewing my papers and sharing his precious experience with me.

I would also like to thank OB Takada, who taught me how to use the equipments when I just joined the lab. His conscientious attitude on doing research impressed me a lot.

I appreciate Mr. Suzuki, Mr. Tada and Mr. Genseki from Analysis Center of Tokyo Tech for their supports in experimental measurements.

I want to thank Qian Xie, who did research with me during the most difficult half of year. I also want to thank Lei Guo, Nagano and other members in the lab to share their experience

with me and help me on my research.

Finally, I want to thank my parents and wife. Their constant support gave me courage to quit my job and pursue my PhD degree.